Collagen Scaffolds for Treatment of Penetrating Brain Injury in a Rat Model

by

Paul Ziad Elias

M.S. Aeronautics and Astronautics
Massachusetts Institute of Technology, 2006

B.S. Bioengineering
University of Washington, 2003

SUBMITTED TO THE HARVARD-MIT DIVISION OF HEALTH SCIENCES AND TECHNOLOGY IN PARTIAL FULFILLMENT OF THE REQUIREMENTS FOR THE DEGREE OF

DOCTOR OF PHILOSOPHY IN BIOMEDICAL ENGINEERING

AT THE

MASSACHUSETTS INSTITUTE OF TECHNOLOGY

February 2011

Signature of Author: _____
Harvard-MIT Division of Health Sciences and Technology
January 28, 2011

Certified by: _____
Myron Spector
Professor of Orthopedic Surgery (Biomaterials), Harvard Medical School
Thesis Supervisor

Accepted by: _____
Ram Sasisekharan
Director, Harvard-MIT Division of Health Sciences and Technology / Edwin Hood Taplin Professor of Health Sciences and Technology and Biological Engineering

Collagen Scaffolds for Treatment of Penetrating Brain Injury in a Rat Model

by

Paul Ziad Elias

Submitted to the Harvard-MIT Division of Health Sciences and Technology on January 28, 2011 in partial fulfillment of the requirements for the degree of Doctor of Philosophy in Biomedical Engineering

ABSTRACT

Recovery from central nervous system (CNS) injuries is hindered by a lack of spontaneous regeneration. In injuries such as stroke and traumatic brain injury, loss of viable tissue can lead to cavitation as necrotic debris is cleared. Using a rat model of penetrating brain injury, this thesis investigated the use of collagen biomaterials to fill a cavitary brain defect and deliver therapeutic agents.

Characterization of the untreated injury revealed lesion volume expansion of 29% between weeks 1 and 5 post-injury. The cavity occupied parts of the striatum and cortex in the left hemisphere, and was surrounded by glial scarring.

Implantation of a collagen scaffold one week after injury resulted in a modest cellular infiltrate four weeks later consisting of macrophages, astrocytes, and endothelial cells. The scaffold was able to fill the cavity and provide a substrate for cellular migration into the defect.

Incorporation of a Nogo receptor molecule aimed at binding inhibitory myelin proteins did not appear to promote axonal regeneration, but resulted in increased infiltration of macrophages and endothelial cells. The increased vascularization observed within the scaffolds represents a modified environment that might be more suitable for regenerative therapies.

A scaffold was also used to investigate the delivery of neural progenitor cells one week after injury. After four weeks, viable implanted cells were found to have differentiated into astrocytes, oligodendrocytes, endothelial cells, neurons, and possibly macrophages/microglia.

These results demonstrate the potential utility of combinatorial therapies involving collagen biomaterials, myelin protein antagonists, and neural progenitors for treatment of CNS injuries.

Thesis Supervisor: Myron Spector
Title: Professor of Orthopedic Surgery (Biomaterials), Harvard Medical School
Senior Lecturer, Harvard-MIT Division of Health Sciences and Technology, MIT

Acknowledgements

I'd like to thank Dr. Spector very much for granting me the opportunity to do research in his laboratory. I learned a great deal throughout this process and I sincerely appreciated his support and enthusiasm along the way. It was a privilege to have a research supervisor who cares so much about his students.

Thank you to my committee members Dr. Ioannis Yannas and Dr. Larry Benowitz for helpful feedback on this research project.

Thank you to all of the students, post-docs, and fellows for being good lab mates and nice people. With regard to this research, thank you to Rahmat Cholas for helping with the first few surgeries and for taking some of the surgical photographs. Thank you to Cathal Kearney for teaching me how to suture. Thank you to Karen Ng for assistance with handling of the biomaterials during one particularly long day of surgery. Thank you to our lab manager Alix Weaver for assistance with all matters pertaining to the lab and also for helping with some of the H&E staining.

Thank you to Dr. Simona Socrate and Dr. Thibault Prevost at MIT for assistance with the mechanical testing.

Thank you to VA investigator Dr. Alice Alexander for assorted pieces of lab wisdom shared over the last few years, and for many interesting conversations. Thank you to VA investigator Dr. Kimberly Leite-Morris for assisting with the initial animal surgeries and for providing very helpful information about how to appropriately care for the animals. Thank you to Diane Ghera and the animal handlers in the animal research facility for contributing to the well-being of the rats throughout my studies.

Thank you to Dr. Daniel Lee and Dr. Paul Weinreb at Biogen Idec for generously providing the soluble Nogo receptor. Thank you to Dr. Fred Gage at the Salk Institute for providing our lab with the neural progenitors. Thank you to James Groer at Dragonfly Inc. for construction and assembly of the PBI apparatus.

To my family, this could not have been achieved without you. Your love and support were essential for making it through this challenging period. Dad, Mom, Maria, Laila – thank you so much.

Table of Contents

List of Figures

List of Tables

List of Equations

Chapter 1: Introduction and Background

1.1 General Introduction

Injuries and diseases of the central nervous system (CNS) are particularly devastating due to the lack of spontaneous tissue regeneration. Stroke, neurodegenerative disease, spinal cord injury, and traumatic brain injuries collectively present a major health care challenge for both the civilian and military populations. A more extensive understanding of the cellular and environmental regenerative limitations involved in CNS lesions will be necessary for the development of effective treatments. While considerable challenges remain, many elements of the physiological injury response in the CNS are now known. This improved body of knowledge has made clear that the complexity of CNS lesions is likely to require combinatorial therapies targeting several distinct components of the pathologies. In general, the factors preventing regeneration can be divided into intrinsic cellular limitations and extrinsic elements of the injury environments [1, 2]. Devising comprehensive methods to simultaneously and adequately address these factors will be a prerequisite for ultimately achieving more satisfactory clinical outcomes.

This work aims to investigate several therapeutic agents with potential utility in treatment of CNS lesions. The starting point for the proposed work is a collagen scaffold that can be implanted into a damaged brain. This biomaterial provides a foundation for subsequent studies of combinatorial therapies involving delivery of a therapeutic protein or a population of neural progenitor cells.

This chapter begins with an overview of some of the major obstacles that must be overcome in the process of developing CNS treatments. This is followed by descriptions of common CNS injuries and diseases, as well as a summary of various research tools used in CNS tissue engineering. The chapter concludes with an outline of the experiments included in this thesis.

1.2 Intrinsic Factors Limiting Regeneration

Intrinsic cellular limitations refer to the insufficient capacity of existing cells to proliferate, grow, and potentially replace damaged or dead cells [1]. A major obstacle lies in the fact that mature neurons do not proliferate, and therefore are unable to repopulate a region of the brain or spinal cord lost to disease or injury. Similarly, mature neurons that undergo damage have a greatly limited ability to extend axons relative to developing cells. One reason for this is the decreased expression of genes such as GAP-43 [3] that regulate the growth of axons and establishment of synapses. Further, various neuronal subtypes differ substantially in their intrinsic axonal growth capability and their response to exogenous environmental factors [4]. While the existence and multipotency of endogenous neural progenitors in the brain and spinal cord have been demonstrated, they appear to be insufficient for robust CNS repair in their native form and number.

1.3 Extrinsic Factors Limiting Regeneration

Although the axonal growth capacity of mature neurons is not as robust as during development, a significant degree of regeneration is theoretically still be possible. This

potential for regeneration is defeated largely by inhibitory factors in the CNS injury environment. It was demonstrated, for example, that neurons from the CNS can extend long distances through a peripheral nerve graft [5]. Identifying and targeting the inhibitory extrinsic elements in the CNS will be necessary for achieving regeneration.

1.3.1 Myelin Proteins

It was discovered early on that oligodendrocyte myelin is inhibitory for growing axons, causing acute growth cone collapse [6]. 3 particular myelin proteins were eventually identified and characterized as major axon growth inhibitors: Reticulon 4 (Nogo) [7], Oligodendrocyte Myelin Glycoprotein (OMgp) [8], and Myelin Associated Glycoprotein (MAG) [9]. Interestingly, it was found that they bind a common receptor, known as Nogo Receptor (NgR) [8, 10-12]. NgR is a 473 amino acid glycosylphosphatidylinositol-anchored (GPI-anchored) protein, which includes 8 leucine-rich-repeat domains that are involved in ligand-binding[13, 14]. Although NgR is a receptor for several signaling molecules, it lacks an intracellular domain and must rely on co-receptors such as P75 [15, 16], LINGO-1 [17], Gt1b, and TROY [18, 19] for intracellular signaling [20]. The intracellular signaling cascade following binding of the NgR complex leads to collapse of axonal growth cones by activation of cytoskeletal regulators such as rhoA GTPase and rho kinase (ROCK) [21, 22]. The NgR pathway has been the subject of much research over the last decade. While many promising results have been obtained, it has become clear that additional approaches will be necessary going forward. Recently, the paired immunoglobulin-like receptor B (PirB) in mice was also found to bind the 3 myelin proteins and act as an inhibitor of axonal regeneration

[23]. This discovery has helped to explain some confounding results previously obtained while studying NgR, particularly the result that NgR knockout mice show only moderately enhanced regeneration after CNS injury [24]. This and other work has demonstrated that blocking the effects of myelin proteins or their downstream targets will be an important part of a comprehensive treatment plan for certain CNS lesions.

Recent findings have suggested that the same myelin proteins involved in growth cone collapse may also have effects on neural progenitor cells (NPCs). The use of NPCs has been hindered in part by a lack of control over differentiation after implantation, with some results suggesting a tendency to either remain undifferentiated or to take on an astroglial phenotype. Similar effects were demonstrated *in vitro* when NPCs expressing NgR were exposed to Nogo or its active inhibitory fragment [25-27]. It is possible then that myelin proteins may play a role in limiting the efficacy of both implanted and endogenous NPCs after injury.

1.3.2 Glial Scar

Another major factor inhibiting axonal regeneration is the presence of a glial scar [28]. While scar tissue in peripheral organs such as skin and peripheral nerve is characterized by fibrous collagen deposition and wound contraction, scar in the CNS is markedly different. Following a CNS injury, resident astrocytes respond to environmental cues by proliferating and taking on a ramified phenotype known as an "activated" astrocyte. The astrocytes, along with microglia, migrate to the site of the injury and surround it with a cellular barrier [29]. Additionally, they deposit extracellular matrix molecules consisting of axon-inhibitory chondroitin sulfate proteoglycans [30].

Until recently, the precise mechanism by which CSPGs inhibit regeneration was unknown. While it had been suggested that the mechanism involved activation of protein kinase C and rho GTPase, evidence for binding to a particular receptor was lacking [31]. It was also observed that disrupting epidermal growth factor (EGFR) signaling blocked some of the inhibitory effects, EGFR was not found to directly bind CSPGs [31]. It was, however, recently discovered that a transmembrane protein tyrosine phophatase (PTPσ) is a receptor for CSPGs, and that disruption of PTPσ after spinal cord injury resulted in enhanced regeneration [32]. As this area of research continues, it is likely that novel therapies will be available to better target the inhibitory nature of the glial scar.

To date, many therapeutic approaches have focused on disrupting either the formation of the glial scar, or the scar itself after the acute injury response has subsided. Approaches of interest include blocking elements of the inflammatory cascade [28], using biomaterials to prevent formation of the cellular barrier [33], and enzymatic degradation of the inhibitory extracellular matrix (ECM) molecules using chondroitinase [31, 34]. While eliminating elements of the glial scar will likely be necessary in developing treatment options, it has been suggested that the timing of such action is of critical importance. Studies have demonstrated positive effects of the reactive astrocytes in early stages following an acute insult [35, 36], and thus it may be essential to allow initial scar formation without inhibition to avoid further injury.

1.3.3 Inhibitory Axon Guidance Molecules

In addition to the myelin proteins that act through NgR, there exist other molecules that can exert inhibitory actions on neurons. While axon guidance molecules

play a crucial role in proper development of the CNS, a subset of them that possess axon-repulsive characteristics are prevalent in lesion sites and act to inhibit regeneration. Netrin-1, for example, continues to be expressed by mature neurons, oligodendrocytes, and Schwann cells. Molecules such as Semaphorins, ephrins and various slits have also been found in the glial scar and CNS myelin. Repulsive guidance molecule A (RGMa) is expressed in the adult spinal cord and appears to play a role in preventing recovery after injury. Neutralizing axon guidance molecules may prove to be an important component of future therapies [37].

1.3.4 Lack of Neurotrophic Factors

Aside from active inhibitors, it may also be that the lesion environment is lacking the trophic factors necessary for neuronal survival and axonal outgrowth. A variety of molecules have been identified and characterized for their ability to promote neuronal survival and growth.

The neurotrophins make up one such class of molecules consisting of nerve growth factor (NGF), brain-derived neurotrophic factor (BDNF), neurotrophin 3 (NT-3), and neurotrophin 4/5 (NT-4/5). Neurotrophins have a major role in promoting neuronal survival, but also act to regulate axon growth, synapse formation, dendrite formation, cell migration, and proliferation. Neurotrophins are known to act through specific tyrosine kinase receptors, with NGF binding to tyrosine kinase receptor A (TrkA), BDNF and NT-4/5 binding to TrkB, and NT-3 to TrkC. Additionally, all neurotrophins can bind to the receptor $p75^{NTR}$, though with lower affinity. The response to individual neurotrophins does, however, vary substantially between neuronal subtypes [38].

Glial cell line-derived neurotrophic factor (GDNF), along with the molecules neurturin, artemin, and persephin compose a distinct group of neurotrophic factors. GDNF acts through a receptor complex involving GNDF family receptor and rearranged during transfection (RET) Trk, with subsequent effects of promoting neuronal survival and axonal regeneration. GDNF has demonstrated particular benefit for survival of motoneurons and dopaminergic neurons, making it a therapeutic candidate for amyotrophic lateral scleroris and Parkinson's disease [38].

Members of the fibroblast growth factor (FGF) family have also been shown to enhance neuronal survival and neurite outgrowth. FGFs can have several distinct effects, such as maintaining calcium homeostasis, regulating enzymes involved in neutralizing reactive oxygen species, and stimulating anti-apoptotic pathways. Further, the FGF-2 (also known as basic FGF) is a mitogen that appears to be important in preventing differentiation of neural (and other) progenitors and maintaining their multipotency [38].

Ciliary neurotrophic factor (CNTF) is another molecule with demonstrated neuroprotective effects [38].

1.4 Injuries to the Central Nervous System

1.4.1 Traumatic Brain Injury: Non-penetrating

Traumatic brain injury (TBI) presents a significant cause of morbidity and mortality in military conflicts and also in the civilian sector. Roadside bombs and improvised explosive devices in Iraq and Afghanistan have made TBI an increasingly

common problem, with few good treatment options. The severity of TBI can range from mild injuries imperceptible by standard imaging modalities, to penetrating injuries causing extensive hemorrhage and loss of brain tissue. From an interventional standpoint, closed head injuries present a difficulty in administering treatment. While considerable work remains in understanding the pathophysiology of such injuries, there is a challenge in determining whether a potential therapy should be administered directly via surgery, or peripherally. Peripheral administration requires that the agent can cross the blood-brain barrier, a topic of considerable pharmacological research. Surgery, on the other hand, presents obvious risks and complications that may outweigh the potential benefit of the therapy.

1.4.2 Traumatic Brain Injury: Penetrating

Penetrating brain injury may be more amenable to therapy administered surgically, due to the fact that surgical intervention is often acutely necessary after the injury. While PBI has unique characteristics not found in closed head injuries, there are similarities particularly in the secondary injury response that may be applicable to other TBI scenarios, as well as ischemic or hemorrhagic insults. By studying potential implantable therapeutics in a model of PBI, one can begin to assess whether such options would be of sufficient benefit to warrant surgical intervention in other CNS lesions.

When relatively high velocity objects enter the brain in a PBI, they create a complex wound resulting largely from radial dissipation of the projectile's kinetic energy. Tissue surrounding the projectile track is rapidly compressed, leading to the formation of a temporary cavity larger than the actual projectile. The projectile injury track is thus

surrounded by a significantly larger amount of injured tissue as a result of the temporary cavity [39]. While the tissue associated with the permanent injury track of the projectile has generally been destroyed, the surrounding peri-lesional area may potentially be salvageable if an appropriate therapy were applied soon enough [40].

The initial mechanical insult of a penetrating brain injury causes disruption of membranes associated with blood vessels, cell bodies, and axons. A large degree of hemorrhage rapidly ensues and intracellular contents of damaged neurons and glial cells are released. The loss of blood supply associated with damaged vessels causes metabolic and ischemic stress to areas of surrounding tissue, while the release of intracellular contents produces an extracellular ionic imbalance (Ca^{2+}, Na^{+}, K^{+}), contributing to diffuse axonal injury. Breakdown of axons leads to release of myelin components that act to inhibit potential regeneration [41].

Release of cytokines, as well as breakdown of the blood-brain-barrier, causes a large inflammatory response consisting of both resident microglia and peripheral leukocytes. Reactive astrocytes proliferate and surround the injury site, creating a glial scar both with their cell bodies and production of axon-inhibitory extracellular matrix (ECM) molecules. With time, a delayed degeneration of axons and neuronal cell bodies remote from the lesion occurs, possibly as a result of lost synaptic targets and retrograde degeneration from sites of axonal injury. It is also thought that myelin proteins may play a role in remote degeneration in the thalamus. Electrophysiological abnormalities ensue and functional deficits become apparent depending on the location and extent of injury. At the injury site, debris and dead cells are eventually cleared and a permanent cavity

remains [42, 43]. Bone and metal fragments remaining in the brain pose a serious risk for infection and seizure.

It has also been suggested that the pressure wave during PBI damages axons that connect to brainstem respiratory centers, leading in some cases to apnea and subsequent death [44].

Treatment options are limited in PBI. Surgical intervention typically involves debridement of necrotic tissue and removal of accessible bone and metal fragments [45]. In many cases, risk of damaging functional brain tissue precludes the removal of all fragments. In these cases, there exists no broad consensus on how aggressively to pursue the removal of embedded fragments [46]. However, recent advances in image-guided surgery present possibilities for improved removal techniques to safely eliminate as much foreign matter as possible from the brain [47]. With better imaging, the surgeons can choose less destructive paths for accessing fragments and potentially minimize damage to viable tissue.

Given the temporal limitations in getting patients, particularly in military settings, to surgery, it is a major challenge to devise an appropriate treatment for the acute injury phase. Although significantly mitigating the primary injury process may not be currently feasible, there may be a great deal that can be done to limit secondary tissue damage. While it has been shown that degeneration of both white and gray matter persists long after traumatic brain injury [48], there are currently no effective pharmacological agents or surgical therapies to significantly disrupt this process. Implantation of a biomaterial or other drug-delivery agent during the time of surgery may allow damaged or ischemic

neural cells to survive. Further, promoting axonal regeneration may prevent the loss of additional neurons by allowing the reestablishment of synapses disrupted by the lesion.

1.4.3 Ischemic Stroke

Ischemic stroke is caused by an interruption of blood supply to the brain, often as a result of thrombosis or embolism. Death of neurons occurs rapidly in the absence of oxygen, leading to permanent neurological damage depending on the duration before reperfusion can be established. While a particularly region of the brain may be damaged beyond repair, there is often a region of ischemic tissue referred to as a penumbra that may be viable with appropriate intervention. For this reason, it is imperative that treatment is sought as soon as possible after recognition of the event. The penumbra and areas more remote from the region are susceptible to further injury and neuronal degeneration [49]. Neuroprotective agents that may improve the amount of spared tissue and decrease remote degeneration are thus a topic of intense research. The complexity of this goal is emphasized by the fact that numerous clinical trials to date have not shown benefits for neuroprotective drugs [50].

The design and application of such therapies depends on knowledge of how ischemia leads to neuronal cell death and degeneration. The ischemic cascade begins with reduction of ATP production due to loss of the oxygen supply. Without adequate energy supplies, ATP-dependent ion pumps fail, disrupting the regular ionic balance and cell potential. Influx of calcium leads to release of glutamate, which excites other cells and results in an even greater calcium influx and eventually more glutamate release. The result of this uncontrolled positive feedback is excitotoxic damage from production of

calcium dependent enzymes. Breakdown of the cell membrane leads to influx of extracellular ions and molecules, and also to release of intracellular contents that further alter the extracellular environment [51].

Application of a biomaterial supplemented with neuroprotective agents and perhaps neural progenitor cells may have the potential to reduce secondary injury and promote regeneration.

1.4.4 Hemorrhagic Stroke

Many of the pathophysiological effects are similar in ischemic and hemorrhagic stroke, but hemorrhagic events tend to be significantly more severe. In addition to the potential for dangerous rises in intracranial pressure due to hematomas, hemoglobin in the blood is cytotoxic and may cause increased neuronal death [52]. Delivery of neuroprotective therapeutics and agents to neutralize hemoglobin toxicity may help clinical outcome.

1.4.5 Spinal Cord Injury

Spinal cord injuries affect several million people worldwide, with a wide range of severities including debilitating conditions like quadriplegia and diaphragm paralysis. Such injuries can result from contusion, compression, and partial or complete severing of the cord [53]. Pathophysiological events include the death of neuronal cell bodies at the injury site, remote degeneration of neurons whose axons have been severed, myelin breakdown, severe inflammation, and formation of a glial scar [54]. As with injuries to

the brain, combinatorial therapies involving biomaterials, cells, growth factors, and antagonists to inhibitory molecules offer significant promise for restoring function.

1.5 Neurodegenerative Diseases

1.5.1 Parkinson's

Parkinson's disease is characterized by loss of dopaminergic neurons of the substantia nigra region of the basal ganglia. These neurons play a direct role in regulation of the striatum as part of the direct and indirect basal ganglia pathways. These pathways contribute to control of cortical excitation through the thalamus, modulating voluntary movement. Pharmacological therapy currently involves administration of L-Dopa, a dopamine precursor that can cross the blood-brain barrier before being metabolized to dopamine. While this helps to control symptoms, it does not stop the progressive loss of the dopaminergic neurons. Alternative therapies are aimed at alterations of the basal ganglia pathways by surgical lesions or an implantable deep brain stimulation device. Cell replacement is a promising therapeutic approach for Parkinson's, as significant progress has been made in directing stem/progenitor cells to differentiate into dopaminergic neurons [55]. Developing a viable dopaminergic cell-scaffold construct for implantation into the substantia nigra could be a potentially beneficial therapeutic strategy.

1.5.2 Alzheimer's

Alzheimer's disease is a common form of dementia that is characterized by the loss of cortical neurons and degeneration in various other brain regions. In addition to marked cortical atrophy, histological analysis of Alzheimer's brains shows accumulation of amyloid plaques and neurofibrillary tangles. Plaques consist of beta amyloid peptides that improperly accumulate due to abnormal folding. Research into the processing and function of amyloid precursor protein (APP) will aid in the understanding of how amyloid plaques form. Therapeutic approaches are aimed at reducing beta amyloid accumulation, though a long-term goal may also be to regenerate lost cortical neurons. Interestingly, it has been found that APP associates physically with the Nogo receptor [56].

1.5.3 Huntington's

Huntington's disease is an autosomal dominant genetic neurological disease that results in an abnormal movement disorder (chorea) and decline in cognitive ability. The disease is caused by a mutation of the Huntingtin gene such that it contains an abnormally large number of trinucleotide repeats [57]. The resulting mutant protein accelerates degeneration of certain subpopulations of neurons in the striatum, frontal cortex, and temporal cortex. Astrogliosis is apparently also increased. While gene therapy may present the best hope for a comprehensive cure, neuroprotection or regeneration of some affected neuronal populations may be a more feasible goal in the shorter term.

1.5.4 Amyotrophic Lateral Sclerosis (ALS)

ALS, also called Lou Gehrig's disease, is characterized by the progressive degeneration of cortical motoneurons. Early symptoms consist of muscle weakness or speech difficulties, but progress eventually to major problems with limb movement and severe muscle atrophy. While the cause is unknown in most cases, a small subset of patients have a genetic form of the disease correlated with a mutation in the superoxide dismutase (SOD1) gene [58]. Potential therapies are aimed at preventing motoneuron degeneration by controlling glutamate release and associated possible excitotoxic effects. Novel neuroprotective agents combined with cell replacement therapy may present effective future strategies.

1.5.5 Multiple Sclerosis

Multiple scleroris (MS) is an autoimmune disease that results in demyelinatin of white matter in the CNS. Demylinated axons have poor conduction capabilities, and as a result virtually any neurological symptom may be present. While some degree of remyelination takes place, particularly in early stages of the diseases, the disease affects oligodendrocytes to a degree that they cannot adequately keep up with the loss of myelin. Therapeutic approaches have included the use of anti-inflammatory medications and immunosuppressants. Cell therapy to promote remyelination is an area of significant research for developing a potential future treatment [59].

1.5.6 Frontotemporal Dementia (FTD)

FTD is a dementia characterized by degeneration of neurons in the frontal and sometimes temporal lobe of the brain [60]. Symptoms of the disease can include lethargy and apathy, or alternatively disinhibition resulting in inappropriate social behavior. While there is no known common cause, some cases appear to be genetic. Therapeutic options are currently extremely limited. Neuroprotective agents or cell replacement may in the future be able to prevent progression of the disease if applied in the early stages.

1.6 Central Nervous System Tissue Engineering

Regeneration of the Central Nervous System is extraordinarily difficult relative to other tissues due its enormous complexity and the abundance of inhibitory factors. Given the variation between regions of the brain and the spinal cord, there is unlikely to be a single therapeutic approach for all problems. To replace a neuronal population with cells of the same subtype and guide them to reestablish connections similar to those lost would be a monumental feat.

1.6.1 Goals in the Field

CNS tissue engineering strategies currently are not necessarily aimed at trying to produce tissue indistinguishable from that which was initially lost, though this remains a long-term goal. At the present time, one can broadly categorize the desired outcomes as cellular replacement, axonal regeneration, and collateral sprouting.

Cellular replacement in some cases is aimed at replacing a particular population of lost neurons or glial cells, depending on the injury or disease. An example would be

potential therapy for Parkinson's disease. The affected neuronal subtype is known, and theoretically it would be appropriate to simply replace the lost dopaminergic neurons with new ones that will survive, make appropriate synapses, and carry out the desired function. While this approach does not claim to be addressing the underlying cause of the pathology, the goal of restoring function may still be possible. If the clinical outcome is as desired, it becomes less important that the histological appearance of the implantation site be exactly as in a healthy brain. Increases or decreases in cell density, proportion of neurons relative to glia, pattern of vascularity, and volume proportion of extracellular matrix may deviate significantly from normal yet still result in an acceptable outcome.

Cell replacement may also be applied in scenarios where a mixed population of cells is lost, such as in a penetrating brain injury. The challenge in this case is greater, as cells with varying and potentially unknown functions are likely lost. The use of stem/progenitor cells in this case offers the promise of restoring lost function if the cells can be induced to replace those which were lost. This represents a major challenge in the field at this time. It has been demonstrated that exogenous cells can survive and integrate when implanted into the brain, but it is difficult to assess exactly how they are functioning and what they are doing to improve outcome.

Promoting axonal regeneration is a more straight forward task, but remains a challenge. In this approach, one aims to neutralize the inhibitory factors in the lesion environment and/or enhance the growth state of neurons whose axons have been damaged. In doing so, neurons may regain some degree of functionality as they

reestablish synapses ideally in the region near the lesion. This may prevent or limit remote neuronal degeneration that has been noted in traumatic brain injuries and strokes.

Induction of collateral sprouting aims to promote structural plasticity of regions that have been spared from the lesion. Rather than replacing cell bodies, it is instead desired to compensate for those lost with the existing neurons. Similar to axonal regeneration, blocking inhibitory factors and stimulating the growth capacity of neurons are promising strategies.

1.6.2 Research Tools and Methods: Biomaterials

Central to the field of regenerative medicine is the use of matrices or scaffolds to promote tissue growth. Such scaffolds can generally serve as ECM analogs for cell attachment, migration, and contraction blocking, as well as delivery vehicles for therapeutics such as cells, nucleic acids, proteins, and anti-inflammatory drugs. Modes of incorporation for therapeutics can range from simple soaking like a sponge, to use of engineered nanoparticles, to covalent bonds formed by cross-linking chemistry. Many materials, both natural and synthetic, have been used for CNS tissue engineering [61].

Synthetic materials provide a great deal of control over the scaffold composition, degradation rate, and mechanical behavior. Poly (ethylene glycol), Poly (ethylene-co-vinylacetate), Poly (glycolic acid), Poly (lactic acid), Poly (lactic-co-glycolic acid), poly (2-hydroxyethyl methacrylate), poly (2-hydroxyethyl methacrylate-co-methyl methacrylate), and Polypyrrole are among the common synthetic materials used. These materials have widely varying properties with respect to protein adsorption, cell adhesion, degradability, degradation rate, mechanical stiffness, pH, and conductivity.

Natural materials are less easily modified, but have advantages such as containing sites for cell adhesion and potentially mimicking native extracellular matrix in composition and material properties. Common materials include agarose, chitosan, methylcellulose, nitrocellulose, collagen, dextran, fibrin, fibronectin, laminin, and hyaluronic acid.

1.6.3 Research Tools and Methods: Neural Stem/Progenitor Cells

While embryonic stem cells still represent exciting and profound possibilities for regenerative medicine, the discovery of neural stem/progenitor cells in the adult brain has spurred a tremendous amount of research. Adult neurogenesis has been confirmed to occur in two regions of the brain: the subventricular zone (SVZ) and the subgranular zone (SGZ) of the dentate gyrus (in the hippocampus). Cells from the SVZ travel along the rostral migratory stream to the olfactory bulb where they become granule neurons and periglomerular neurons. Cells from the SGZ migrate into the granule layer of the dentate gyrus, becoming granule neurons. Both cell types can be harvested and expanded in culture containing FGF-2. Culturing can be done either in monolayer or as neurospheres, with monolayer culture typically requiring coating the culture flasks with laminin to promote adhesion. SVZ and SGZ progenitors have been used in various applications and shown to differentiate into various cell types. It appears that while they are indeed multipotent progenitors that can become neurons, astrocytes, and oligodendrocytes, they may not be able to differentiate into all neuronal subtypes. Additionally, their differentiation has been shown to be highly regulated by the specific environment into which they are implanted. For example, when SGZ cells were implanted into the

neonatal retina, they expressed neuronal and astrocytic markers while taking on morphologies of Muller, amacrine, bipolar, horizontal, and photoreceptor cells. In the healthy adult retina, however, the cells did not attain morphologies of normal retinal cells [62].

Although neurogenesis appears to only occur in the SVZ and SGZ, neural progenitors have been found elsewhere in the cortex, substantia nigra, and spinal cord. Stimulating these existing progenitors to proliferate and differentiate in large numbers is an active area of research.

1.6.4 Research Tools and Methods: Neurotrophic Factors

Neurotrophic factors, such as NGF, BDNF, NT-3, and GDNF have been used to promote neuronal survival, neurite outgrowth, and axonal regeneration. While the number of studies is extensive, an important emphasis on neurotrophic factor synergy has developed. For example, it has been shown that combinatorial therapy with FGF-2, NT-3, and BDNF improved the degree of retinal ganglion cell regeneration by an amount larger than the sum of each individually [63]. Similarly, the combination of NT-3 and BDNF proves more effective than each individually in nerve growth after spinal cord injury [64].

While not specifically categorized as a growth factor, the purine nucleoside inosine has been shown to promote axonal regeneration activating the protein kinase Mst3b, a key component of the cell-signaling pathway through which trophic factors regulate axon growth [65-67]. Combining inosine with various growth factors and antagonists to inhibitors may improve the prospects for regeneration even further.

1.6.5 Research Tools and Methods: Antagonists to Nerve Growth Inhibitors

A variety of effective strategies have been devised for blocking the effects of inhibitory molecules in the CNS lesion environment. A multitude of experimental approaches for blocking the myelin proteins are currently in use. Among them are antibodies against the Nogo, MAG, and OMgp, antibodies against the Nogo Receptor, a soluble Nogo receptor fusion protein to intercept myelin proteins before reaching the cell surface, phospholipase C to release NgR from neuronal membranes, gene knockout, siRNA gene knockdown, rho/ROCK inhibitors, and others. Many of these approaches will likely work equally well in blocking effects of myelin proteins that also act through the PirB receptor [68].

The glial scar has also been targeted with the chondroitinase ABC enzyme that cleaves inhibitory chondroitin sulfate proteoglycans in the lesion environment [31].

1.7 Outline of this Research

This research will investigate the use of a collagen scaffold alone, or in combination with neural progenitors or a soluble Nogo receptor for improving histological outcome after penetrating brain injury. Type I collagen has been chosen for this work based on its utility in peripheral nerve studies and its ability to be modified in terms of composition (e.g. addition of glycosaminoglycans), architecture (e.g. pore size),

biocompatibility in other tissues, and cross-linking. Additionally, collagen does not appear to have axon inhibitory properties like the native brain ECM consisting of proteoglycans and glycosaminoglycans. The neural progenitors to be used have been provided by Professor Fred Gage of the Salk Institute, and were harvested from the hippocampi of adult rats. The use of adult cells eliminates the ethical concerns associated with embryonic stem cells, and as already described, these cells can differentiate into neurons, oligodendrocytes, and astrocytes. The soluble Nogo receptor has been selected based on its ability to block Nogo, MAG, and OMgp to prevent them reaching endogenous NgR or PirB receptor. This allows one to effectively block all 3 proteins and both receptors with a single molecule, whereas antibodies would have to be targeted to each individually.

The first part of this thesis will describe mechanical testing of collagen scaffolds of varying collagen concentration. Through indentation testing and viscoelastic modeling, the scaffold properties are compared to those of the *in situ* rat brain. A collagen scaffold with properties reasonably similar to those of the rat brain is then chosen for *in vivo* studies.

The second part of the thesis involves the characterization of a bilateral PBI lesion in rats at 1 week at 5 week time points through histological, histomorphometric, and immunohistochemical methods. Additionally, the implantation of collagen scaffolds is evaluated for safety of the material *in vivo* and potential to fill the defect and interact with surrounding tissue.

The third part of the thesis employs a larger biomaterial scaffold to attempt to fully fill the PBI defect. The implantation of a collagen scaffold loaded with soluble

Nogo receptor (sNgR) is studied at 4 week and 8 week post-implantation time points and compared with the scaffold alone.

The final part of the thesis investigates the implantation of a collagen scaffold seeded with adult hippocampal progenitor cells. The survival of the cells is evaluated, along with their potential for differentiation into neurons, astrocytes, oligodendrocytes, endothelial cells, and macrophages.

Chapter 2: Viscoelastic Characterization of Rat Cerebral Cortex and Type I Collagen Scaffolds for Central Nervous System Tissue Engineering

2.1 Introduction

Mechanical testing of brain tissue has become an increasingly important topic in a variety of fields. With the elevated incidence of traumatic brain injury (TBI) over the last decade in the military conflicts in Iraq and Afghanistan, there has been an increased focus on studying the brain's response to blasts, blunt trauma, and penetrating projectiles. In these injuries, the mechanics of both the initial physical insult and secondary responses such as rises in intracranial pressure due to hemorrhage and swelling are of interest [40, 69, 70]. For both experimental and computational modeling approaches [69], basic data on the brain's bulk mechanical properties contribute to a more thorough understanding of the brain injuries under study . Macromechanical modeling complements the ongoing research into cellular mechanics of TBI-associated processes such as diffuse axonal injury [71].

Brain mechanics are also highly relevant in neurosurgery for understanding of pathological conditions [72, 73], as well as for modern procedures [73] and training techniques [74]. The mass effect of a growing tumor has highly negative implications for patient outcome due to compression of surrounding brain tissue with the potential for herniation [75]. To accurately simulate the growth of a tumor and its subsequent mechanical effects on the brain could be of clinical utility in estimating the risk of herniation or other adverse outcomes. Such information could potentially help physicians in determining the appropriate timing and course of action for individual patients.[76]. Similarly, the surgical management of patients with brain hemorrhage or edema (e.g.

after TBI) may be aided by additional knowledge of how the brain responds to increases in volume and pressure within the skull [70].

Modeling of brain mechanics has an integral role in newer technologies for neurosurgical training. While the opportunities for training in neurosurgical procedures are obviously limited by various constraints of clinical and educational institutions, simulated or "virtual" surgery has the potential to offer meaningful complimentary training [74, 77]. With appropriate modeling of the brain mechanics, the simulated surgery is intended to recreate with accuracy how the brain feels and responds to surgical manipulations [78].

In the area of CNS regenerative medicine, there is emerging evidence that neural cells may sense and respond to the mechanical stiffness of substrates they come in contact with. Several results indicate that neurons prefer a soft substrate with stiffness comparable to that of brain tissue, while astrocytes prefer stiffer surfaces. Using agarose hydrogels, it was demonstrated that dorsal root ganglion neurons show an increasing rate of neurite extension with decreasing matrix stiffness [79]. Similarly, neurons from the mouse spinal cord show increased neurite branching on polyacrylamide gels as their compliance increases [80]. In a mixed coculture of neurons and astrocytes on fibrin scaffolds, it was found that scaffolds with stiffness similar to brain selected for neurons over glia [81]. Both mesenchymal and neural progenitor cells have also displayed a tendency to differentiate into neurons on compliant substrates [82, 83].

For the design of biomaterials intended for implantation into a CNS lesion, it may then be beneficial to characterize the mechanical properties of the material and understand how they relate to properties of the brain. While it is not supposed at this

point that a material should need to have properties identical to the brain to be effective, one may nonetheless aim to create a biomaterial that approximately reproduces certain aspects of the mechanical behavior. To demonstrate the characterization of such a material and comparison with the brain, type I collagen scaffolds fabricated with varying collagen concentrations are examined in this work. Similar scaffolds have been used in a number of regenerative medicine applications involving skin [84], conjunctiva [85], peripheral nerve [86], and spinal cord injury [87].

2.1.1 Indentation Testing

Standard compression, tension, or shear testing of very soft tissues can be challenging due to the difficulty of preparing the specimens without damage and ensuring that assumptions regarding friction and uniformity of the contact area are justified [88]. To test the cerebral cortex in one of these modalities requires removal of the brain from the skull and a careful dissection to separate cortical tissue from deeper brain structures without damaging the tissue. A convenient alternative is to use indentation testing, which precludes the necessity of removing the brain from the skull and requires no physical attachment of the tissue specimen to the testing device. Indentation solutions for viscoelastic materials have also been recently developed [89, 90].

While creep testing may be more similar to some physiological scenarios in which the brain or a biomaterial is under a nearly constant force, load control at very small forces can be difficult to implement. The stress-relaxation testing conducted in this work provides an alternative approach to investigate viscoelastic phenomena, but with the relative ease of controlling displacement rather than force.

Indentation testing combined with linear viscoelastic modeling has not to our knowledge been previously conducted for the collagen biomaterials used in this work. While data on brain mechanical properties exists in the literature, it has been commented that many studies show large discrepancies in results [91]. Further, there are relatively few studies reporting specifically on properties of the rat brain. The rat is of particular interest because of its prevalence in studies relating to a variety of brain injuries and diseases. The data and methodology in this study may have utility for some of the applications already mentioned, but will also add an independent verification of the only published study on indentation of the rat brain [92]. This work adds the application of a five-element Maxwell viscoelastic model to the brain indentation data. The model is developed by expanding the published solution for spherical-tip indentation of a viscoelastic material characterized by three linear elements in a standard viscoelastic material configuration [89]. The three-element model is found in this work to be insufficient for modeling the brain and scaffold relaxation responses, prompting the use of the five-element model. The approach described provides a convenient method for indentation testing and linear viscoelastic modeling of soft tissues and biomaterials. While a linear model is generally not sufficient to describe the full range of behavior of such materials [91], it is potentially useful over a limited range of strains and strain rates [91, 93] and may aid in making simple comparisons between materials.

2.2 Experimental Methods

2.2.1 Rat Brain Preparation

Five adult female Lewis rats, whose primary use was for non-neurologic experiments, were sacrificed by carbon dioxide asphyxiation. The top of the skull was removed and the dura was resected to expose the frontal and parietal lobes. Tissue was kept moist with phosphate buffered saline throughout the dissection and testing procedure. All testing was completed well within the six hour time window before the expected onset of significant tissue degradation [94, 95]. Each brain was tested at four locations in the cortex (right and left frontal and parietal lobes), based on previous data showing the cortex can reasonably be considered as homogeneous [91, 95]. For each analysis parameter, an ANOVA was conducted to confirm that there was no effect of indentation location before the separate measurements on the same brain were pooled [95].

2.2.2 Collagen Scaffold Fabrication

Type I collagen scaffolds (0.5%, 0.75%, 1.0%, 1.5% weight:volume) were fabricated from porcine microfibrillar collagen (Geistlich Biomaterials, Wolhusen, Switzerland). A suspension of the collagen was first made in 0.001 N HCl, brought to pH 3, and mixed with a stir bar for 20 minutes. The slurry was blended at 15,000 RPM (Ultra Turrax T18 blender, IKA, Staufen, Germany) for 30 minutes at 4° C, brought again to pH 3, and blended for an additional 2 hours. The slurry was then centrifuged for 10 minutes at 5500 RPM to remove air bubbles, and mixed with a pipette to ensure homogeneity. The slurry was poured in a metal mold and placed into an AdVantage Benchtop Freeze Dryer (VirTis, Gardiner, NY). The temperature was decreased at a controlled rate to -20° C over 180 minutes and held at -20° C for 60 minutes.

Sublimation was conducted at a temperature of 0° C and pressure of 200 mTorr for 1020 minutes. Scaffolds were then dehydrothermally cross-linked overnight at 105° C under vacuum. Additional chemical cross-linking was conducted using the water soluble agent 1-ethyl-3-(3-dimethylaminopropryl)carbodiimide hydrochloride (EDC) (Sigma-Aldrich Inc, St. Louis, MO) with addition of N-hydroxysuccinimide (NHS) to increase the reaction rate [96]. EDC cross-linking involves activation of carboxylic acid groups that react with free amine groups in lysine residues to form amide bonds. Scaffolds were hydrated with water prior to crosslinking for 2 hours with an EDC to NHS ratio of 5:2. Six scaffolds of each collagen concentration underwent indentation testing.

2.2.3 Mechanical Testing

Mechanical tests were performed on a Zwick/Roell Mechanical Tester (Model NO. Z2.5/TN1S, Zwick GmbH & Co) with a Zwick load cell (Part No. BTC-LC0020N.P01). Scaffolds and brain specimens were indented with a 1 mm radius hemispherical polyoxymethylene indenter to a depth of 0.5 mm at a displacement rate of 0.1 mm/sec, and held at constant displacement for 5 minutes to allow for relaxation. Stress relaxation data was collected at a sampling rate of 10 Hz.

2.2.4 Signal Processing

Data processing was done using Matlab Version 7.6 (The MathWorks Inc., Natick, MA). The Matlab signal processing tool was used to perform low-pass filtering on brain and scaffold data before application of the five element viscoelastic model using the Matlab curve fitting tool.

2.2.5 Statistics

The StatView statistical package (version 5.0.01, SAS Institute Inc., Cary, NC) was used for all statistical tests. Values are reported as mean ± standard error. One-factor analysis of variance (ANOVA) was used to evaluate significance for the effect of collagen concentration on mechanical properties of the collagen biomaterials. Post hoc comparisons between scaffold groups were made using Fisher's protected least squares differences. Unpaired t-tests were used to compare differences between brain properties and those of the various scaffold groups. A p-value of 0.05 was used to establish statistical significance.

2.3 Analytical Methods

2.3.1 Linear Elastic and Viscoelastic Modeling for Indentation of Rat Brain and Collagen Biomaterials

To make an idealized characterization of the materials based on an elastic modulus, one can employ the solution for indentation of an elastic half-space with a rigid hemispherical indenter [92, 95, 97]. The load P is given as a function of the indentation depth δ, the indenter radius R, the Poisson's ratio ν, and the shear modulus G. For an incompressible material (Poisson's ratio of 0.5), the shear modulus G for this loading scenario is given in Equation 1. One can use Equation 1 to calculate idealized short term and long term shear moduli from a stress-relaxation curve by evaluating the peak force at the end of the loading phase and the approximately asymptotic load at the end of the relaxation period [92, 95].

$$G = \frac{3P}{16\delta\sqrt{R}\delta^{3/2}}$$

Equation 1: Spherical-tip indentation solution for the shear modulus of an incompressible linearly elastic material

To proceed with a viscoelastic characterization, one can apply the correspondence principle [90]. The correspondence principle makes use of the fact that Laplace transformed viscoelastic governing equations are of the same form as the elastic governing equations. If the elastic solution is known, the transform of the viscoelastic solution is obtained by substitution of time dependent (s-dependent) material properties for the time independent parameters in the elastic equations. This procedure has been demonstrated for both flat punch and spherical-tip indentation of viscoelastic materials [89, 90]. In both cases, the viscoelastic material was modeled with three elements, namely a spring in series with a parallel arrangement of a spring and dashpot. The spherical-tip viscoelastic indentation solution for the three-element model is given in Equation 2.

$$P(t) = \left(\frac{16}{9}\sqrt{\delta^3 R}\right)E_1\left(\left(\frac{E_1}{E_1+E_2}\right)e^{-\frac{(E_1+E_2)t}{3\eta}} + \left(\frac{E_2}{E_1+E_2}\right)\right)$$

Equation 2: Spherical-tip indentation solution of a viscoelastic material modeled with three linear elements

It was attempted to use the above equations to fit the relaxation profiles of the brain and scaffold data, with the understanding that a more complex model might be necessary.

While staying within the realm of linear viscoelasticity, a slightly more complex model involving five elements was used to fit the data. The five-element model (Figure

1) is an example of a generalized Maxwell model, which may contain an arbitrary number of parallel spring-dashpot elements.

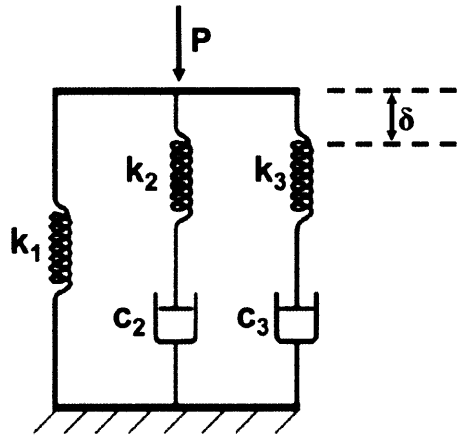

Figure 2.1. Five-element viscoelastic model under load P and displacement δ.

To extend the use of the correspondence principle from the three-element model that Cheng et al. employed [89] to the five-element model, one may begin by deriving the governing differential equation for the system in Figure 1 under load P and displacement δ. After writing equilibrium and geometric compatibility equations, Laplace transforms are taken with a step displacement of magnitude δ_0 substituted for the general displacement δ. The resulting relationship between the transformed load $\hat{P}$ and transformed displacement $\hat{\delta} = \frac{\delta_0}{s}$ is given in Equation 3.

$$\hat{P} = \frac{k_1\delta_0}{s} + \frac{k_2 c_2 \delta_0}{k_2 + c_2 s} + \frac{k_3 c_3 \delta_0}{k_3 + c_3 s} = \left(\frac{k_1}{s} + \frac{k_2}{s + \frac{k_2}{c_2}} + \frac{k_3}{s + \frac{k_3}{c_3}} \right) \delta_0$$

Equation 3: Laplace transformed relationship between load P and step displacement δ_0.

To go from the load and displacement relationship to one between stress and strain, it is first necessary to separate deviatoric from volumetric stress and strain. One can then

write a completely analogous relationship between deviatoric stress and strain [89, 90] in which the spring constants are replaced by shear moduli G_1, G_2, G_3, and the dashpot constants replaced by viscosities η_2, η_3. The transformed relationship is given in Equation 4, where $\hat{\sigma}'_{ij}$ is the transformed deviatoric stress and $\hat{e}'_{ij}$ is the transformed deviatoric strain.

$$\hat{\sigma}'_{ij} = \left(G_1 + \frac{G_2 s}{s + \frac{G_2}{\eta_2}} + \frac{G_3 s}{s + \frac{G_3}{\eta_3}} \right) \hat{e}'_{ij}$$

Equation 4: Laplace transformed relationship between deviatoric stress and strain for a viscoelastic material modeled with five linear elements.

For an elastic material, deviatoric stresses and strains are related by twice the shear modulus. As a result, in the indentation solutions for elastic materials, the correspondence is made with the viscoelastic material by replacing 2G with the time dependent (s-dependent) term in parentheses in Equation 4. Taking the inverse Laplace transform produces the solution in the time domain. For the elastic hemispherical indentation solution in Equation 1, substituting for 2G, solving for P, and taking the inverse Laplace transform with a step displacement input results in Equation 5a. The solution for flat punch indentation is found by the same method and is given in Equation 5b. Note that the values η_2/G_2 and η_3/G_3 are the time constants for the two exponentials in each equation.

$$P(t) = \frac{8}{3}\left(G_1 + G_2 e^{-\frac{G_2}{\eta_2}t} + G_3 e^{-\frac{G_3}{\eta_3}t} \right) \sqrt{R}\,\delta_0^{\,3/2}$$

Equation 5a: Spherical-tip indentation solution for a viscoelastic material modeled with five linear elements and subjected to a step displacement δ_0

$$P(t) = 4R\left(G_1 + G_2 e^{-\frac{G_2}{\eta_2}t} + G_3 e^{-\frac{G_3}{\eta_3}t} \right)\delta_0$$

Equation 5b: Flat punch indentation solution for a viscoelastic material modeled with five linear elements and subjected to a step displacement δ_0

To determine the material properties from experimental stress-relaxation data, two approaches are available. The first is to use a curve-fitting program, such as the MATLAB curve fitting tool. The simplicity and accuracy of this method are preferable, and as such it was used in this investigation. The second method is an explicit analytical approach, making use of experimental values at particular time points and taking advantage of particular aspects of the two-exponential behavior found in Equation 5a and Equation 5b.

The analytical procedure will be briefly described for the flat punch indentation solution. For approximations of step loading, the peak load is considered as being the load at time 0. From Equation 5b, one can see that P(t=0) depends on the sum of the shear moduli. Similarly, if one considers a time point near the end of relaxation (approximated as $t = \infty$), then $P(t=\infty)$ depends on G_1. Next, consider three time points t_1, t_2, t_3 in the relaxation phase. Choosing t_2 and t_3 to be relatively large, the term with G_3 is taken to be negligible by assuming it to have the shorter time constant. As a result, the equations for $P(0)$, $P(\infty)$, $P(t_1)$, $P(t_2)$, and $P(t_3)$ become sufficient for uniquely determining G_1, G_2, G_3, η_2, and η_3 to within an approximation consistent with the previous assumption. G_1 is determined directly from the experimental value $P(\infty)$ as seen in Equation 6. To determine G_2, one can use the ratio of $\frac{P(t_2)-P(\infty)}{P(t_3)-P(\infty)}$ to find an

expression for $\frac{G_2}{\eta_2}$, which can then be used with the expression $P(t_2) - P(\infty)$ to arrive at Equation 7. With G_2 and the ratio $\frac{G_2}{\eta_2}$ known, η_2 is calculated using Equation 8. For G_3, P(t=0) is evaluated to obtain G_3 in terms of G_1 and G_2. With G_1 and G_2 already determined, G_3 is found from Equation 9. η_3 is found in terms of G_1, G_2, and G_3, or $P(\infty)$, G_2, and G_3 by manipulation of the expression for $P(t_1)$, yielding Equation 10.

$$G_1 = \frac{P(\infty)}{4R\delta_0}$$

Equation 6: Determination of G_1 from estimation of the experimental value $P(\infty)$

$$G_2 = \frac{P(t_2) - P(\infty)}{4R\delta_0} e^{\left(\frac{1}{t_3 - t_2}\right) \ln\left(\frac{P(t_2) - P(\infty)}{P(t_3) - P(\infty)}\right) t_2}$$

Equation 7: Determination of G_2 from experimental values $P(t_2)$, $P(\infty)$.

$$\eta_2 = \frac{t_3 - t_2}{\ln\left(\frac{P(t_2) - P(\infty)}{P(t_3) - P(\infty)}\right)} \frac{P(t_2) - P(\infty)}{4R\delta_0} e^{\left(\frac{1}{t_3 - t_2}\right) \ln\left(\frac{P(t_2) - P(\infty)}{P(t_3) - P(\infty)}\right) t_2}$$

Equation 8: Determination of η_2 from experimental values $P(t_2)$, $P(t_3)$, and $P(\infty)$.

$$G_3 = \frac{P(0) - P(\infty)}{4R\delta_0} - \frac{P(t_2) - P(\infty)}{4R\delta_0} e^{\left(\frac{1}{t_3 - t_2}\right) \ln\left(\frac{P(t_2) - P(\infty)}{P(t_3) - P(\infty)}\right) t_2}$$

Equation 9: Determination of G_3 from experimental values $P(0)$, $P(t_2)$, $P(t_3)$, and $P(\infty)$.

$$\eta_3 = \frac{-G_3}{\ln\left(\frac{P(t_1) - P(\infty)}{4RG_3\delta_0} - \frac{G_2}{G_3} e^{-\frac{G_2}{\eta_2} t_1}\right)} t_1$$

Equation 10: Determination of η_3 from experimental values

The five material parameters are thus approximately determined to fit the experimental data with the five element model.

To characterize the brain and collagen biomaterials, the MATLAB curve fitting program is used to determine the material parameters from the experimental relaxation data for hemispherical indentation. As a means of comparing the two materials, as well as comparing the brain data with other published literature, several measures are used.

First, a comparison of the idealized elastic shear modulus for the loading phase is made based upon the elastic solution for spherical-tip indentation (Equation 1). The brain data is compared to available literature values, while the brain and scaffolds are also compared. Similarly, a comparison of the idealized long term shear modulus is made by using the load at the end of the relaxation period in the same equation. Next, the five material parameters G_1, G_2, G_3, η_2, and η_3 are compared for the materials. Their relationship to the relaxation behavior of the materials is clarified by examination of the two time constants of decay corresponding with ratios of shear moduli to viscosities. Finally, the relaxation behavior of the materials is analyzed by calculating the extent of relaxation relative to the maximum load attained during the indentation. Specifically, the percent relaxation is calculated by taking 1 minus the ratio of the final load to the peak load.

2.4 Results

2.4.1 Stress-Relaxation Behavior of Rat Brain and Collagen Scaffolds

The stress-relaxation curves for the collagen scaffolds showed similar general viscoelastic behavior for the various collagen concentrations (Figure 2). Scaffolds exhibited rapid relaxation upon cessation of the loading phase, with forces reaching approximately asymptotic levels by the end of the 5 minute hold at constant displacement. Higher force levels were observed for higher collagen concentrations, with 1.5% scaffolds having markedly larger forces than any other group. The rat brain also showed the expected viscoelastic behavior with fast initial relaxation and forces eventually reaching an approximate plateau. Rat brain curves appeared to have maximum forces similar to some of the scaffolds, but lower forces at the end of relaxation.

Attempts to fit experimental data with the three-element viscoelastic model in Equation 2 revealed that a single exponential is not sufficient to accurately describe brain or scaffold relaxation. This is consistent with previous indentation testing of porcine brain [95], but had not been previously determined for the collagen scaffolds used in this study. The five-element model, however, provided good fits (R^2 generally above 0.90) for both the brain and scaffold relaxation profiles (Figure 2). 0.5% scaffolds were not able to be fit well due to resolution limitations of the load cell during data acquisition of the relaxation phase.

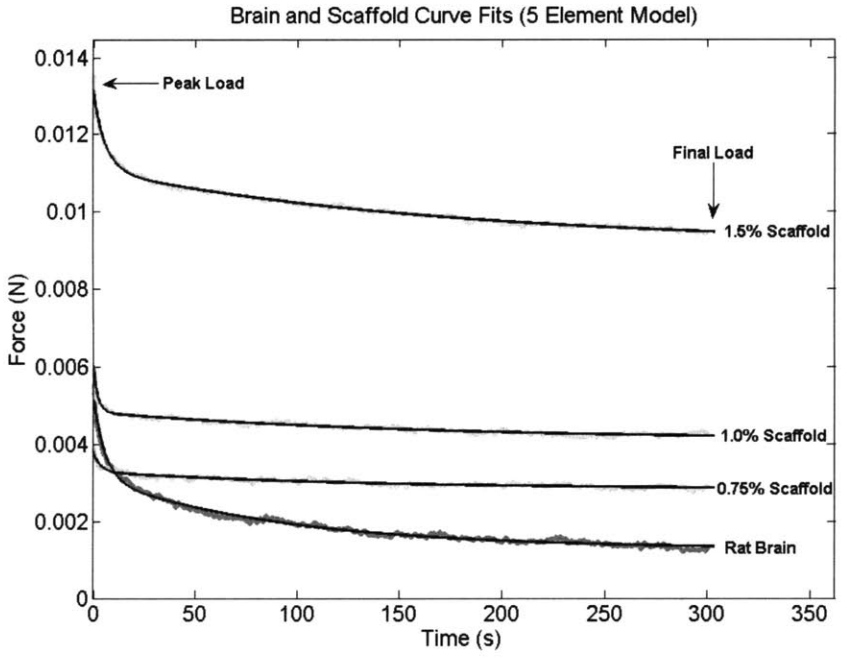

Figure 2.2. Representative brain (n=5) and collagen scaffold (n=6) relaxation data fitted with the five-element viscoelastic model.

2.4.2 Idealized Short and Long Term Elastic Shear Moduli

The idealized elastic shear modulus for the loading phase increased significantly with increasing collagen concentration (one-factor ANOVA; $p<0.001$; power=1.0) for the scaffolds (Figure 3). Individual contrasts by post hoc testing also revealed significant differences in the short term moduli of all scaffold groups. The rat brain was significantly stiffer than the 0.5% ($p<0.001$) and 0.75% ($p=0.013$) scaffolds, and significantly less stiff than the 1.5% scaffold ($p<0.001$). The difference between the modulus of the brain and the 1.0% scaffold was not statistically significant. Moduli ranged from 1.0 ± 0.04 kPa for the 0.5% scaffold up to 7.5 ± 0.37 kPa for the 1.5 % scaffold.

The idealized long term elastic shear modulus (Figure 3) similarly showed a significant effect of collagen concentration ($p<0.001$; power=1.0). The rat brain modulus

was significantly lower than 0.75% (p=0.002), 1.0% (p=0.002), and 1.5% (p<0.001) scaffolds, but not significantly different from the 0.5% scaffold. Moduli ranged from 0.7 ± 0.02 kPa for 0.5% collagen scaffolds to 4.2 ± 0.45 kPa for 1.5% scaffolds.

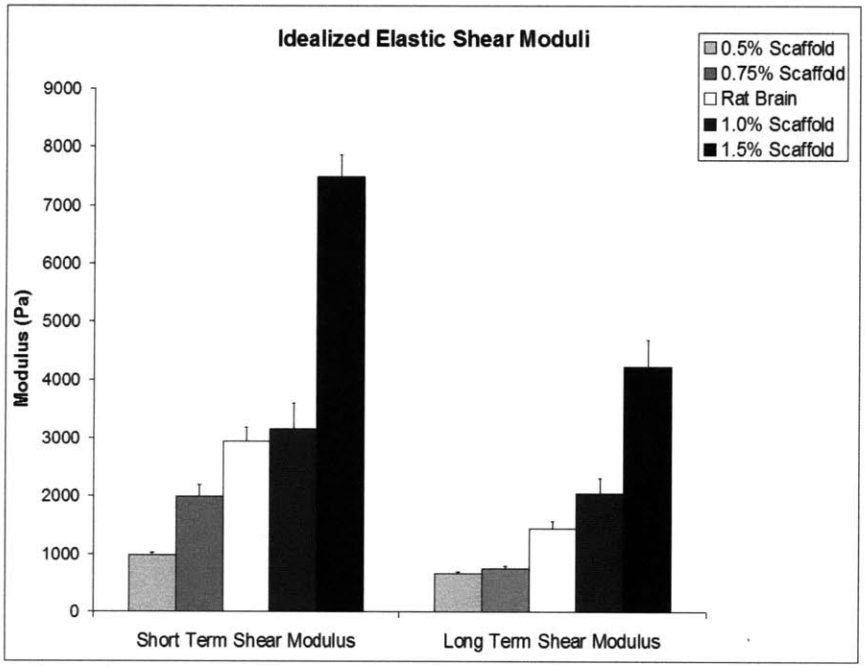

Figure 2.3. Idealized short term and long term elastic shear moduli

2.4.3 Five-Element Model Parameters (G_1, G_2, G_3, η_2, η_3)

The three shear moduli G_1, G_2, and G_3 (Figure 4) in the five-element model all increased with increasing collagen concentration for the scaffolds (p=0.002; power=1.0, p<0.001; power=1.0, p<0.001; power=1.0, respectively). G_1 values ranged from 1.6 ± 0.10 kPa for the rat brain to 7.9 ± 0.99 kPa for the 1.5% scaffolds, with the brain modulus being significantly less than the 0.75% scaffold (p=0.003). G_2 values ranged from 0.4 ± 0.08 kPa for 0.75% scaffolds to 2.7 ± 0.18kPa for 1.5% scaffolds, with the rat brain modulus of 2.0 ± 0.15 kPa being significantly greater than the 1.0% scaffold (p=0.005), and significantly less than 1.5% scaffold (p=0.017). G_3 values ranged from 0.5 ± 0.09

kPa for 0.75% scaffolds to 3.4 ± 0.35 kPa for 1.5% scaffolds, with the rat brain modulus of 1.8±0.20 kPa again falling between 1.0% (p=0.001) and 1.5% (p=0.004) scaffolds.

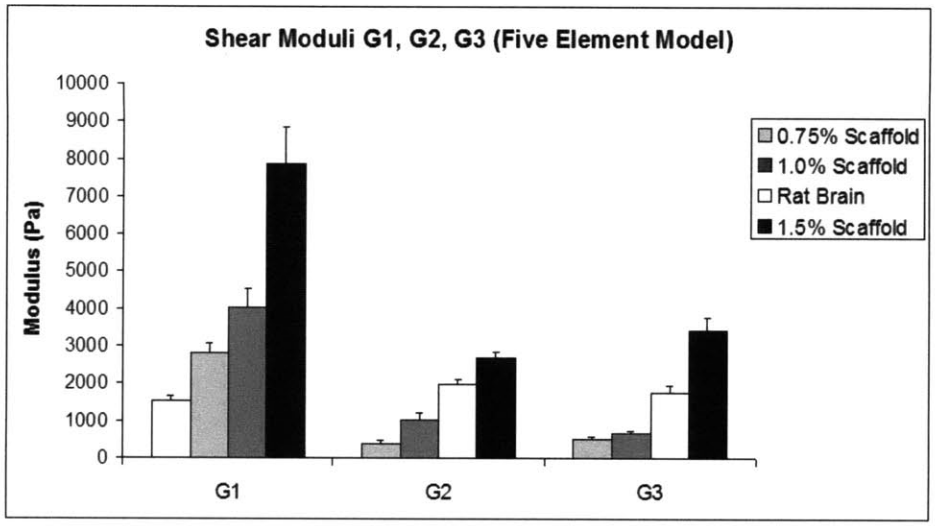

Figure 2.4. Shear moduli G_1, G_2, G_3 for rat brain and collagen scaffold stress-relaxation data fit with the five-element viscoelastic model

The viscosities η_2 and η_3 (Figure 5) also increased significantly with increasing collagen concentrations ($p<0.001$; power=1 for both). η_2 ranged from 1.1 ± 0.19 kPa*s for 0.75% scaffolds to 15.4 ± 0.98 kPa*s for 1.5% scaffolds, with rat brain viscosity of 11.0 ± 0.44 kPa*s being between 1.0% ($p<0.001$) and 1.5% ($p=0.004$) scaffolds. The viscosity η_3 ranged from 98.1 ± 27.1 kPa*s for 0.75% scaffolds to 648.2 ± 90.1 kPa*s for 1.5% scaffolds. Rat brain had a viscosity η_3 of 148.7 ± 6.8 kPa*s, which was significantly less than the 1.5% ($p<0.001$) and 1.0% ($p=0.02$) scaffolds, but not significantly different from 0.75% scaffolds.

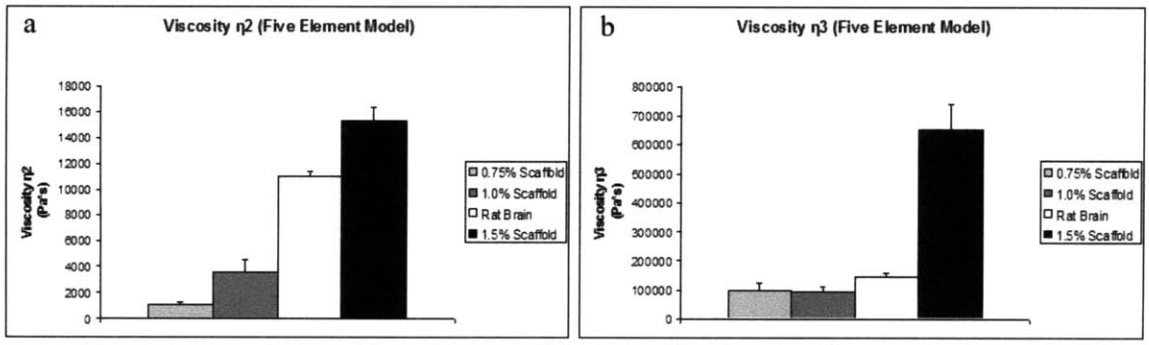

Figure 2.5. Viscosities η_2 (a) and η_3 (b) for rat brain and collagen scaffold stress-relaxation data fit with the five-element viscoelastic model

2.4.4 Relaxation Time Constants

The time constant $\tau_1 = \eta_2/G_2$ (Figure 6a) increased with increasing collagen concentration for the scaffolds ($p=0.006$; power=0.89). 0.75% and 1.0% scaffolds had respective τ_1 values of 3.0 ± 0.35 s and 3.3 ± 0.86 s, which were not significantly different from each other, but were significantly lower than the 1.5% τ_1 value of 5.8 ± 0.19 s ($p=0.003$ and $p=0.007$, respectively). The brain had a τ_1 value of 5.7 ± 0.30 s, which was significantly larger than τ_1 for the 0.75% ($p<0.001$) and 1.0% ($p=0.042$) scaffolds, but not significantly different from the 1.5% scaffold. While $\tau_2 = \eta_3/G_3$ (Figure 6b) did not vary significantly with collagen concentration for the scaffolds, the brain was found to have a significantly shorter time constant than the 0.75% ($p=0.046$), 1.0% ($p=0.049$), and 1.5% scaffolds ($p<0.001$).

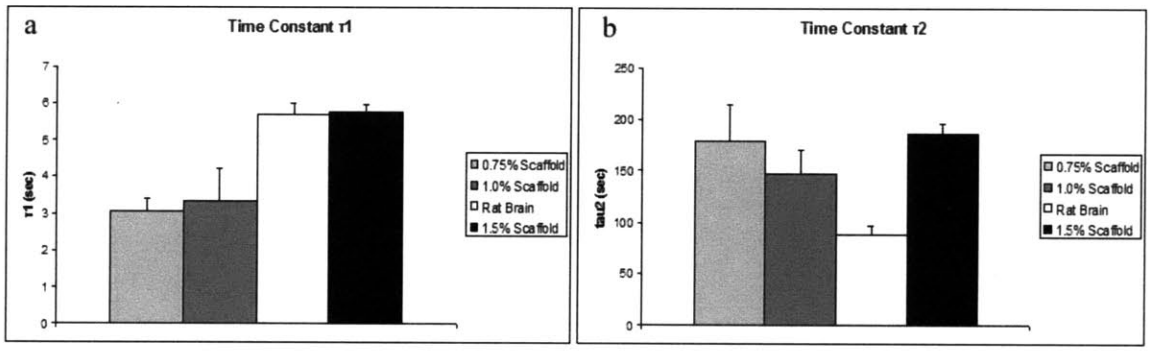

Figure 2.6. Time constants τ_1 (a) and τ_2 (b) for rat brain and collagen scaffold stress-relaxation data fit with the five-element viscoelastic model.

2.4.5 Percentage Force Relaxation

The percentage relaxation (Figure 7) increased with increasing collagen concentration for the scaffolds ($p=0.001$; power=0.98), with values of 27.4 ± 1.29%, 34.9 ± 1.6%, and 44.1 ± 3.78% for 0.75%, 1.0%, and 1.5% scaffolds, respectively. Rat brain had a relaxation percentage of 74.1 ± 1.22%, which was significantly larger than the 1.5% scaffold ($p<0.001$).

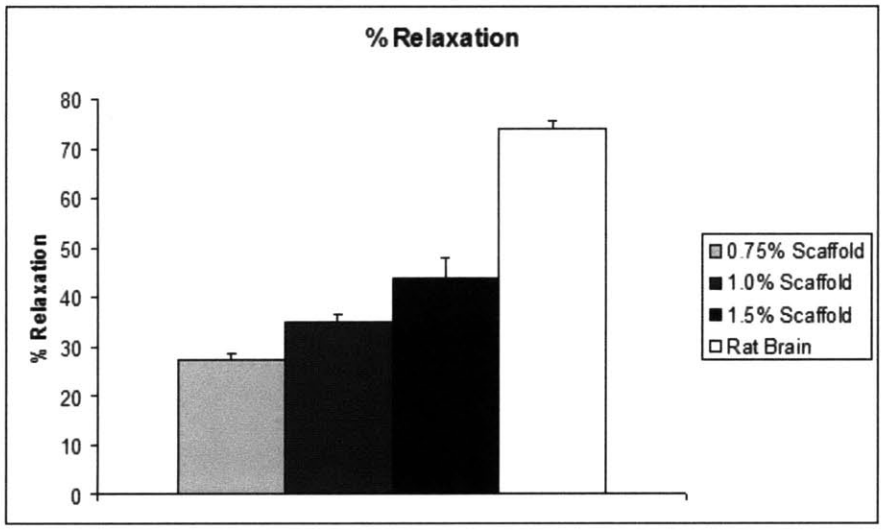

Figure 2.7. Percentage Relaxation (1-final load/peak load) for brain and scaffold materials.

2.5 Discussion

The application of viscoelastic modeling to collagen scaffold stress-relaxation data acquired by indentation testing has not been previously reported. Studies that have tested porous collagen and collagen-glycosaminoglycan scaffolds similar to those in this work have done so in standard tension and compression configurations and reported properties such as the Young's modulus [98, 99], tensile strength [100], and compressive

yield strength [98]. The published Young's modulus values are on the order of approximately 1-6 kPa [98, 99] for scaffolds fabricated and tested under varying conditions, which compares favorably with the short term moduli in this study.

The finding that the rat brain stress-relaxation curves can be fit relatively precisely with two exponentials is consistent with previous data on stress-relaxation of porcine brains [95]. It is observed that the relaxation is generally too steep in the initial phase and too slow at the later time points to be fit well with a single exponential. We have shown that type I collagen scaffolds exhibit similar behavior with respect to a stress-relaxation profile that can be fit well by a minimum of two exponential curves.

The idealized short and long term shear moduli for the brain show reasonable consistency with previously published indentation data on rat brain. The short term and long term moduli found in this study were 2.9 ± 0.23 kPa and 0.8 ± 0.04, respectively, while Gefen et al. reported values of 1.7 ± 0.68 kPa and 0.5 ± 0.25 kPa [92]. While different studies of brain tissue have reported properties varying by as much as an order of magnitude [91], the relative agreement here is encouraging. The consistency between these two independent studies using different indenter radii and indentation depths gives confidence in the reliability of the testing modality and the validity of assumptions made in application of the theoretical indentation solution. Additionally, a recent study conducted unconfined compression testing on the rat cerebral cortex and reported a value of 1.0 ± 0.17 kPa [98]. This result is not far from the values obtained through indentation, and the lower value could be due to the use of a much slower displacement rate.

In Figure 3 it can be seen that the 1.5% collagen scaffold has disproportionately large short and long term moduli relative to the other scaffolds. This result can be explained based on previous work that has modeled collagen scaffolds as open-cell foam materials [101]. The open-cell foam model predicts that for such materials the Young's modulus varies in proportion to the square of the relative density (defined as the density of the porous material divided by the density of the solid material from which it is made) [99, 101]. This property, taken with recent data illustrating a linear increase in relative density with increasing collagen concentration for scaffolds [99], suggests that the Young's modulus should increase with the square of the collagen concentration. (It is noted that the scaffolds in the study by Harley et al. included chondroitin 6-sulfate at a proportion 10 times less by weight than collagen.) A plot of the short term shear modulus found in this study versus the square of the collagen concentration produces a linear relationship (R^2=0.998) which is consistent with the predicted behavior (not shown). The long term shear modulus shows a similar linear relationship (R^2=0.997) with the square of the collagen concentration.

Comparison of the brain idealized shear moduli with the collagen scaffolds showed that the 0.5% scaffolds are much more compliant than the brain during loading, while 1.5% scaffolds are much stiffer. 0.75% and 1.0% scaffolds had short term moduli that were similar to the brain, with the 1.0% scaffold being most similar. The 0.5% scaffold, however, had the most similar long-term modulus. While the relative importance of the short and long term moduli with respect to cell behavior in a biomaterial has yet to be elucidated, one can speculate that the scaffolds with properties much stiffer than the brain may not be ideal for promoting primarily neuronal survival or

differentiation [81-83]. Additional considerations for use of these or similar biomaterials might include the ease of handling, the *in vivo* degradation rate, and the resistance to pore collapse. One can generally expect the stiffer scaffolds to have better handling properties, slower degradation rates, and increased resistance to pore collapse due to increased strut stiffness. The importance of such factors can vary significantly among applications [86, 102-104].

In the five-element model, the parameter G_1 was lower for the brain than for the 0.75%, 1.0%, and 1.5% scaffolds. G_1 is related to the long term load, and illustrates that the relaxation behavior for the brain differs substantially from the scaffolds by having a lower force at the end of relaxation. This is essentially the same information as is found from the idealized long term shear modulus, except that the modulus here relates to a particular element in the viscoelastic model rather than a general solution for indentation of an elastic material.

G_2, G_3, η_2, and η_3 values for the brain were in between the 1.0% and 1.5% scaffold. The viscosities relate to the relaxation behavior as one of the determinants of the time constants of decay, while the moduli affect both the peak force during the loading phase and also the relaxation behavior. Relative to the biomaterials, the model parameters reflect the observation that the brain behaves more like the scaffolds of higher collagen concentration in loading. In relaxation, however, there appear to be elements of the behavior similar in some respects to the scaffolds of both higher and lower collagen concentration. This is evident upon examination of the time constants themselves. The time constant τ_1 for the brain is most similar to the 1.5% scaffold, with the 0.75% and 1.0% time constants being significantly shorter. τ_2 for the brain, however, is shorter than

0.75%, 1.0%, and 1.5% scaffolds. The modeling confirms the observation that the brain generally relaxes to its long-term load faster than the scaffolds, even though the low collagen concentration scaffolds have shorter τ_1 time constants that contribute to their relatively steep decay immediately at the onset of relaxation.

A major difference between the brain and scaffold mechanical behavior is illustrated in the results for percentage relaxation. The brain not only relaxes faster than the scaffolds, but it relaxes by a much greater amount (i.e. to a much lower force). In considering biomaterials for use in soft tissues, this result may be of particular interest. Forces applied to the scaffold from cells or surrounding tissue are likely to be sustained and of nearly constant magnitude. While the result of the material would be to creep in that scenario, the phenomenon is similar to stress-relaxation. If it were desired to match the behavior of the material to the tissue in which it was implanted, the degree of relaxation would be an important factor to consider. For the scaffolds, the increase in relaxation with increasing collagen concentration may be the result of increased water uptake by the scaffold struts. Increasing the collagen concentration further would likely achieve more relaxation, but the associated increase in stiffness might not be compatible with the desired application. While there are clearly limitations in terms of how a biomaterial can be manipulated to alter its mechanical properties, addition of other materials to form a composite can be a helpful tool. As an example, elements of brain extracellular matrix such as hyaluronic acid can be incorporated into a collagen scaffold so that it more closely resembles the brain from a material standpoint [98, 105]. Addition of hyaluronic acid could potentially increase the amount of water in the struts of a hydrated scaffold, which may then result in a greater degree of relaxation without

increasing the stiffness as collagen has been shown to do. Adjusting the proportion of each material offers a strategy to significantly alter the mechanical properties of the scaffold [98].

2.6 Limitations

While the five-element viscoelastic model is shown to fit the stress-relaxation curves reasonably well, it is limited in several respects. First, the brain is known to exhibit nonlinear behavior [72, 106]. While a linear model can be useful for a restricted range of strains and strain rates, a nonlinear model would be necessary to characterize the material more accurately for a wide range of loading conditions [91]. The indentation solution also relies on isotropy and homogeneity of the material, an assumption which does not hold as one looks at other brain regions besides the cerebral cortex. Deeper brain structures and white matter tracts such as the corpus collosum are known to exhibit anisotropic mechanical behavior [91]. The model used in this work would thus be inappropriate for describing behavior of other brain structures.

2.7 Conclusion

A five-element viscoelastic model has been used in conjunction with indentation testing to characterize mechanical properties of rat cerebral cortex and various collagen scaffold biomaterials. The brain and scaffolds both exhibit relaxation behavior that cannot be accurately fit with a single exponential, but can be fit well with the two exponentials of the five-element model. The brain exhibited behavior similar to the 1% collagen scaffold in the loading phase, but was appreciably different from each scaffold

in the relaxation. The viscoelastic modeling identifies several parameters that can be used to characterize materials and therefore potentially changed to arrive at a mechanically suitable material for *in vivo* or *in vitro* work. For the purposes of CNS tissue engineering, it remains to be seen how the variation in mechanical properties may affect *in vivo* physiological responses to a particular biomaterial.

Chapter 3: Characterization of a Bilateral Penetrating Brain Injury in Rats and Evaluation of a Collagen Biomaterial for Potential Treatment

3.1 Introduction

Penetrating brain injury (PBI) represents a particularly severe form of traumatic brain injury encountered in both military and civilian sectors. Projectiles (e.g. bullets, shrapnel) that enter the brain result in very high mortality, but are not uniformly fatal [107]. The path and velocity of the projectile are important determinants in whether an individual will survive, with single hemisphere injuries, frontal lobe injuries and lower projectile velocities associated with better outcomes [108-112]. While estimates of overall mortality vary widely, one general estimate suggests up to 30% of individuals suffering PBI in combat achieve long term survival [39]. Unfortunately, the treatment options for patients remain limited mainly to surgical debridement [45] and medical management of subsequent neurological symptoms [44]. With a more thorough understanding of the physiology of PBI, potential therapies could be devised and administered at the time of initial surgery and perhaps also in subsequent surgeries.

Previous studies of penetrating brain injury have actually fired projectiles into the brains of animals including cats [113, 114], rabbits [115], and monkeys [116, 117]. Studies of these kinds have generally been discontinued, prompting the development of different animal models.

Toward this end, a rat model to simulate a ballistic penetrating brain injury was recently developed at the Walter Reed Army Institute of Research (WRAIR) [40]. The key feature of PBI simulated by the model is the creation of a large temporary cavity resulting from dissipation of kinetic energy while a projectile passes through the brain. Various studies have demonstrated evidence [39] that the temporary cavity in PBI is several times larger than the volume of tissue damaged solely from the path of the

projectile [45, 118, 119]. The injury model involves inserting a metal probe into the brain to mimic the projectile path and inflating a balloon attached near the probe tip to simulate the temporary cavity. The model has been shown to produce neurological deficits, electrophysiological abnormalities, and histological features consistent with what is known about PBI from larger animal models and from human pathology [40, 42, 43, 120]. It is noted that certain PBI features such as retained bone and metal fragments, along with subsequent infectious processes, are not reproduced [121]. The model nonetheless provides a useful method for studying several aspects of PBI pathophysiology through the creation of a standardized cavitary defect.

Published work using the PBI model has focused on characterization of a frontal, unilateral injury at time points up to 1 week post-injury. While one study evaluated survival and behavioral outcomes following a bilateral injury [122], a histological characterization similar to that of the frontal injury has not been conducted for a bilateral injury. Additionally, the progression of the PBI lesion several weeks after the injury has not been studied. This work aims to characterize the bilateral PBI injury at 1 week and 5 week time points using histomorphometric and immunohistochemical methods. It is observed that the permanent cavity that eventually forms in the brain as the result of PBI lends itself to the possibility of treatment through implantation of a biomaterial. The biomaterial might act as a suitable delivery vehicle for pharmacological or cellular therapeutic agents to mitigate injury progression or promote regeneration. As a preliminary step towards developing such a treatment, this work will also evaluate the effects of implanting a preformed collagen scaffold either immediately or 1 week after the injury.

3.2 Materials and Methods

3.2.1 Experimental Design

Four groups of animals were used in this study, with all undergoing surgical administration of a bilateral penetrating brain injury. The injury involved inflation of the PBI balloon to a volume equal to approximately 10% of the rat brain volume. Group 1 was administered the injury and allowed to survive for 1 week before sacrifice. Group 2 was administered the same injury but was then implanted with a type I collagen scaffold and sacrificed after 1 week. Group 3 underwent the injury, but was allowed to survive for 5 weeks. It is noted that at 1 week post-injury, the Group 3 animals underwent a sham surgery to serve as controls for Group 4. Group 4 underwent the injury, and 1 week later had a second surgery to implant a collagen scaffold. Group 4 animals were sacrificed 4 weeks after implantation of the scaffold (5 weeks post-injury). The experimental groups are summarized in Table 1.

Table 1: Experimental Groups

	Group 1 (n=5)	Group 2 (n=5)	Group 3 (n=6)	Group 4 (n=5)
1st surgery	Injury without intervention	10% injury with scaffold implantation	Injury without intervention	Injury without intervention
2nd surgery	N/A	N/A	Sham implantation surgery 1 week post-injury	Scaffold implantation 1 week post-injury
Sacrifice time (post-injury)	1 week	1 week	5 weeks	5 weeks

3.2.2 Penetrating Brain Injury Apparatus

Technical details of the PBI apparatus (Dragonfly Inc., Ridgeley, WV) have been described in several publications [40, 42]. Briefly, the apparatus consists of components including a balloon-tipped probe, a stereotaxic frame (Kopf, Tujunga, CA), a piston-cylinder pneumatic device, and a pendulum. The pendulum is dropped under gravity to drive the piston, forcing the air in the cylinder through tubing of smaller diameter and generating a pressure impulse to rapidly inflate the balloon. The balloon, which takes the shape of an ellipsoid, has been reported to remain inflated on average for less than 6.6 ms.

3.2.3 Collagen Scaffold Fabrication

Type I collagen scaffolds (1.0% weight:volume) were fabricated from medical grade porcine microfibrillar collagen (Geistlich Biomaterials, Wolhusen, Switzerland). A suspension of the collagen was first made in 0.001 N HCl, brought to pH 3, and mixed with a stir bar for 20 minutes. The slurry was blended at 15,000 RPM (Ultra Turrax T18 blender, IKA, Staufen, Germany) for 30 minutes at 4° C, brought again to pH 3, and blended for an additional 2 hours. The slurry was then centrifuged for 10 minutes at 5500 RPM to remove air bubbles, and mixed with a pipette to ensure homogeneity. The slurry was poured in a metal mold and placed into an AdVantage Benchtop Freeze Dryer (VirTis, Gardiner, NY). The temperature was decreased at a controlled rate to -40° C over 180 minutes and held at -40° C for 60 minutes. Sublimation was conducted at a temperature of 0° C and pressure of 200 mTorr for 1020 minutes. Scaffolds were then dehydrothermally cross-linked overnight at 105° C under vacuum. Biopsy punches were

used to cut scaffolds 3 mm in diameter and approximately 3 mm in thickness for implantation. Published work using similar scaffolds has determined the pore size to be approximately 100-150 μm. Similar collagen scaffolds have been used in several published studies from our research group.

3.2.4 Surgical Procedure and Animal Care

24 male Sprague-Dawley rats were used in this study. All procedures were approved by the Boston VA Healthcare System Institutional Animal Care and Use Committee.

Animals were shaved, anesthetized with isoflurane, and positioned in a stereotaxic frame where the anesthetic delivery was maintained through a nosecone. A circulating water heating pad was used to maintain body temperature throughout the surgery and also for several hours during the post-operative recovery. Heart rate and blood oxygen saturation were monitored from a probe on the foot during the procedure.

After sterilizing the skin with 13% povidone iodine solution, a midline incision was made along the top of the head to expose the skull, followed by a lateral incision extending from the posterior aspect of the midline incision and passing just anterior to the left ear (Figure 3.1a). With the top of the skull and the left side of the head exposed, a portion of the left temporalis muscle was excised with care taken to avoid damaging the temporal branch of the facial nerve (Figure 3.1b). With the lateral aspect of the skull exposed, a 3 mm diameter window was drilled in the skull at a position 1 mm anterior to bregma and 3 mm ventral to bregma (Figure 3.1c). The PBI probe was then positioned with the tip at the surface of the brain (Figure 3.1d) before pausing to briefly ensure stability of the animal's vital signs.

The PBI probe was then inserted into the brain, with the tip advancing 10 mm from the surface of the left hemisphere into the right hemisphere. The PBI balloon was inflated to a diameter of 6.3 mm to create an injury encompassing approximately 10% of the rat brain volume. It is noted that the balloon is several mm proximal to the tip of the probe, such that the balloon inflation is predominately in the left hemisphere despite the probe tip being in the right hemisphere. This scenario mimics a projectile entering the left hemisphere and dissipating its kinetic energy before coming to rest in the right hemisphere. Following the balloon inflation, the probe was retracted from the brain and bleeding was controlled using Gelfoam. Animals in Group 2 underwent implantation of a cylindrical collagen scaffold 3 mm in diameter and 3 mm thick into the defect at this time. Groups 1, 2, and 3, had no intervention. The cranial window was covered (Figure 3.1e) with a Bio-Gide collagen membrane (Geistlich Biomaterials, Wolhusen, Switzerland) and the surgical incision was closed with a 4-0 suture (Figure 3.1f).

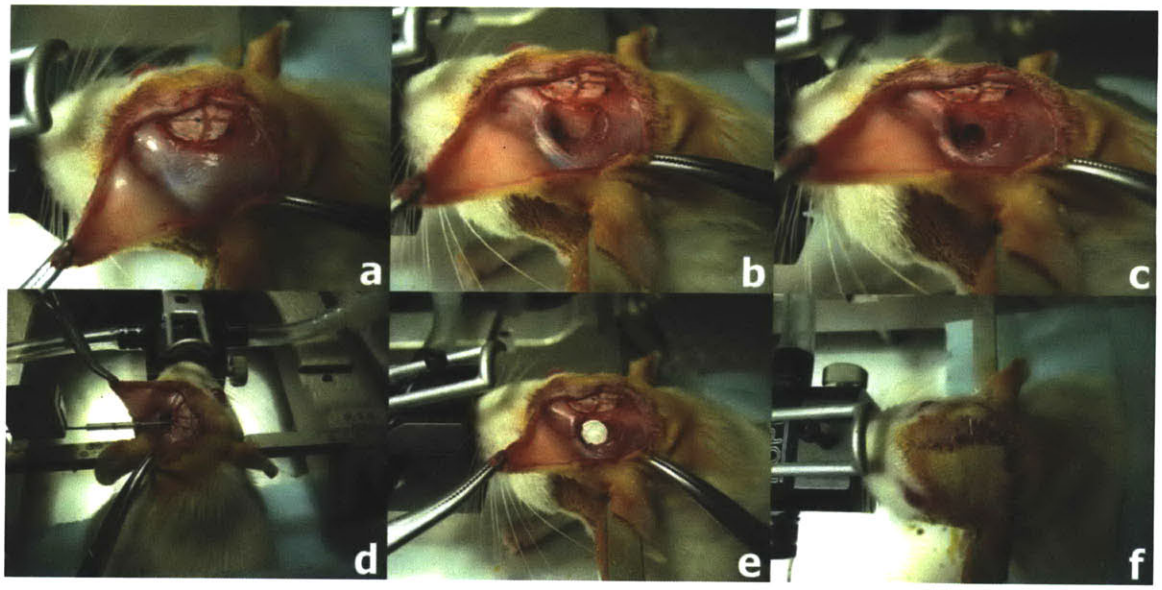

Figure 3.1. PBI Surgical Procedure. a) Lateral aspect of the head with the temporalis muscle exposed. b) Lateral surface of the skull exposed with part of the temporalis muscle excised. c) Cranial window though which the PBI probe will be inserted. d) PBI probe in place just prior to

insertion into the brain. e) Collagen membrane covering the cranial window following the injury. f) Incisions closed with 4-0 sutures.

1 week after the injury, animals in Groups 3 and 4 underwent a second surgery. A second incision was made parallel to the lateral incision from the first surgery (Figure 3.2a), enabling access to the defect site (Figure 3.2b). After removing the collagen membrane covering the cranial window (Figure 3.2c), the lesion site was exposed (Figure 3.2d). Group 4 animals had a collagen scaffold implanted at this time (Figure 3.2e), while Group 3 animals had only the surgery without scaffold implantation. The cranial window in each case was covered again with a collagen membrane (Figure 3.2f) and the incision closed with a 5-0 suture.

Following all surgeries, animals were allowed to recover in warmed cages with additional oxygen administered through a nose cone. Food and water were provided at bedding level. Animals were initially placed on their side within the cage while recovering from anesthesia and the surgical trauma. Buprenorphine (0.05 mg/kg) was given for pain relief, while Cefazolin (20 mg/kg) was given to prevent infection.

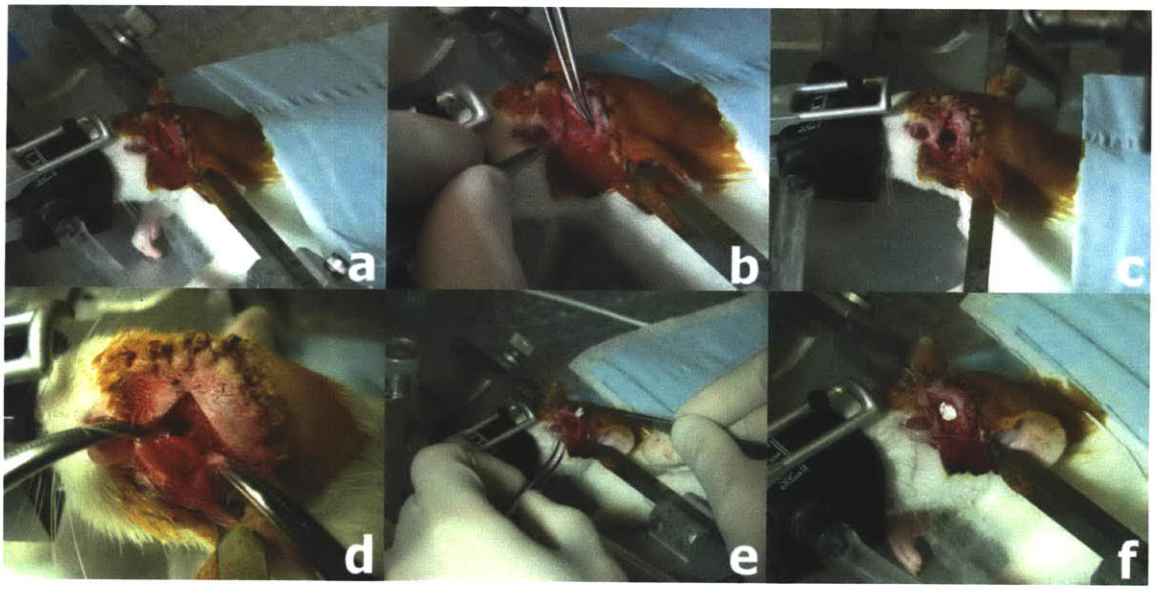

Figure 3.2. Collagen Scaffold Implantation Surgery. a) Incision to expose the site of the cranial window. b) Scar tissue covering the collagen membrane and cranial window. c) Cranial window exposed. d) Cranial window exposed (different animal). e) Implantation of the collagen scaffold into the defect. f) Collagen membrane covering the cranial window prior to closing the incision

3.2.5 Animal Sacrifice and Specimen Processing

Before sacrifice, animals were deeply anesthetized with an intraperitoneal injection of sodium pentobarbital (150 mg/kg). When all reflexes were lost, surgical scissors were used to cut through the skin, muscle, and thorax to expose the heart. Animals were then transcardially perfused (Figure 3.3) with 150 mL cold heparanized PBS (20 units/mL) followed by 250 mL cold 4% paraformaldehyde solution (USB corporation 19943, Cleveland, OH). Brains were extracted and immersed in 4% paraformaldehyde for 2-3 days at 4° C. Brains were processed through reagent alcohol (70% - 10 min, 80% - 90 min, 95% - 2 x 90 min, 100% - 2 x 90 min, 100% - 90 min under vacuum), xylene (3 x 90 min), and paraffin (2 x 180 min under vacuum, 58° C). Samples were then embedded in paraffin and sectioned on a microtome at 5 μm. Sections were taken at approximately 1 mm intervals spanning the lesion. Slides were dried on a warmer at 60° C for several hours.

Figure 3.3. Transcardial Perfusion

3.2.6 Histology and Immunohistochemistry

Sections were stained with hematoxylin and eosin for histomorphometric analysis and for general histologic observation of the injury. Slides were first deparrafinized (xylenes: 2 x 5 min, 100% reagent alcohol: 2 x 3 min, 95% alcohol: 2 x 2 min, 80% alcohol 1 x 1 min) and rehydrated (5 min water rinse). Slides were stained in Gill's hematoxylin for 3 minutes, rinsed for 5 minutes, and stained in eosin for 45 seconds. Slides were processed through 95% alcohol (2 x 2 min) and xylenes (2 x 2 min) before being coverslipped with Cytoseal.

The fluorescent dye Fluoro-Jade C (Millipore AG325) was used for visualization of degenerating in the thalamus. Sections from approximately 2.5 mm posterior to bregma were deparrafinized and rehydrated prior to incubation in 0.06% $KMnO_4$ (Sigma 223468) for 20 minutes. After 3 rinses in deionized water, slides were then stained with 0.00015% Fluoro-Jade C solution for 20 minutes and rinsed 3 more times in water. Slides were dried on a warmer at 60° C for 10 minutes, placed in xylene for several minutes, and coverslipped with Cytoseal mounting medium.

Antibodies, dilution factors, and antigen retrieval methods used for immunohistochemistry are summarized in Table 2. The staining procedure was conducted at room temperature. Following deparrafinization, rehydration, and antigen retrieval, slides were rinsed with wash buffer (Dako S3006) containing TBS and 0.05% Tween 20. Slides were blocked for 2 hours with Dako protein block (Dako X0909) prior to addition of the primary antibody for 2 hours. Following 3 rinses with wash buffer, the secondary antibody was added for 1 hour. After 3 more rinses, a 100 ng/mL solution of

the fluorescent DNA stain 4',6-diamidino-2-phenylindole (DAPI) was added for 30 minutes. 3 final rinses with wash buffer were performed and the slides were then placed in TBS for 3 minutes. The slides were transferred to a 0.1% solution of Sudan Black (Sigma 199664) dye for 20 minutes in to reduce tissue autofluorescence. Following 3 rinses in TBS, slides were coverslipped with Immu-mount aqueous mounting medium (Thermo Scientific 9990402).

Table 2: Immunohistochemistry reagents (Abbreviations: rb (rabbit), ms (mouse), gt (goat),

1° Antibody	Source	Retrieval	Dilution	2° Antibody
GFAP (rabbit polyclonal)	Dako (Z0334)	0.1% Protease XIV 25 min (Sigma P5147)	1:500	Dylight 488 donkey anti-rabbit IgG (Jackson ImmunoResearch 711-485-152)
Von Willebrand Factor (rabbit polyclonal)	Dako (A0082)	0.1% Protease XIV 40 min (Sigma P5147)	1:100	Dylight 488 donkey anti-rabbit IgG (Jackson ImmunoResearch 711-485-152)
Doublecortin (goat polyclonal)	Santa Cruz (sc-8066)	Citrate buffer pH 6, 2 min 120° C (Dako S1699)	1:100	Dylight 488 donkey anti-goat IgG (Jackson ImmunoResearch 705-485-003)
CD68 (mouse monoclonal IgG)	Serotec (MCA341R)	0.1% Protease XIV 20 min (Sigma P5147)	1:200	Dylight 549 donkey anti-mouse IgG (Jackson ImmunoResearch 715-505-150)
NeuN (mouse monoclonal IgG)	Millipore (MAB 377)	Citrate buffer pH 6, 1 min 120° C (Dako S1699)	1:200	Dylight 549 donkey anti-mouse IgG (Jackson ImmunoResearch 715-505-150)
CNPase (mouse monoclonal IgG)	Abcam (ab6319)	Citrate buffer pH 6, 20 min 95° C (Dako S1699)	1:500	Dylight 549 donkey anti-mouse IgG (Jackson ImmunoResearch 715-505-150)
CS56 (mouse monoclonal	Sigma (C8035)	0.1% Protease XIV 40 min	1:100	Rhodamine donkey anti-mouse IgM (Jackson

IgM)		(Sigma P5147)		ImmunoResearch 715-025-020)

3.2.7 Imaging

Light microscope images were taken with an Olympus camera interfaced with a Olympus BX51 microscope, while fluorescent images were captured an Olympus DP71 camera interfaced with an Olympus BX60 microscope. Adobe Photoshop CS3 was used for minor image processing procedures such as cropping and adjustment of levels to reduce background [123].

3.2.8 Histomorphometric Analysis

Lesion area was demarcated in hematoxylin and eosin stained sections at approximately 1 mm intervals spanning the lesion. The lesion was defined by areas of obvious necrosis with lack of cellularity, along with regions of dense macrophage infiltration, hemorrhage, gliosis, and vacuolization. A linear interpolation was used to reconstruct an approximate volume, with the volume between sections being equal to the average of the areas multiplied by the distance between them.

3.2.9 Statistics

Numerical values are reported at mean ± standard error, and all statistical analysis was performed using Statview (version 5.0.01, SAS Institute Inc., Cary, NC). Unpaired t-tests were used to compare differences between experimental groups, with a p-value of 0.05 used for determining statistical significance.

3.3 Results

3.3.1 Animal Survival, Recovery, and Qualitative Behavioral Observations

21 out of 24 animals survived for the intended duration of their experimental groups. 2 of the 3 deaths occurred during the surgery to administer the injury, while the third occurred the day after the injury. All animals undergoing a second surgery (Groups 3 and 4) survived with no apparent adverse effects of the surgery or the implanted biomaterial.

Following administration of the injury, animals generally remained on their side for 1-3 hours before gradually righting themselves and withdrawing from the oxygen nosecone. Variability was observed in the degree to which animals would then begin grooming, ambulating, and eating. As recovery progressed several days after injury, the animals generally groomed themselves well and kept the incision site clean (Figure 3.4a). Animals undergoing a 2nd surgery similarly kept both incision sites very clean (Figure 3.4b). No signs of infection were apparent in any of the animals.

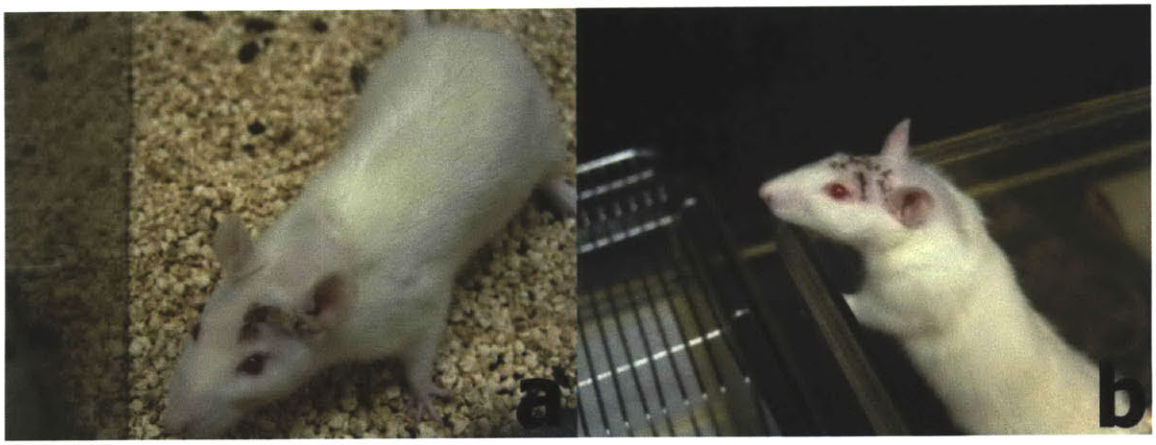

Figure 3.4. Incision sites following surgery. a) 1 week post-injury. b) 5 days after 2nd surgery (different animal)

Figure 3.5 shows the average weight progression for each group as a percentage of their weight at the time of the first surgery. Animals in Group 1 (Figure 3.5a) and Group 2 (Figure 3.5b) typically lost weight in the first 2-3 days after the injury, but thereafter recovered and continued to maintain or gain weight for the duration of the study. In each group, the average weight started to increase by the 3rd day after surgery. Animals in Group 3 (Figure 3.5c) and Group 4 (Figure 3.5d) showed similar weight loss following injury, but generally lost little or no weight after the second surgery.

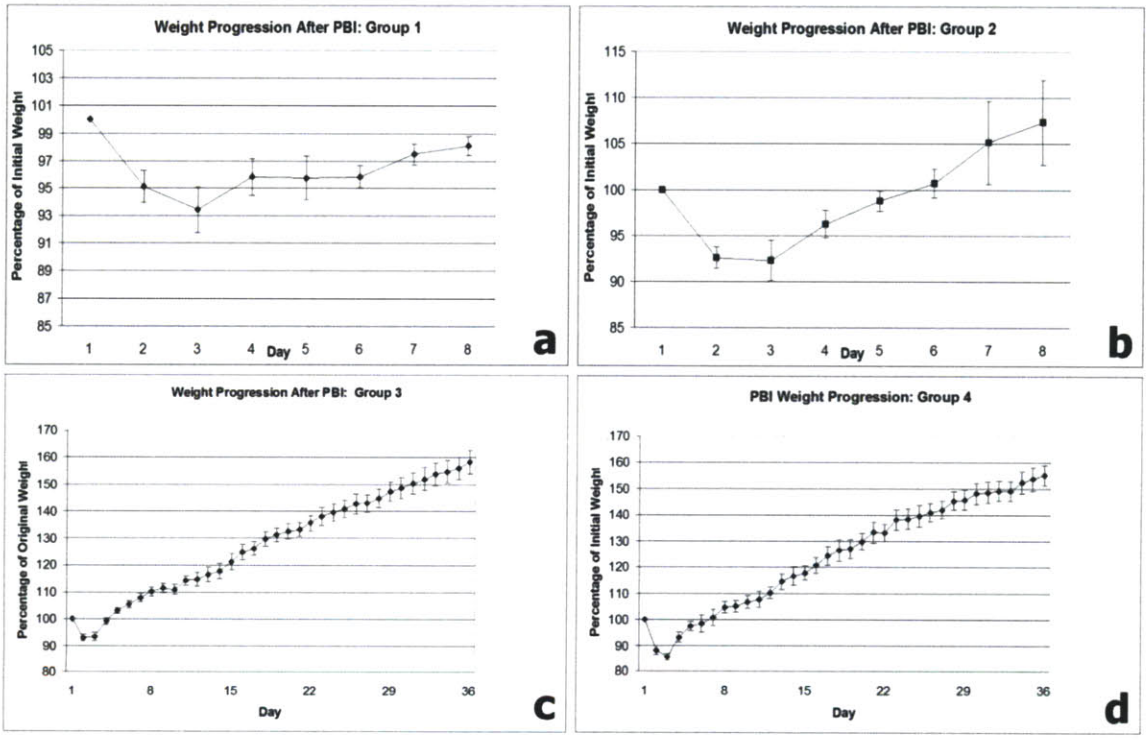

Figure 3.5. Weight Progression After PBI and Scaffold Implantation. a) Animals in Group 1 lost weight on average in the first 2 days after surgery, and thereafter began to gain weight again. b) Animals in Group 2 showed a similar trend to Group 1. c) Animals in Group 3 maintained their weight on average after the second surgery (Day 8). d). Animals in Group 4 showed a similar trend to those in Group 3.

Following the injury, animals consistently showed a decreased ability to use their right forelimb for grasping food while eating. Additionally, a slight tremor of the head was observed in some animals. Both the forelimb deficit and the tremor appeared to

mostly resolve within 3-4 days based on observation of the animals eating, grooming, and ambulating normally. It is likely, however, that sensitive functional and behavioral tests would detect some degree of persistent deficit even at later time points.

3.3.2 Lesion Characteristics and Volume

The site of the lesion was very obvious upon observation of the brain after extraction (Figure 3.6a). Histologically, the bilateral PBI was observed after 1 week to cause a large amount of damage to the left striatum, as well as lesser injury to elements of sensory and motor cortex, corpus callosum, external capsule, and the lateral ventricles (Figure 3.6b). In Group 1 and Group 2, the lesion at 1 week consisted of a large amount of necrotic debris (Figure 3.6c and Figure 3.6d), with dense infiltration of macrophages, areas of hemorrhage, and some areas of vacuolization within the striatum. The size of the cavity was smaller than the entire lesion, as much of the dead tissue had not yet been cleared.

At 5 weeks, however, Groups 3 and 4 revealed that the cavity had become much larger as most of the necrotic debris had been removed (Figure 3.7b). Injured structures were largely same, though the injury appeared to have expanded to include virtually the entire left striatum. Although a few areas of necrosis persisted within the cavity and notably at the edge of the corpus callosum (Figure 3.7c and Figure 3.7d), most of the remaining tissue appeared viable and without dense macrophage infiltration.

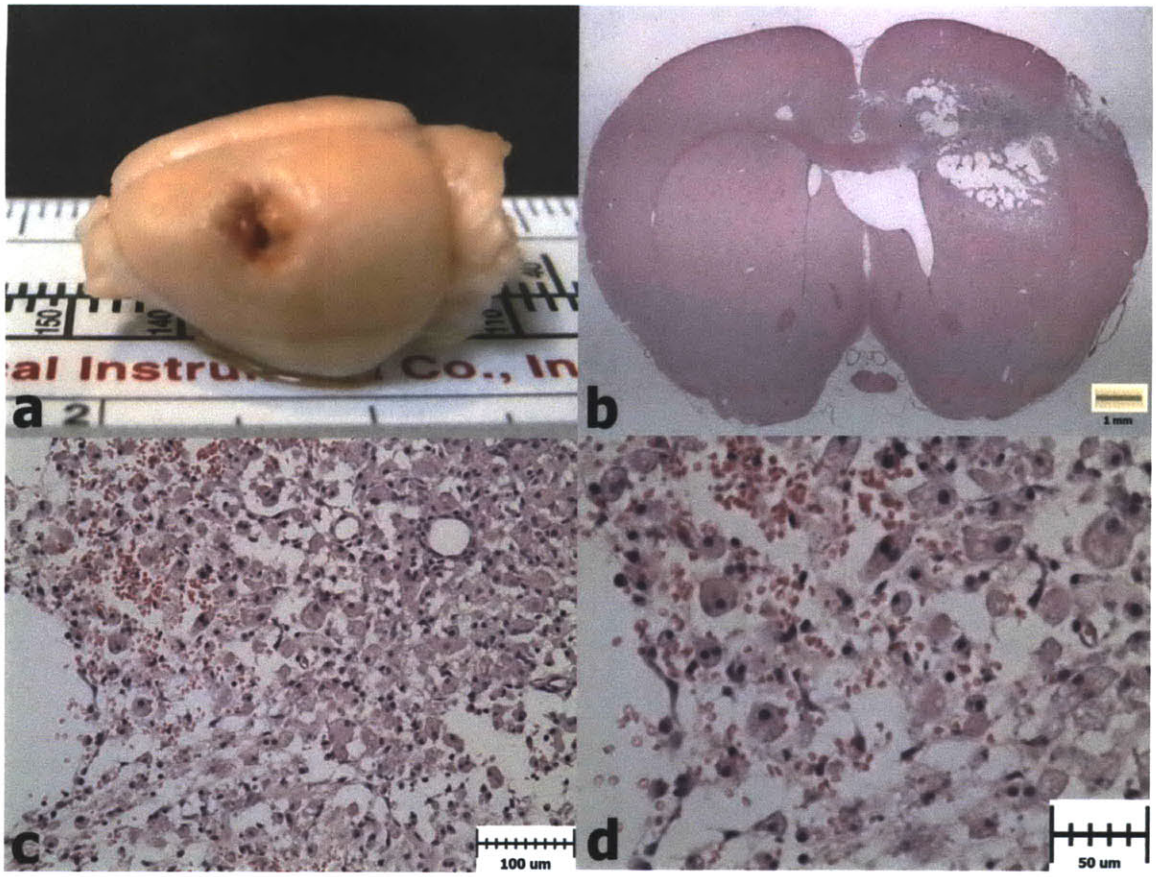

Figure 3.6. H&E Histology 1 Week after PBI (Group 1). a) PBI lesion evident in the extracted brain from a Group 1 animal. b) H&E coronal section showing damaged regions of cortex, striatum, lateral ventricle, external capsule, and corpus callosum after 1 week. c) Necrotic tissue being cleared by macrophages. d) Higher magnification image showing erythrocytes and engorged macrophages in the lesion site.

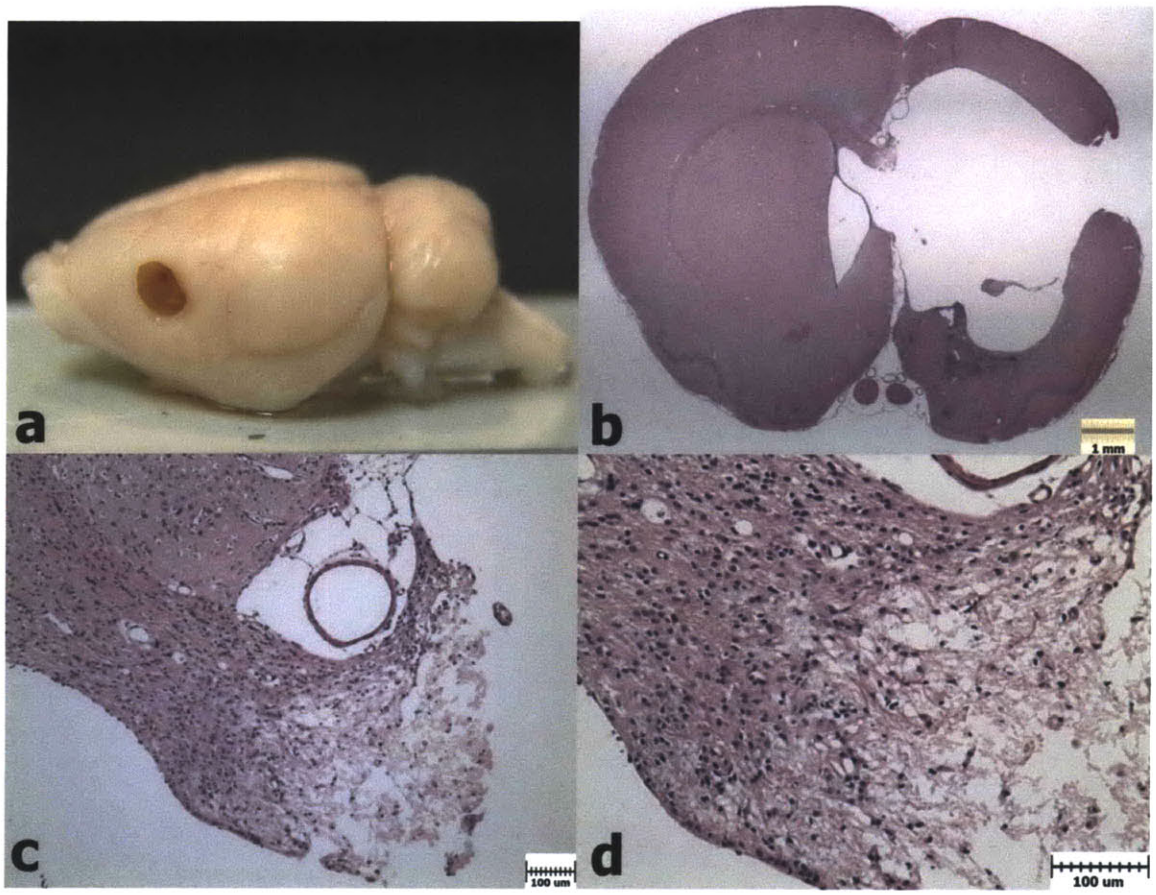

Figure 3.7. H&E Histology 5 Weeks after PBI (Group 3). a) PBI lesion after 5 weeks in the extracted brain of a Group 3 animals. b) H&E image showing the large PBI cavity in the left hemisphere at 5 weeks. c) Degeneration in the corpus callosum at 5 weeks. d) Higher magnification of the corpus callosum showing necrotic white matter with macrophage infiltration.

The volume of the bilateral PBI lesion was calculated to be 51.2 ± 3.7 mm^3 and 51.9 ± 4.4 mm^3 after 1 week in Groups 1 and 2, respectively. At 5 weeks, the Group 3 and 4 volumes were 65.9 ± 2.7 mm^3 and 85.1 ± 12.9 mm^3, respectively. Lesion volumes are summarized in Figure 3.8. Comparisons between groups revealed that the lesion volume at 5 weeks in Group 3 was significantly greater than the volume at 1 week in Group 1 ($p = 0.010$). Similarly, the Group 3 volume was significantly greater than that of Group 2 ($p=0.020$). The Group 4 volume was significantly greater than those of Group 1

and Group 2 (p=0.036 and p=0.041, respectively), but was not significantly different from Group 3.

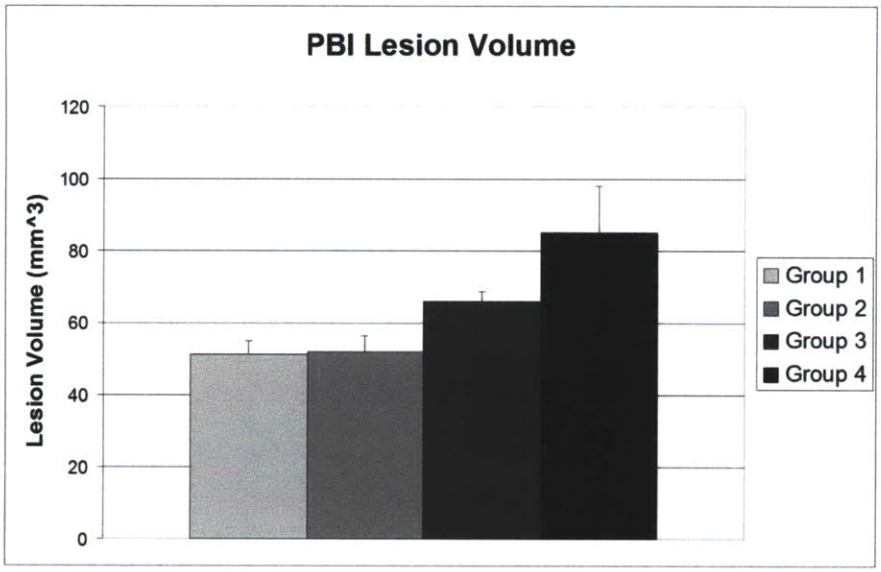

Figure 3.8. PBI Lesion Volumes. Group 3 and 4 volumes were significantly greater than Group 1 (p=0.010, p=0.036, respectively) and Group 2 (p=0.020, p=0.041, respectively) volumes.

3.3.3 Scaffold Localization and Cellular Infiltration

Scaffolds in Group 2 generally remained intact within the lesion site 1 week after implantation (Figure 3.9b). The volume of the scaffold appeared to fill most, but not all of the lesion site. The scaffolds were generally localized to the injured regions in the ipsilateral striatum and cortex, and were often in contact with some tissue that appeared viable. The scaffolds were observed to have open pores without apparent degradation of the scaffold struts. Cells from the surrounding tissue appeared to have infiltrated the scaffolds in relatively small numbers (Figure 3.9c). Many of the cells had morphology similar to that of macrophages in the surrounding tissue. Erythrocytes were also observed within the scaffolds (Figure 3.9d).

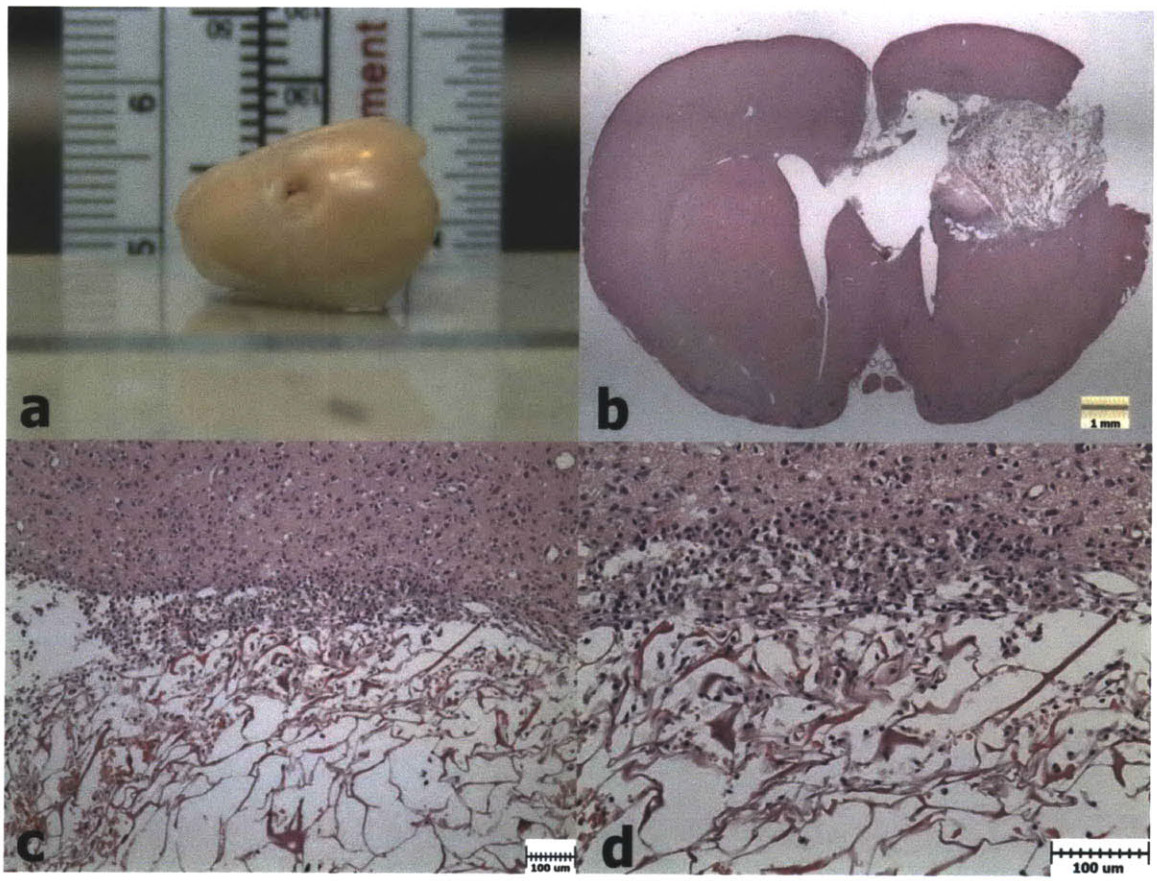

Figure 3.9. H&E Histology 1 Week after PBI and Scaffold Implantation (Group 2). a) Extracted brain showing a collagen scaffold in the PBI lesion. b) H&E histology showing the collagen scaffold within the PBI lesion. c) Cellular infiltration at the superior edge of the scaffold. d) Higher magnification view showing cells along the scaffold struts

Group 4 scaffolds were observed to be much smaller than the size of the lesion at 5 weeks, and did not come close to filling the volume of the cavity (Figure 3.10a and Figure 3.10b). The scaffolds were also poorly integrated into the surrounding tissue, with only a fraction of their surface areas contacting viable tissue. The scaffolds were found localized to the lateral aspect of the lesion, and in 2 cases were partially adhered to the inside of the skull. One of the adhered scaffolds was not recognized as such, and was lost

during extraction most likely due to inadvertently removing it with a portion of the skull. In the remaining 4 samples, the scaffold pores were open and there was some cellular infiltration which appeared qualitatively similar to Group 2 (Figure 3.10c and Figure 3.10d). The integrity of the scaffolds appeared to be maintained with no obvious signs of degradation present.

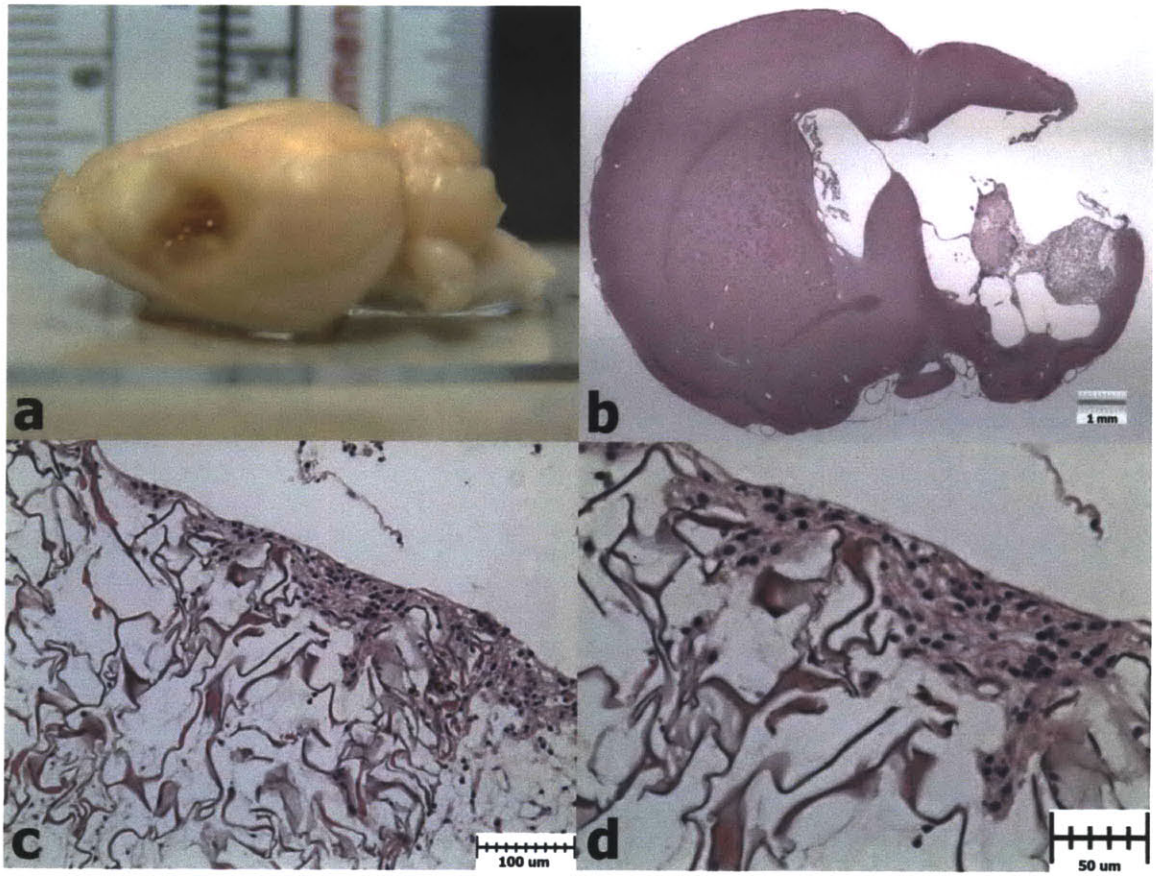

Figure 3.10. H&E Histology 4 Weeks after Scaffold Implantation (Group 4). a) Extracted brain with a collagen scaffold in the lesion site. b) H&E histology showing a collagen scaffold at the lateral edge of the PBI cavity. c) Cellular infiltration along the superior edge of the scaffold. d) Higher magnification image showing cells within the scaffold

3.3.4 Glial Scarring and Inflammation: GFAP, CS56 and CD68

GFAP staining showed reactive astrocytes surrounding the lesion in all groups. At 1 week (Group 1 and 2), GFAP reactivity was absent within much of the necrotic lesion while being primarily localized outside the collection of inflammatory cells within and bordering the necrosis (Figure 3.11). There was little GFAP reactivity seen within the scaffold in Group 2 (Figure 3.12).

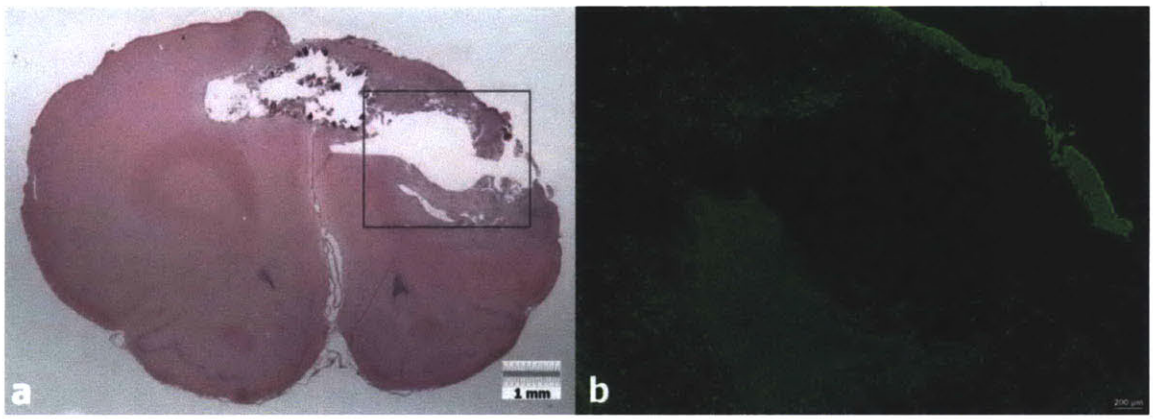

Figure 3.11. GFAP Staining Surrounding the PBI Lesion after 1 Week (Group 1). a) H&E histology showing a PBI lesion after 1 week. b) GFAP staining surrounding the lesion site.

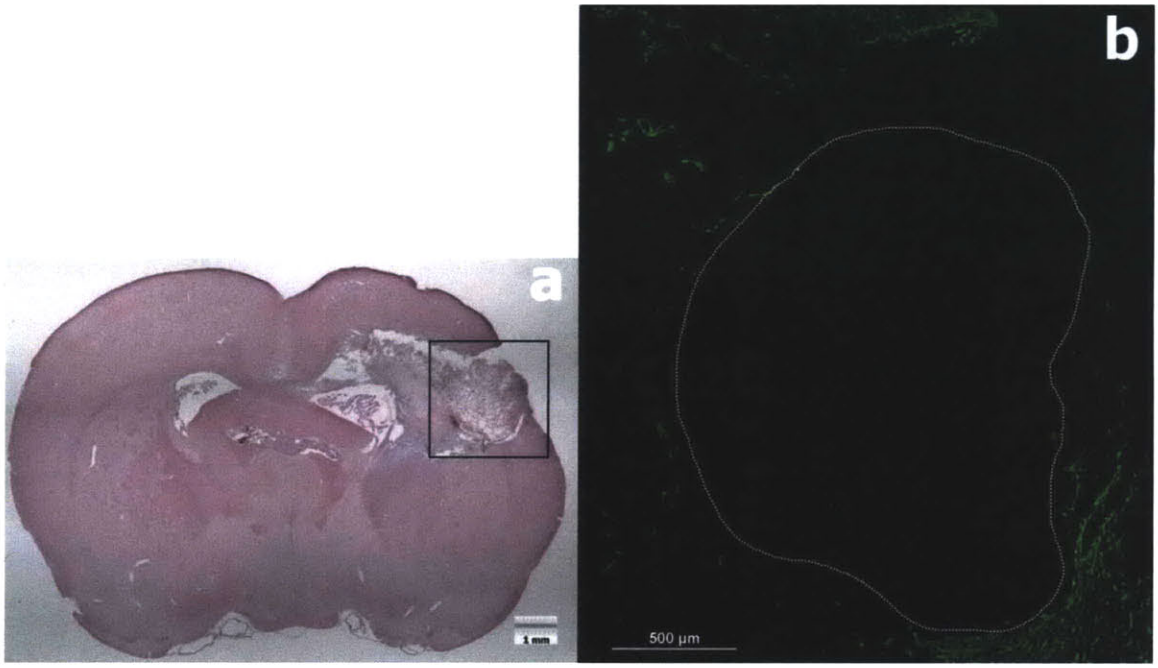

Figure 3.12. GFAP Staining Surrounding the Implanted Collagen Scaffold after 1 Week (Group 2). a) H&E image showing a collagen scaffold within the defect site after 1 week. b) GFAP reactivity surrounding the lesion, with very little staining within the scaffold.

At 5 weeks (Groups 3 and 4), GFAP reactivity bordered most of the cavity with a band of intense staining (Figure 3.13). There was, however, variability in the degree of gliosis surrounding the lesion at various locations. Figure 3.14 illustrates a relatively thick band of gliosis surrounding the cavity at a coordinate near the anterior boundary of the lesion. GFAP expression in Figure 3.14 also appears to be upregulated throughout much of the ipsilateral hemisphere, and not only in the immediately vicinity of the cavity. There were scattered GFAP positive cells at a low density within the scaffold of Group 4 (Figure 3.15).

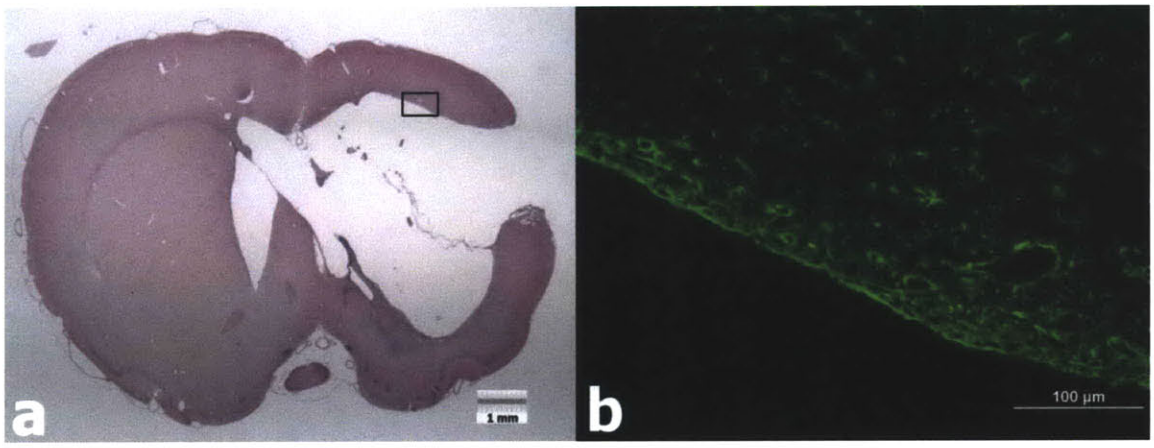

Figure 3.13. GFAP Reactivity Bordering the PBI Cavity at 5 Weeks (Group 3). a) H&E image of the PBI lesion after 5 weeks. b) GFAP reactivity along the superior edge of the cavity.

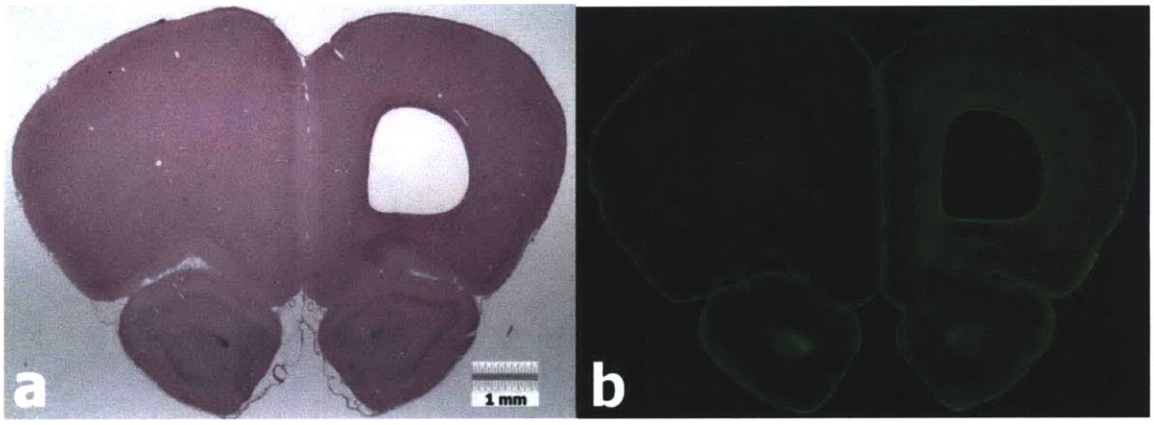

Figure 3.14. GFAP Reactivity Near Anterior Aspect of Lesion at 5 weeks (Group 3). a) H&E image of the anterior portion of the PBI cavity. b) GFAP staining bordering the cavity and extending throughout much of the ipsilateral hemisphere.

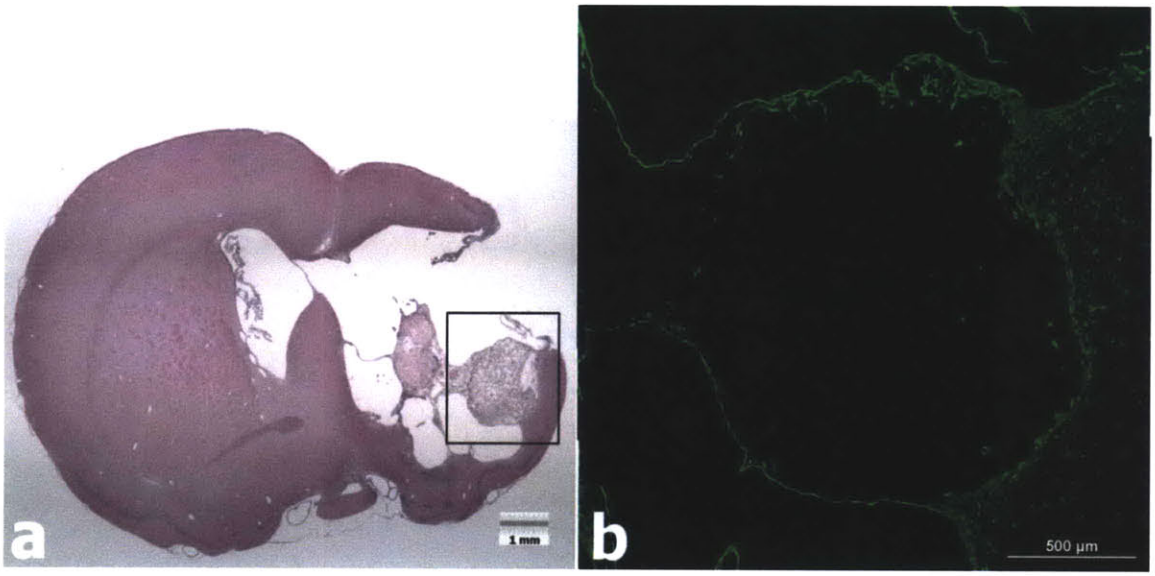

Figure 3.15. GFAP Reactivity Surrounding the Implanted Collagen Scaffold (Group 4). a) H&E histology showing an implanted scaffold. b) GFAP reactivity surrounding the lesion with a relatively small amount of staining within the scaffold

While the degree of GFAP reactivity within the scaffolds of Group 2 and Group 4 was low relative to the surrounding tissue, astrocytes could be detected along the scaffold struts at high magnification (Figure 3.16). The density of astrocytes in Group 2 was 12.1 ± 2.0 cells/mm^2, which was significantly less (p=0.053) than the density of 19.0 ± 2.1 in Group 4 (Figure 3.17).

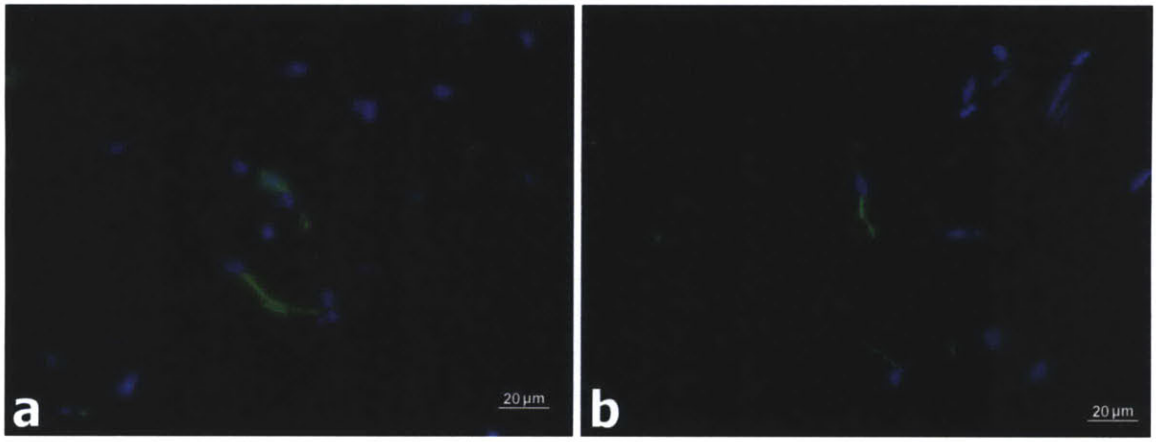

Figure 3.16. GFAP positive astrocytes within the collagen scaffolds of Group 2 and Group 4. a) Astrocytes within a scaffold after 1 week (Group 2). b) Astrocytes within a scaffold after 4 weeks (Group 4). Green: GFAP, Blue: DAPI

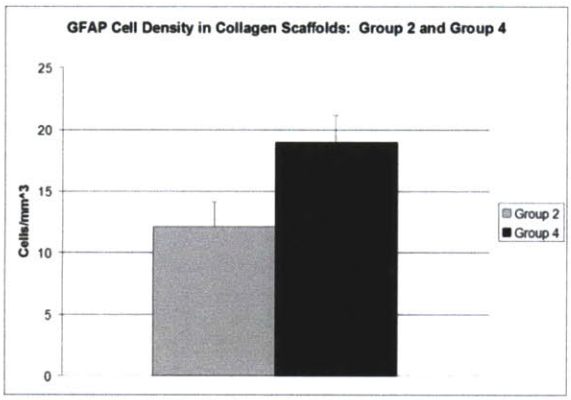

Figure 3.17. GFAP Cell Density in Collagen Scaffolds (Group 2 and Group 4). The density of astrocytes in Group 4 scaffolds was significantly greater than in Group 2 scaffolds (p=0.053).

CS56 staining showed relatively high background staining of the normal extracellular matrix, but also demonstrated increased staining around the border of the lesion (Figure 3.18).

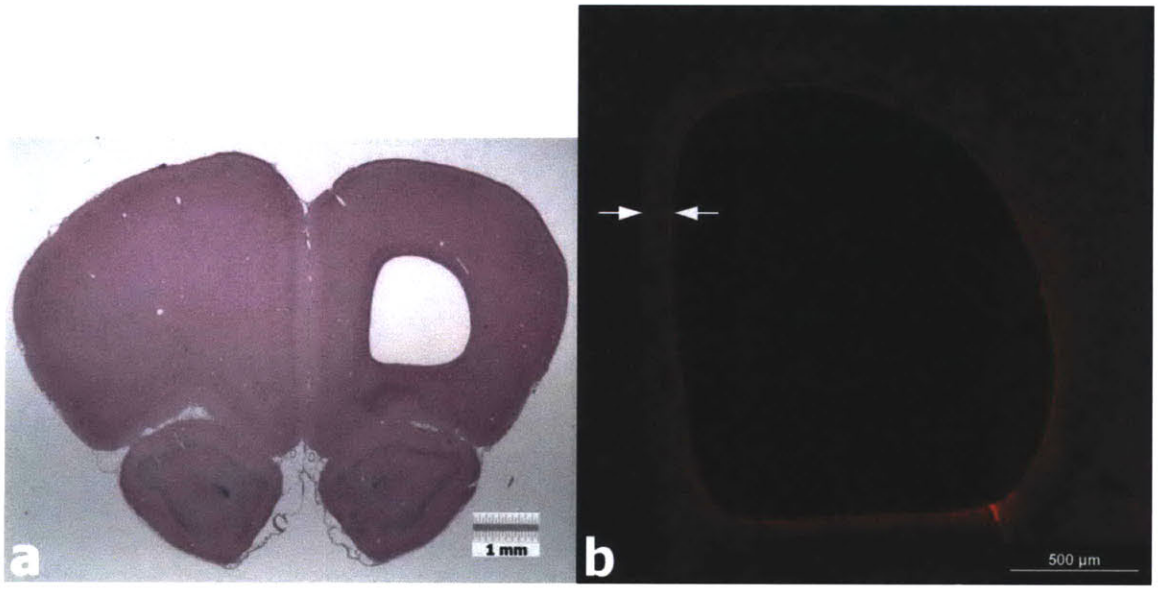

Figure 3.18. CS56 Reactivity Surrounding the PBI Lesion at 5 Weeks (Group 3). a) H&E image of a PBI lesion after 5 weeks. b) Increased CS56 reactivity bordering the PBI cavity.

CD68 staining confirmed the phenotype of many of the inflammatory cells as macrophages. Additionally, widespread reactivity could be observed throughout regions including the cortex, striatum, external capsule, and corpus callosum (ipsilateral and contralateral). The macrophage infiltrate was very dense at 1 week (Figure 3.19), while far fewer macrophages were observed at 5 weeks. However, at 5 weeks CD68 reactivity persisted both near the lesion and remotely in white matter tracts.

In Group 2 and Group 4, CD68 staining showed that many of the cells that had infiltrated the scaffold were macrophages. The density of CD68-positive macrophages in Group 2 scaffolds was 50.5 ± 7.2 cells/mm^2, while the density in Group 4 scaffolds was 39.0 ± 6.0 cell/mm^2. The difference was not statistically significant.

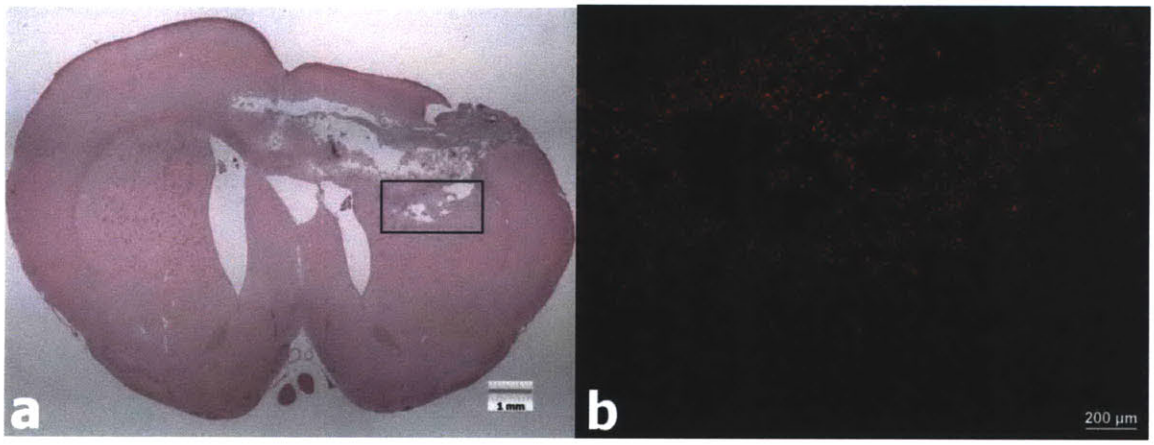

Figure 3.19. CD68 Staining of the PBI Lesion after 1 Week (Group 1). a) H&E image of a PBI lesion. b) Numerous CD68 positive macrophages in the lesion site at 1 week.

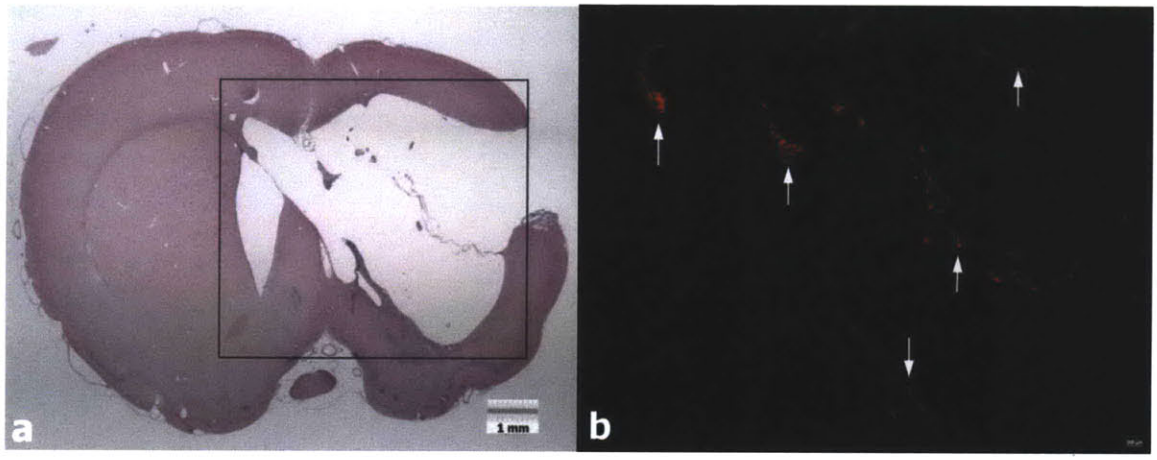

Figure 3.20. CD68 Staining of PBI Lesion After 5 weeks (Group 3). a) H&E image of a PBI lesion at 5 weeks. b) Reduced CD68 staining at 5 weeks relative to the lesion at 1 week. Staining is evident around the border of the lesion and in the small amount of remaining cellular debris.

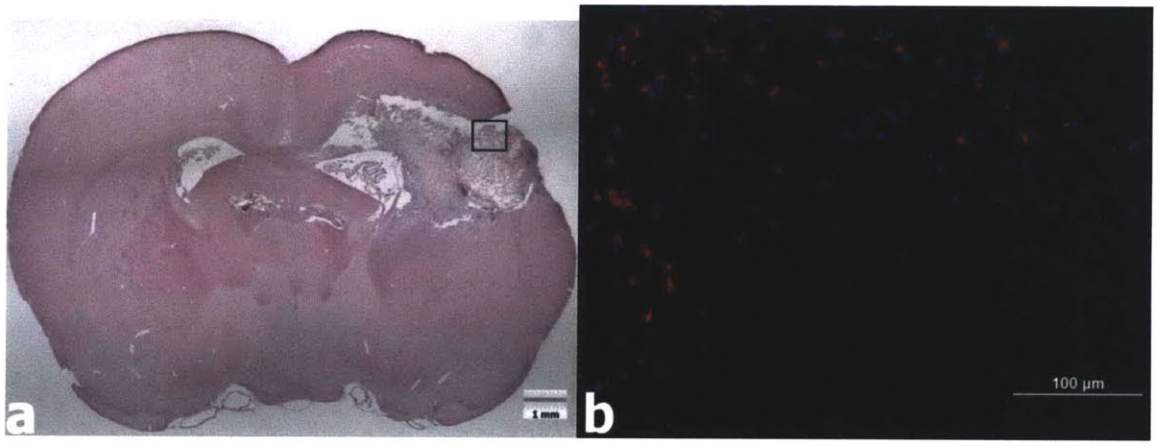

Figure 3.21. CD68 Staining within a collagen scaffold after 1 week (Group 2). a) H&E image of collagen scaffold within a PBI lesion after 1 week. b) CD68 staining of macrophages within the collagen scaffold (Red: CD68, Blue: DAPI)

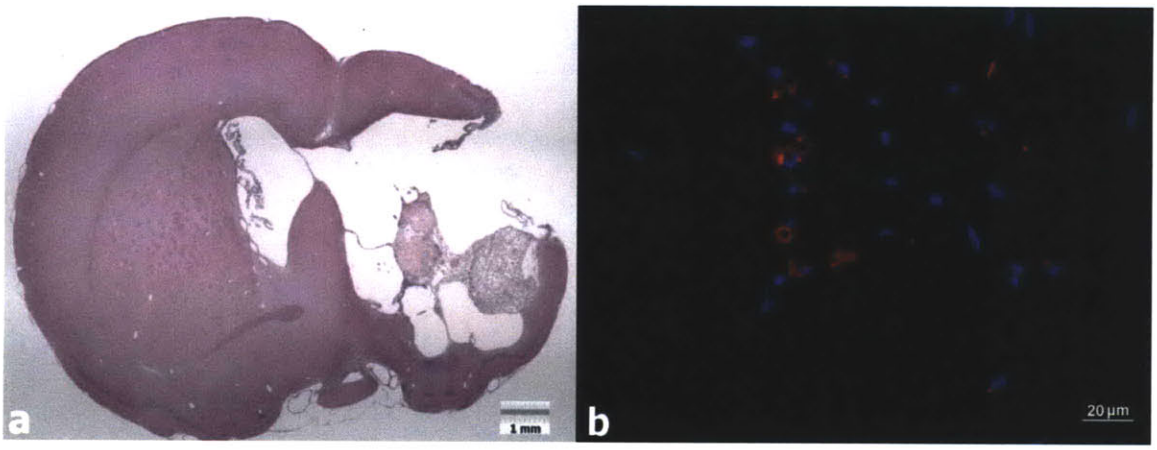

Figure 3.22. CD68 Staining within a collagen scaffold after 4 weeks (Group 4). a) H&E image of a collagen scaffold within a PBI lesion. b) CD68 staining of macrophages within the collagen scaffold (Red: CD68, Blue: DAPI)

3.3.5 Blood Vessels and Endothelial Cells: Von Willebrand Factor

VWF staining displayed many blood vessels within and surrounding the lesion site in response to the injury. At 1 week, vessels were present throughout the areas of necrosis (Figure 3.23), while at 5 weeks many vessels bordered the large lesion cavity (Figure 3.24). An occasional VWF positive cell or vessel was found within the scaffolds of Group 2 (Figure 3.25a), with density being 0.9 ± 0.4 per mm^2. A small number of VWF positive cells/vessels was also found in Group 4 (Figure 3.25b), with the density being 4.7 ± 2.1 per mm^2. The difference between Groups 2 and 4, however, did not reach statistical significance ($p=0.09$).

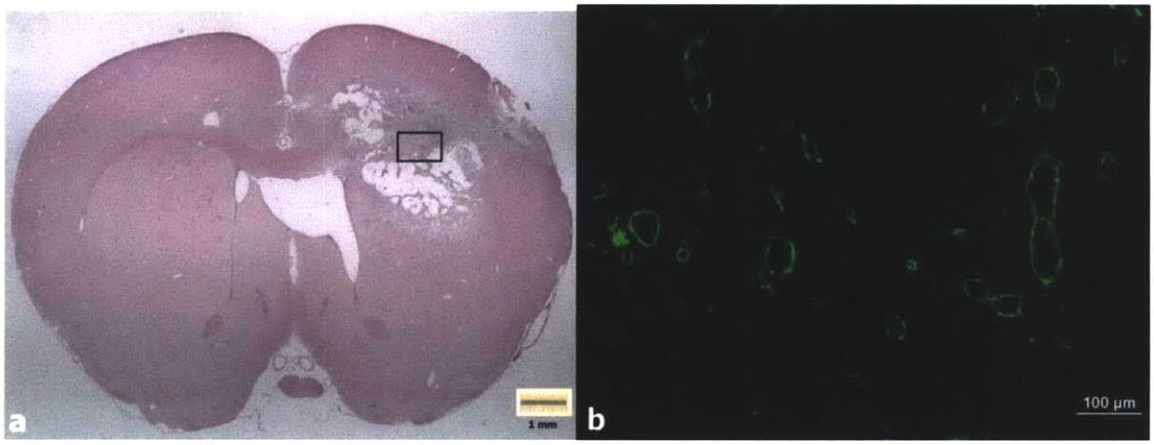

Figure 3.23. VWF staining of blood vessels within the PBI lesion after 1 week (Group 1). a) H&E histology of a PBI lesion after 1 week. b) Numerous VWF positive blood vessels in the lesion site.

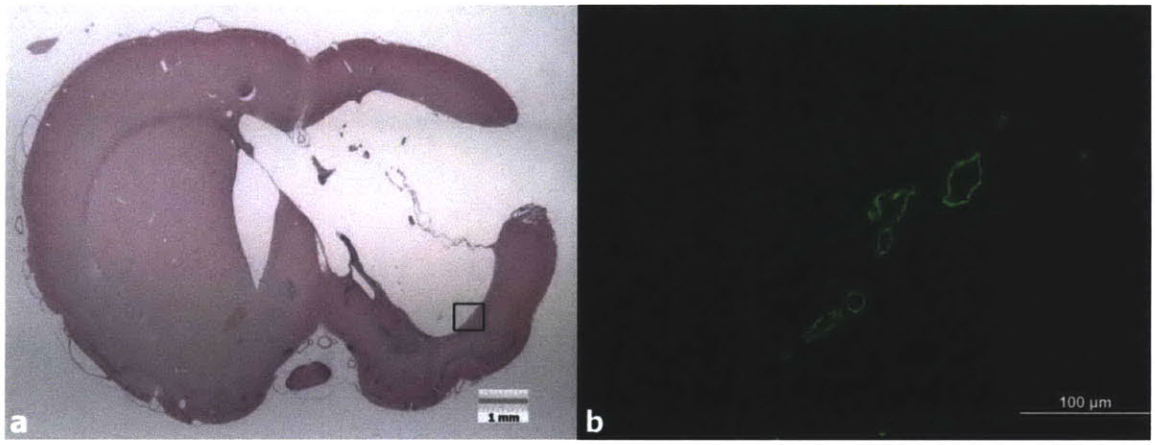

Figure 3.24. VWF staining of blood vessels bordering the PBI cavity after 5 weeks (Group 3). a) H&E image of a PBI lesion after 5 weeks. b) Blood vessels along the border of the PBI cavity.

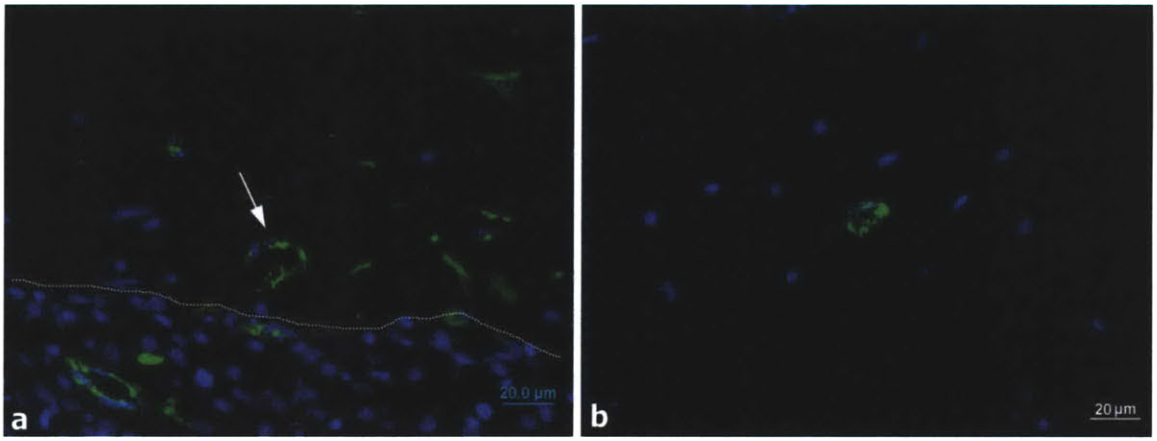

Figure 3.25. VWF staining in collagen scaffolds after 1 week (Group 2) and 4 weeks (Group 4). a) VWF positive cells/vessels in a collagen scaffold from Group 1. The approximate scaffold border is indicated with a white dotted line. b) VWF cell/vessel in a collagen scaffold from Group 4.

3.3.6 Neuronal Degeneration: Fluoro-Jade C

A large number of degenerating neurons were present in the thalamus 1 week after the injury in Groups 1 and 2. While individual neurons stained brightly (Figure 3.26c and Figure 3.26d), there was also diffuse reactivity throughout areas of neuropil and extracellular matrix (Figure 3.26b). Regions of the thalamus showing evidence of degeneration included the laterodorsal, mediodorsal, ventrolateral, ventromedial, ventral posteromedial, and ventral posterolateral nuclei. Additionally, white matter reactivity was present throughout much of the ipsilateral internal capsule. The positive staining of neuronal cell bodies was generally restricted to the ipsilateral hemisphere, though a few degenerating cells could also be found in the contralateral thalamus. Groups 1 and 2 looked qualitatively similar in terms of the regions and approximate number of cells that were degenerating.

At 5 weeks post-injury, far fewer FJC positive cells were observed in the relative to 1 week. Only a few scattered cells could be detected in the thalamus, though there was some persistent staining of the neuropil and extracellular matrix. Additionally, white matter reactivity in the internal capsule persisted.

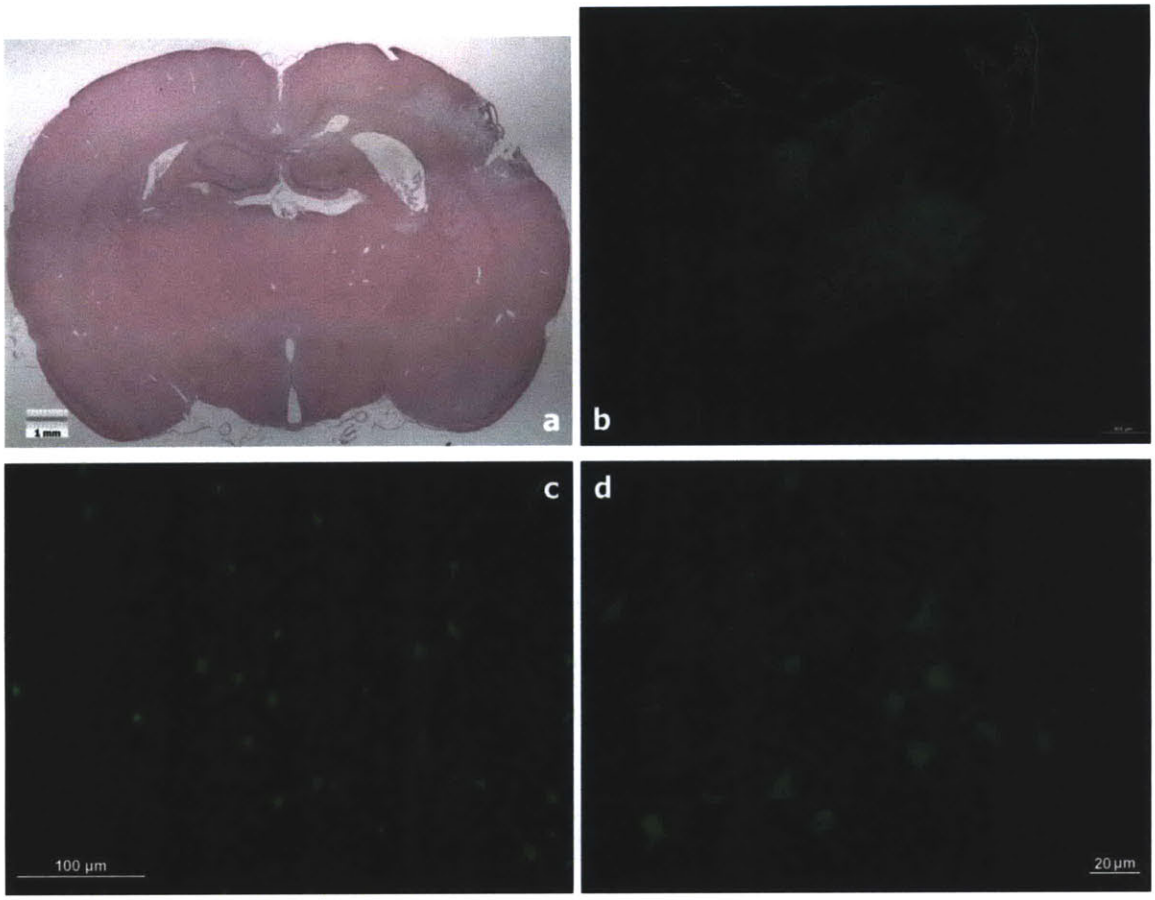

Figure 3.26. Fluorojade staining of degenerating neurons 1 week after PBI (Group 1). a) H&E section from Group 1 including thalamic nuclei. b) Low magnification Fluorojade C staining showing reactivity in the thalamus and internal capsule. c) Neuronal cell bodies in the thalamus staining positively. d) Higher magnification image of degenerating neurons in the thalamus

3.3.7 Oligodendrocytes and Myelinated Axons: CNPase

At 1 week, there was a distinct absence of CNPase staining in and immediately around the lesion site (Figure 3.27b). A clear discontinuity was observed in the corpus callosum (Figure 3.27b), a white matter structure that would normally pass through the lesion area. Superior regions of the striatum that would normally have white matter bundles also showed an absence of staining. More inferior areas of the striatum showed preserved, but abnormal staining of white matter bundles. Relative to the contralateral hemisphere

(Figure 3.27d), the damaged white matter appeared to be filled with circular areas that did not stain (Figure 3.27e). Farther from the lesion, the CNPase staining regained an appearance similar to the contralateral hemisphere.

At 5 weeks, with most of the necrotic tissue of the lesion cleared, CNPase staining was observed around the borders of the lesion area (Figure 3.28b). In some cases CNPase positive axons traversed a path immediately along the edge of the cavity and possibly overlapping with areas of gliosis (Figure 3.28c).

While no CNPase staining was observed within the borders of the scaffolds in Groups 2 (Figure 3.29b) and 4 (Figure 3.30b), the CNPase staining did pass directly along the scaffold edges in some cases.

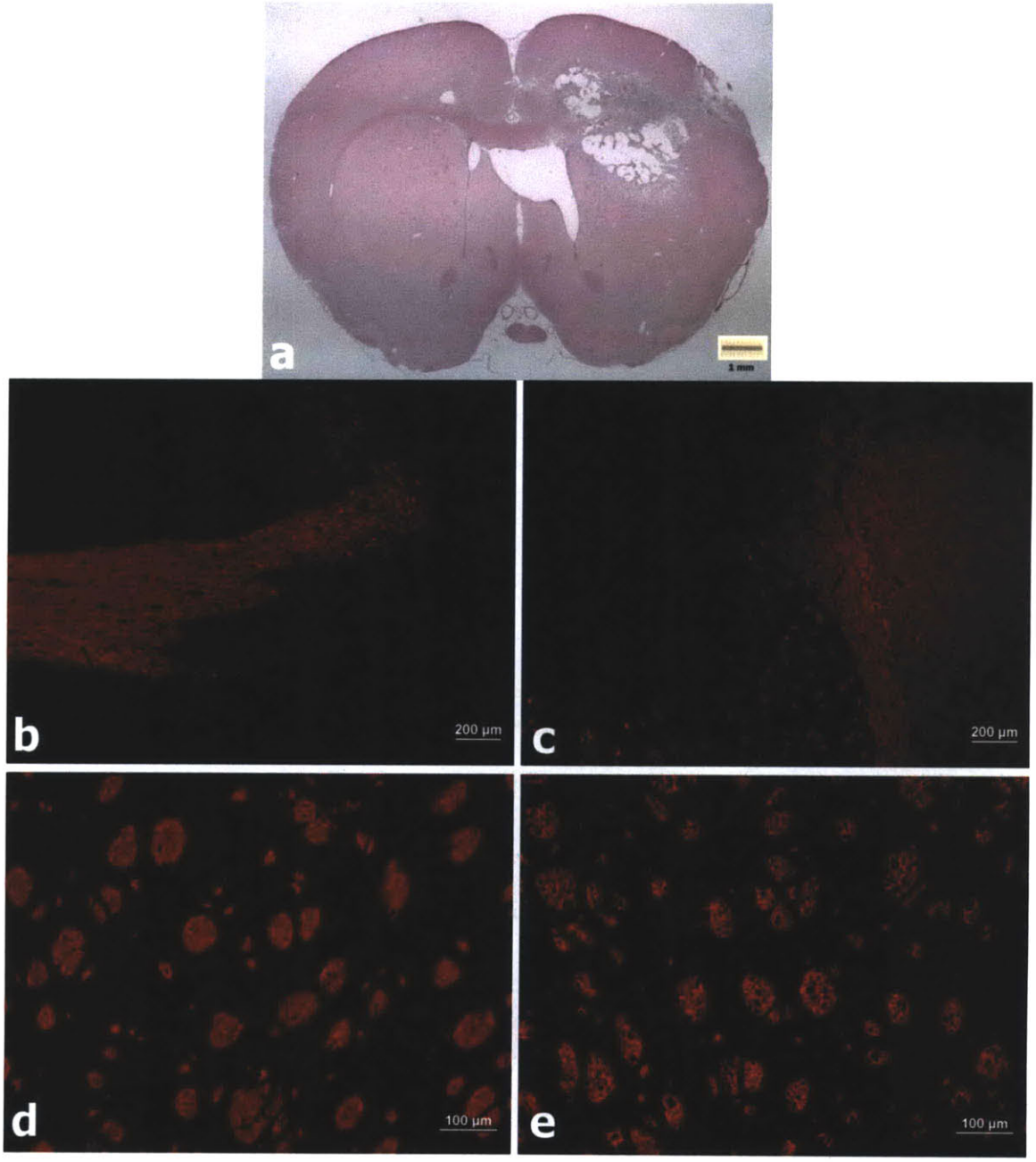

Figure 3.27. CNPase staining 1 week after PBI (Group 1). a) H&E histology of a PBI lesion after 1 week. b) Discontinuity of CNPase staining in striatum. c) Discontinuity of CNPase staining in corpus callosum. d) Normal striatum in the contralateral hemisphere. e) Damaged striatum in ipsilateral thalamus.

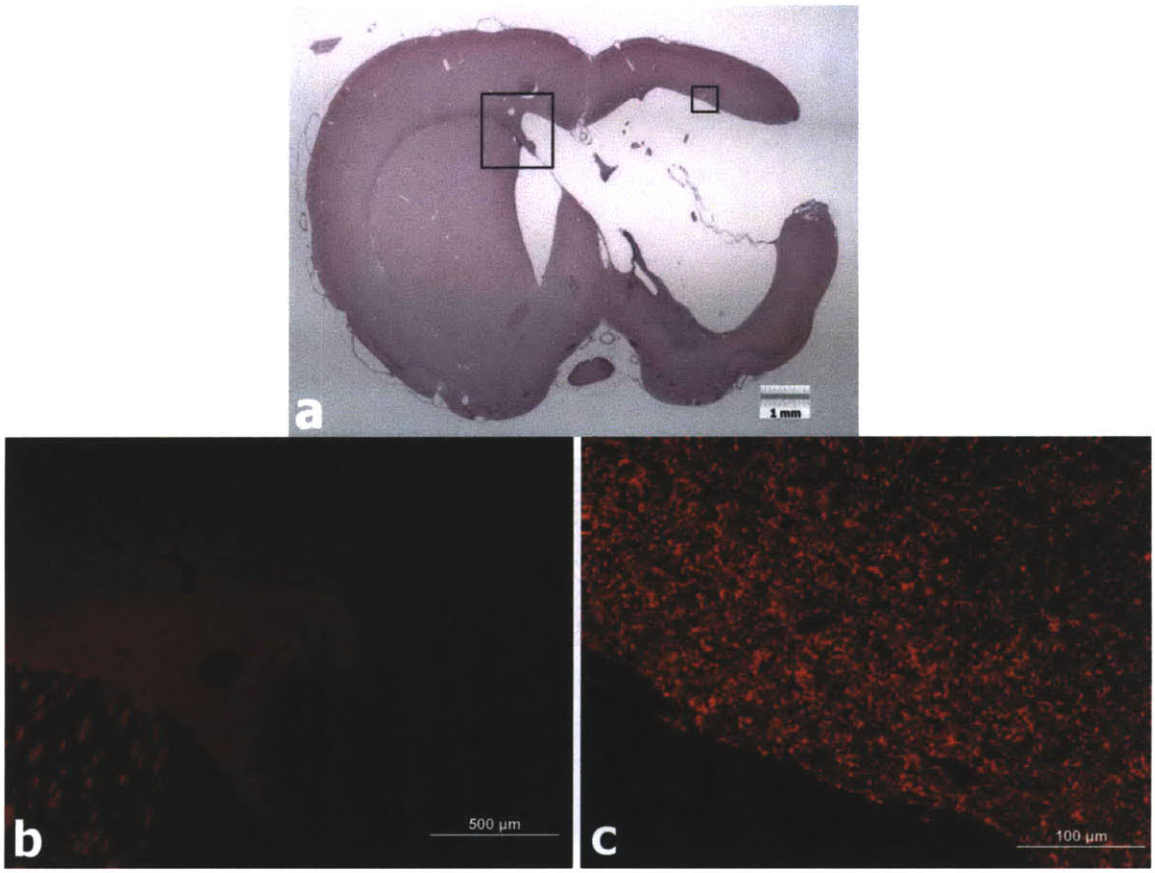

Figure 3.28. CNPase staining 5 week after PBI (Group 3). a) H&E histology of a PBI lesion after 5 weeks. b) Discontinuity of CNPase staining in the corpus callosum. c) CNPase staining along the superior edge of a PBI lesion

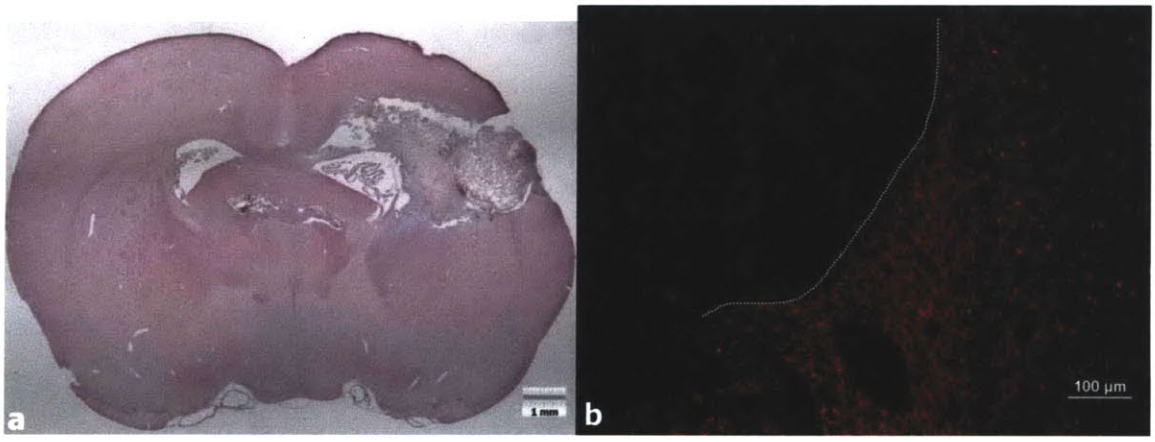

Figure 3.29. CNPase staining surrounding a collagen scaffold after 1 week (Group 2). a) H&E histology showing a collagen scaffold in a PBI lesion after 1 week. b) CNPase staining along the border (white line) of a collagen scaffold at 1 week.

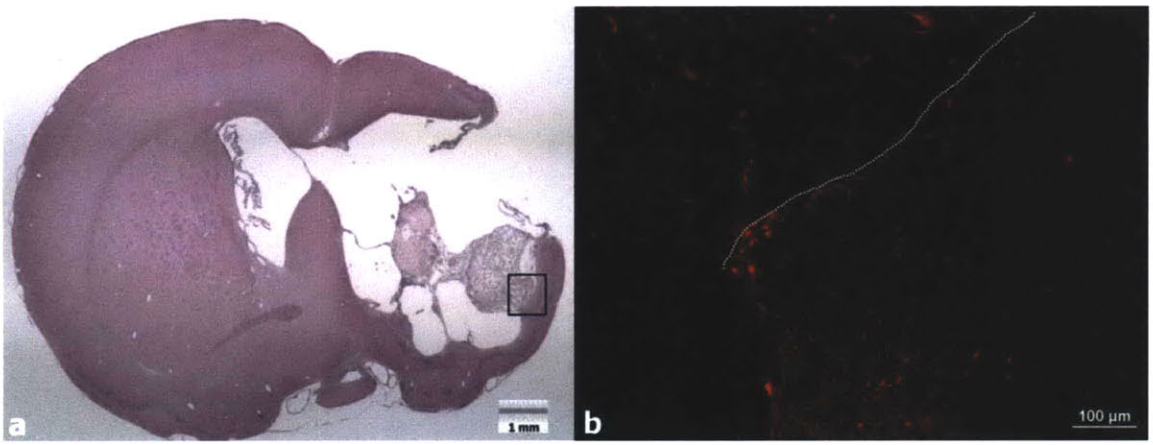

Figure 3.30. CNPase staining at the border of a collagen scaffold after 4 weeks (Group 4). a) H&E histology of a collagen scaffold in the PBI lesion after 4 weeks. b) CNPase staining near the border (white line) of a collagen scaffold.

3.3.8 Post-mitotic Neurons: NeuN

1 week after injury, no NeuN positive neurons could be detected within the lesion site (Figure 3.31b). The neuronal loss was found mainly in the striatum, though it extended to cortical layers in certain areas. After 5 weeks, NeuN positive neurons could be detected in close proximity to the border of the PBI cavity (Figure 3.32b).

No neurons could be detected in the scaffolds of Group 2 and Group 4. In Group 2, there was a significant area of necrosis separating the areas of NeuN staining from the scaffold in many places (Figure 3.33b). In Group 4, areas were observed in which neurons were located closer to the scaffold border (Figure 3.34b).

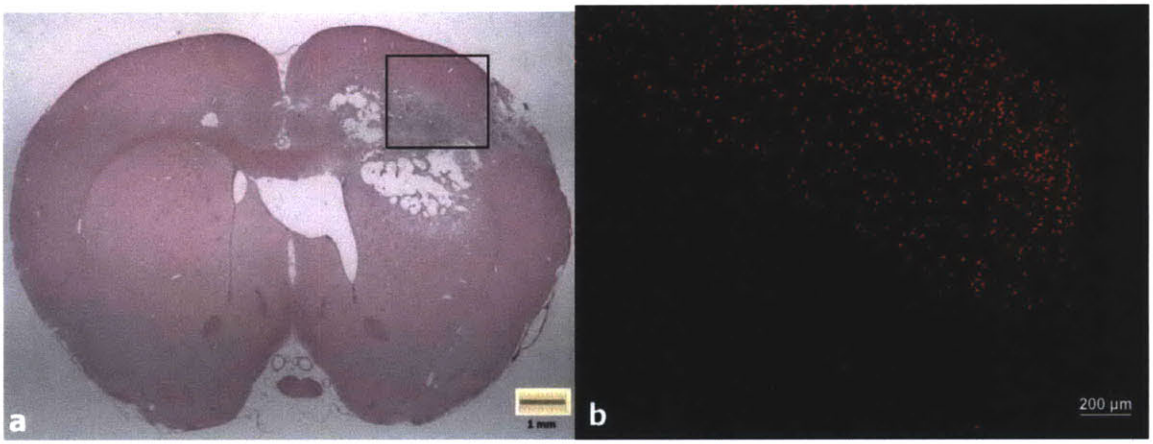

Figure 3.31. NeuN staining near the PBI lesion after 1 week (Group 1). a) H&E image of a PBI lesion after 1 week. b) NeuN staining extending from the border of the PBI lesion into the viable cortex. There is a complete absence of staining within the lesion.

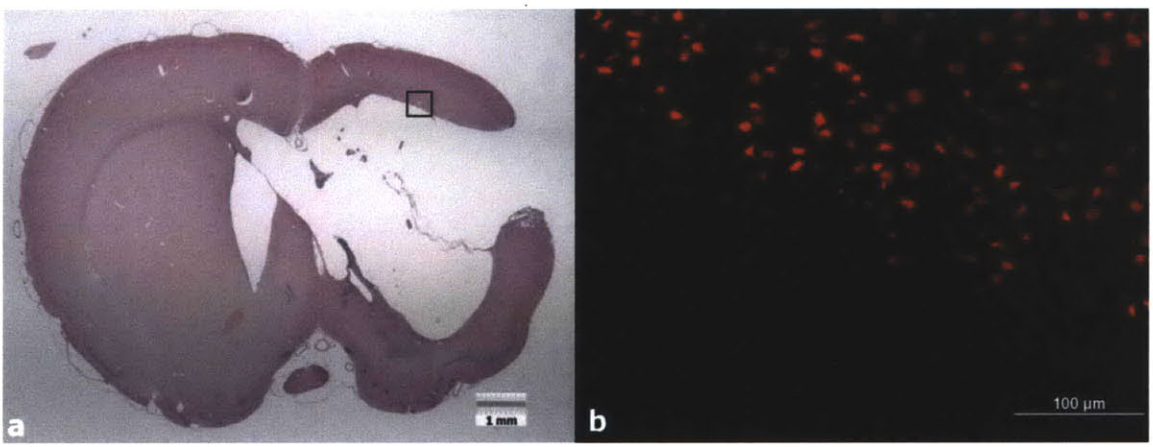

Figure 3.32. NeuN staining bordering the PBI lesion after 5 weeks (Group 3). a) H&E image of a PBI lesion after 5 weeks. b) NeuN positive neurons in close proximity to the cavity border.

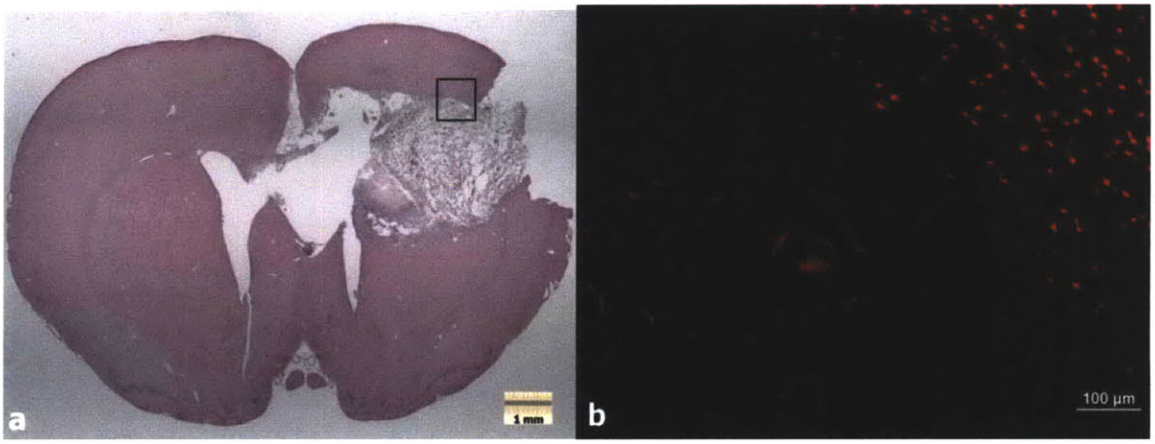

Figure 3.33. NeuN staining near a collagen scaffold after 1 week (Group 2). a) H&E image of a collagen scaffold within a PBI lesion after 1 week. b) Absence of NeuN staining within the collagen scaffold.

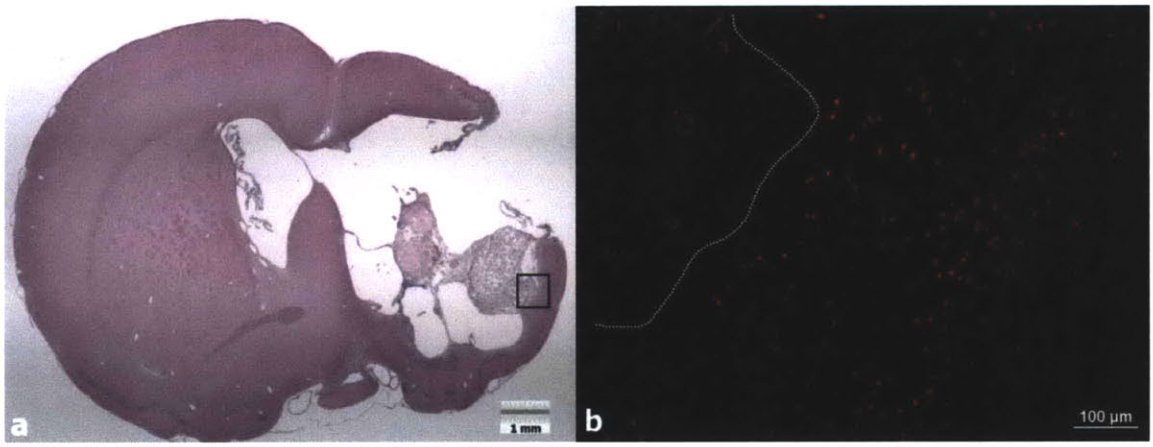

Figure 3.34. NeuN staining bordering a collagen scaffold after 4 weeks (Group 4). a) H&E image of a collagen scaffold within a PBI lesion after 4 weeks. b) NeuN positive neurons near the edge (white line) of a collagen scaffold.

3.3.9 Neural Progenitors: Doublecortin

Cells staining positive for Doublecortin were observed in the vicinity of the lesion, particularly in areas close the lateral ventricles. In Group 1 (Figure 3.35b) and Group 3 (Figure 3.36b), DCX positive cells could be observed in some cases to have migrated from the subventricular zone to the medial border of the PBI lesion. The proximity of the lesion site to the subventricular zone seemed to be the main determinant of whether DCX positive cells were located in the lesion. While DCX positive cells could be also be found near the lesion sites of Groups 2 and 4, no DCX positive cells were observed within the collagen scaffolds.

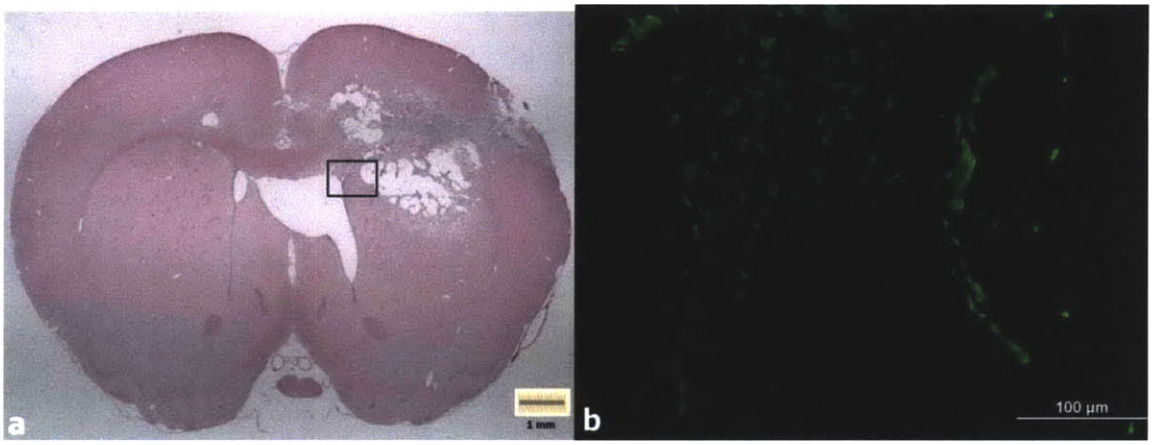

Figure 3.35. Doublecortin staining near the medial border of a PBI lesion after 1 week (Group 1). a) H&E image of a PBI lesion after 1 week. b) DCX positive cells spreading from the subventricular zone to the medial border of the PBI lesion.

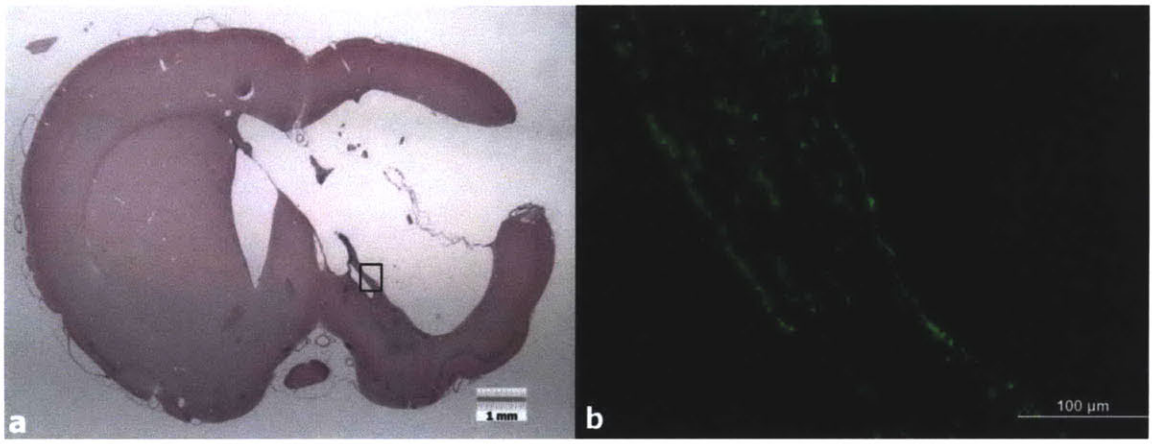

Figure 3.36. Doublecortin staining near the medial border of the PBI cavity after 5 weeks (Group 3). a) H&E image of a PBI lesion after 5 weeks. b) DCX positive cells along the medial border of the PBI cavity.

3.4 Discussion

Despite the extent of the bilateral penetrating brain injury, the rate of survival among the rats was relatively good. Following the initial trauma of the injury, the surviving animals recovered very well and after several days typically displayed no problems with

ambulating, eating, or grooming. The absence of mortality during or after the scaffold implantation was important in establishing the safety of the procedure, and also safety of the implanted material over the time course studied.

Many general characteristics of the lesion 1 week after injury were similar to those reported for the unilateral frontal injury [40], as would be expected. However, some differences were also noted beyond what might be expected simply due to the difference in the anatomical location of the injury. In particular, previous work with the frontal injury has noted that most necrotic tissue is cleared by one week, leaving the permanent cavity in the brain. In contrast, we have found that at 1 week in the bilateral injury, there remains an abundant amount of necrotic tissue still in the process of being cleared by macrophages. We have found that by 5 weeks, the cavity appears well formed with most, but not all, debris cleared. In addition, the entire lesion appears to grow significantly beyond its size at 1 week, with the 5 week lesion being 28% larger. It is noted that the animals surviving for 5 weeks in Group 3 underwent sham surgery at 1 week, which could have caused additional damage resulting in a larger lesion. Any such additional injury from the sham surgery was expected to be very small relative to the PBI. This is supported by previous work comparing the PBI to various surgeries involving insertion of the probe without inflating the balloon [40]. Minimal injury was found in those procedures, which themselves were much more severe than the sham surgery we conducted.

The time course of clearance of necrotic debris and cavity formation is important in determining the appropriate size for a biomaterial, as well as the time of implantation. Further, a particular therapeutic agent delivered may only be suitable for implantation at a

particular time point. For example, certain neuroprotective agents would likely need to be delivered very shortly after the injury to have maximum efficacy in sparing viable tissue [124]. However, the use of a biomaterial at an early time point may be precluded by the lack of space in the lesion, as the permanent cavity has not yet formed. While a material can be implanted shortly after an injury, it may not fill the cavity after several weeks *in vivo*. An early time point also may not be appropriate for cellular therapies, given that the hemorrhage and cellular debris of the injury environment are cytotoxic [125].

Implantation at a later time point allows for the cavity to form, and thus for the biomaterial to fill it. The injury environment may be more hospitable for cellular therapies or pharmacological agents intended for axonal regeneration. The major drawback of delayed intervention is that the injury will progress uninhibited during the period between the injury and the therapy. The potential for limiting the damage of the injury is thus greatly reduced.

In either case, the possibility for combinatorial therapeutic approaches still exists. A neuroprotective pharmacological agent could be administered peripherally shortly after injury, with biomaterial and/or cellular agents delivered surgically at a later time.

In the choice of a biomaterial size, it should be noted that there is a significant risk of damaging viable tissue if a large material is forced into the brain lesion before a suitable cavity is available. To address this issue for small and large materials alike, the mechanical properties of the material should be taken into account. Using a soft material with characteristics reasonably similar to brain tissue may help to reduce the risk of damage during implantation. With an appropriate material, one might implant a large,

but soft, material into a small cavity such that the material will expand to continue to fill the cavity as it grows larger. We have recently conducted a study of viscoelastic mechanical properties of collagen scaffolds in order to help in selecting appropriate scaffolds for future *in vivo* implantation experiments.

The reactive gliosis observed after the bilateral injury was notable in comparison to published studies of the unilateral frontal injury. In particular, it has been reported that GFAP upregulation after PBI peaks around 3 days and returns to a level of very low reactivity by 7 days [42]. We have found that in the bilateral injury, the reactive gliosis persists at high levels at 7 days, and appears to be upregulated in both hemispheres even at 5 weeks post-injury. The increased severity of a bilateral injury relative to the frontal injury may be a possible explanation for the difference. With a larger volume of tissue damaged, it is not surprising that the extent of GFAP upregulation may be increased as the astrocytes surround the injury and isolate it from the rest of the brain. The persistent upregulation at 5 weeks is somewhat surprising, but is consistent with the timescale observed for the lesion to progress to a well-defined cavity largely free of necrotic tissue.

The relatively small number of astrocytes detected within the scaffolds is interesting in that some studies using scaffolds in the brain have reported astrocytes as a major component of cellular infiltration [126-131]. For example, a study using a gelatin-siloxane hybrid material reported 5 times as many astrocytes as microglia/macrophages within the scaffold after 60 days [126]. Implantation of a hyaluronic acid-poly-D-lysine copolymer hydrogel also resulted in more astrocytes relative to macrophages at time points of 1, 3, and 6 weeks [127]. However, our study and others indicate a wide variability in the degree of astrocyte infiltration into materials implanted in the brain [33,

132-135]. This may be attributable to factors such as the injury model, the implantation time, the duration of the study, and obviously the material composition of the scaffold. While many of the studies have used synthetic materials or a combination of natural and synthetic, one group used a collagen scaffold fairly similar to the one in this study [133]. It was found that a 2% collagen scaffold was surrounded by regions of gliosis after 1 month, but that astrocytes largely did not infiltrate the scaffold. Although we observed a larger degree of astrocyte infiltration in our work, the predominance of macrophages in the scaffold relative to astrocytes is consistent between the two studies. It can be concluded that astrocytes do not seem to have a strong affinity for type I collagen as a substrate *in vivo*.

Astrocyte infiltration is of significance in part because it has been suggested that a scaffold may modify the formation or persistence of a glial scar [33, 127, 128, 134]. By encouraging astrocytes to move into the lesion and away from the border, one might prevent organization of the cellular and extracellular matrix barrier that inhibits axonal regeneration. This reduction of the glial scar would ostensibly facilitate regeneration of axons and migration of endogenous or exogenous cells to repair the damaged region. Given the complexity and existing ambiguity of the astrocyte response to injury, such a presumption is questionable. It has been shown that eliminating the astrocyte response following injury actually has deleterious, rather than beneficial effects [35, 36, 136]. While reducing gliosis in the long term may in fact reduce inhibitory factors blocking axonal regeneration, is it not clear whether partially blocking the short-term response of reactive astrocytes would have therapeutic benefit.

The ring of CS56 upregulation surrounding the lesion cavity is consistent with previous reports of the glial scar composition [30, 137]. Cleavage of chondroitin sulfate proteoglycans remains a target for regenerative therapies, as delivery of chondroitinase ABC has been shown to allow for increased axon growth after injury [31, 138]. Delivery of chondroitinase using a collagen scaffold is one such possibility for administration of therapy.

CD68 staining illustrated the massive macrophage response to the injury after 1 week, along with the decreased, but persistent presence at 5 weeks. In the normal rat brain, CD68 staining is virtually entirely negative. In the short term after injury, the macrophage response is likely due to both resident microglia and peripheral monocytes that enter when the blood-brain barrier loses integrity. Resident perivascular monocytes in the brain also play a role. At 5 weeks, however, the blood brain barrier has likely been restored. The presence and distribution of macrophages at this time point suggests that they may be more likely of microglial origin.

Many of the cells present in the collagen scaffold after 1 week were CD68 positive macrophages. The cells in the scaffold did not appear to be engaging in a particularly robust foreign body response, as no multinucleated giant cells were detected. Rather, it may be that the cells were responding to the necrotic debris in and around the area, which to some degree entered the scaffold. Red blood cells, for example, could be observed within the scaffold and various macrophages appeared to be phagocytosing them. The cellular reaction to the scaffolds at 4 weeks was not different in terms of the density of macrophages. Similar to the case with astrocytes, there is wide variability in reported macrophage infiltration among previous studies [128, 133]. No authors report

an explicit absence of macrophages, while nearly all mention the definite or likely presence of macrophages among the cells within the biomaterials [33, 126-134]. Our results and previous published studies emphasize that macrophages are likely to respond to virtually any material implanted into the brain. Macrophages can play a beneficial role if they a participate in degrading a biomaterial along a desired time frame. Ideally, the degradation of the material will be accompanied by synthesis of new tissue at a similar rate. In the brain, this synthesis of new tissue could refer to a deposition of vascularized extracellular matrix that could serve as a substrate for endogenous or exogenous cells to repopulate a lesion site. The extent of the macrophage response is also important due to the complex role that these cells can play in mediating inflammation, survival, and even regeneration among neural cells. Further, an excessive macrophage response consisting of uncontrolled proliferation and formation of giant cells can have deleterious effects [139].

The decrease in degenerating neurons in the thalamus from 1 week to 5 weeks reflects the stabilization of the lesion. Given that the balloon expanded mostly in the ipsilateral hemisphere, it is not surprising that most of the degenerating neurons would be found in the ipsilateral thalamus. The relative lack of positive staining in the contralateral hemisphere indicates that the damage caused by the probe in the right hemisphere was small in comparison to the balloon expansion in the left hemisphere. White matter reactivity in the internal capsule and corpus callosum suggest the possible presence of axonal damage persisting long term. This is consistent with the fact that Wallerian degeneration in the CNS occurs much slower that in the peripheral nervous system [140].

The pattern of NeuN at 1 week reveals the extent of the injury and begins to inform about where the lesion ends. Similarly, the areas of CNPase staining at 1 week give an idea of where the white matter structures have maintained or lost integrity. In injured or damaged axons, CNPase is one of the first proteins lost. Therefore its presence 1 week after the injury suggests largely viable myelinated axons. At 5 weeks, NeuN and CNPase staining give a clear picture of how close to the cavity border the viable neurons and oligodendrocytes localize. In some areas, there appears to be overlap between the glial scar and CNPase staining. Given that elements of the glial scar are inhibitory for regenerating axons, it is likely that this white matter is spared rather than regenerated. It is interesting to note, nonetheless, that the presence of dense GFAP positive regions of glial scar does not preclude functional axons from traveling through it. It is also revealing to observe the distortion of normal anatomic organization in response to the large brain cavity. In particular, areas of the corpus callosum traverse a path that goes much farther in the superior direction on the left side than that less injured right side.

The lack of NeuN or CNPase positive cells in the scaffold at 1 week is not surprising. The small scaffold in the middle of the large lesion had little opportunity to come in contact with viable tissue from which neurons or oligodendrocytes might migrate. Similarly, at 5 weeks the scaffolds were dwarfed by the size of the lesion and there would be little chance of a regenerative response taking place in them. While previous studies have noted some small amounts of staining for neurites and axons within implanted biomaterials [33, 128, 129, 134, 141], these results do not appear to be indicative of a robust regenerative response.

The apparent increase in vascularity surrounding the lesion is consistent with the infiltration of macrophages and subsequent remodeling to create the PBI cavity. Although there were only few vessels and/or endothelial cells observed inside the collagen scaffolds, the numerous vessels surrounding them are an important observation. In order for a cellular therapy to be successful, there will certainly need to be a vascular supply present in order for the cells to remain viable for any significant period of time. With the knowledge that an implanted scaffold will develop vascularity surrounding and potentially inside it, the delivery of cells becomes a possibility. Based on the time frame for vascularization, one could potentially implant the scaffold and then deliver the cells via a targeted injection at a later time. Despite the limited vascularization in this study, It is also noted that increased vascularization within the scaffold might be possible with a larger scaffold that better fills the lesion. Studies using other biomaterials have reported vascularization of the implanted scaffolds when they are in contact with the surrounding tissue [33, 127-129, 132, 135]. A comparison with the collage scaffold work of Nakada et al. [133], shows a similar degree of vascularization. Group 4 scaffolds in our work had a density of 4.7 ± 2.1 vessels per mm^2 after 4 weeks *in vivo*, compared with 0.6 ± 0.4 per mm^2 in that study after 1 month. Addition of adipose derived stromal cells in their work resulted in an increased vessel density of 4.6 ± 1.2 per mm^2.

The presence of DCX positive neural progenitors near the lesion site may also be of benefit in the application of new thereapeutic approaches. While the doublecortin positive cells were not found in the scaffolds, they were in the vicinity of the injured areas. In regions of the injury near the subventricular zone, it appeared as though DCX positive cells migrated towards the lesion. DCX positive cells could be seen along the

border of the lesion and within the edges of the cavity. The fate of progenitors from the subventricular zone has been studied in stroke models, where it was revealed that DCX positive neuroblasts can migrate to the damaged striatum and express markers of medium spiny neurons [142-144]. While many of these cells undergo apoptosis, some are thought to survive with functional integration [145]. Cells from the subventricular zone have also been noted to proliferate and migrate to injured regions followed traumatic brain injury [146-149]. Although the fate of some subventricular zone cells appears to be astrocyte differentiation with contribution to glial scarring, it is not clear whether DCX positive cells are among these [146]. DCX positive cells may have a capacity to replace striatal neurons as in stroke, but it is unclear whether they could potentially replace lost cortical neurons [149]. A scaffold delivering a chemoattractant such as stromal derived factor 1 (SDF-1) [150] or stem cell factor (SCF) [151] might improve recruitment of the progenitors to the lesion site and scaffold.

This work has provided a histological characterization of a bilateral penetrating brain injury and examined similarities and differences in comparison to published work with a frontal unilateral injury. The progression of the lesion from 1 week to 5 weeks has also been described, with a notable increase in the size of the lesion and brain cavity. This information contributes to an understanding of the pathophysiology of penetrating brain injury, but also provides guidance in the development of a therapeutic approach using biomaterials. Based on our initial work implanting a 3 mm diameter collagen scaffold in the PBI lesion, we have seen that the scaffold must be significantly larger in order to fill the PBI cavity after several weeks. Further, it is noted that cellular

infiltration of the scaffolds after 1 week and 5 weeks consists mostly of macrophages, although astrocytes, and endothelial cells are also present.

Acknowledgements

We thank Dr. Kimberly Leite-Morris and Rahmat Cholas for valuable assistance with the initial animal surgeries and surgical photographs. We also thank Alix Weaver for assistance with the hematoxylin and eosin staining.

Chapter 4: Treatment of Penetrating Brain Injury in a Rat Model Using Collagen Scaffolds Loaded with Soluble Nogo Receptor

4.1 Introduction

Injuries to the brain caused by trauma, cerebrovascular events, and certain neurodegenerative diseases lead to necrosis and permanent loss of brain parenchyma [152]. These brain lesions persist in the long term due to intrinsic cellular growth limitations and extrinsic inhibitory factors in the injury environment that together prevent robust structural regeneration [1]. Among the most potent of these inhibitory factors are proteins found in normal myelin which are released as myelinated axons degenerate [153, 154]. The myelin proteins Nogo [155], myelin associated glycoprotein (MAG) [156], and oligodendrocyte myelin glycoprotein (OMgp) [157] have been identified as major inhibitory factors in the CNS injury environment which induce acute growth cone collapse of regenerating axons. It has also been shown that all three proteins bind to Nogo Receptor 1 (NgG1), initiating cytoskeletal rearrangement through the Rho/ROCK pathway [158]. A variety of therapeutic strategies have been devised to disrupt this process following brain and spinal cord injuries including: antibodies against the myelin proteins and NgR1, siRNA knockdown of NgR1, vaccines against myelin proteins, and intracellular agents to disrupt the Rho/ROCK pathway [68]. Another approach is the use of a recombinant soluble Nogo receptor (sNgR) molecule aimed at preventing the myelin proteins from reaching NgR1 on the cell surface [159]. sNgR has the advantage of targeting all three myelin proteins simultaneously, while avoiding cytotoxicity and other problems associated with intracellular agents that much cross the cell membrane. Additionally, it has recently been shown that the myelin proteins can inhibit axon growth through the binding of an independent receptor, paired immunoglobulin-like receptor B (PirB) [23]. Application of sNgR can thus block the effects of the myelin proteins by

preventing them from reaching cellular NgR1, PirB, or any other unknown receptors for which they may have affinity. Delivery of sNgR is thus the focus of this study.

In addition to showing efficacy in blocking myelin proteins *in vitro*, sNgR has been used in *in vivo* studies of spinal cord injury and stroke [160-163]. Functional, electrophysiological, and histological improvements were noted upon administration of the protein for several weeks.

Unfortunately, therapeutic agents directed at central nervous system pathology face the obstacle of the blood brain barrier preventing passage of large molecules . One method for avoiding this issue is to deliver the drug directly to the brain, rather than administering it peripherally. Some experimental animal studies have used micropumps to allow for continuous delivery over weeks or months, but this approach is not convenient for human clinical applications in brain injury. As an alternative, the use of an implantable biomaterial may provide a feasible method of drug delivery in clinical scenarios that may already require a neurosurgical procedure. For example, severe wartime traumatic brain injuries involving penetration of the skull often require debridement surgery to remove bone and projectile fragments that have entered the brain [164]. It has also been demonstrated in an animal model the tissue damage extends beyond the track of the projectile [113, 116]. The major source of injury actually comes from dissipation of the projectile's kinetic energy, causing a large temporary cavity to expand within the brain [113]. While the temporary cavity is short-lived, the injury caused by compression of the surrounding tissue persists. Over time, the area of necrosis along the projectile path spreads to include the injured surrounding tissue and eventually the necrotic debris is cleared by macrophages [43]. The resulting cavitary defect remains

permanently. This cavity may thus afford the possibility of implanting a biomaterial to fill the defect and deliver a therapeutic agent with the capacity to promote regeneration.

In this study we investigated the implantation of a collagen scaffold in a rat model of bilateral penetrating brain injury, along with the effects of loading the scaffold with soluble Nogo receptor. We first sought to evaluate the ability of the scaffold to fill the defect. Based on our previous work with the injury model, we observed that the lesion cavity expanded significantly between 1 week and 5 weeks after injury. Implantation of a scaffold at an early time point is thus complicated by the fact that there is limited space in the lesion site. However, waiting several weeks until the cavity has fully formed forgoes the possibility of the therapeutic agent having a beneficial effect on mitigating the secondary injury process. An implantation time point of 1 week post-injury was thus chosen in an attempt to satisfy both concerns. In addition to trying to fill the defect, we studied the interaction of the scaffold with the surrounding brain tissue and identified the various cell types in and around the scaffold. Similarly, we evaluated whether the delivery of sNgR could affect the brain-scaffold interaction while potentially mitigating the injury progression and promoting axonal regeneration.

4.2 Materials and Methods

4.2.1 Experimental Design

3 groups of male Sprague-Dawley rats (n=7) were used in the study, each being administered a bilateral penetrating brain injury. In the injury model, a balloon-tipped probe is inserted into the brain and the balloon is rapidly expanded to mimic the

temporary cavity caused by a projectile. The balloon was inflated to a volume approximately equal to 10% of the rat brain volume when creating the injury. 1 week post-injury, animals underwent a second surgery in which they were implanted with either a collagen scaffold alone (Group 5), or a scaffold loaded with sNgR (Group 6 and Group 7). Group 5 and 6 were sacrificed 4 weeks after scaffold implantation (5 weeks post-injury), while Group 7 was sacrificed 8 weeks after scaffold implantation (9 weeks post-injury). The experimental groups are summarized in Table 3.

Table 3. Experimental Groups

	Group 5 (n=7)	Group 6 (n=7)	Group 7 (n=7)
1st surgery	Injury without intervention	Injury without intervention	Injury without intervention
2nd surgery	Implantation of collagen scaffold	Implantation of collagen scaffold loaded with sNgR	Implantation of collagen scaffold loaded with sNgR
Sacrifice time (post-injury)	5 weeks	5 weeks	9 weeks

4.2.2 Penetrating Brain Injury Apparatus

The PBI model was developed at the Walter Reed Army Institute of Research and has been used in several published studies to date [40, 42, 43, 120, 122, 165-170]. The model aims to simulate damage to the brain caused by a projectile by mimicking both the destruction of tissue along the projectile path, as well as the temporary cavity formed by dissipation of the projectile's kinetic energy. The injury is created by inserting a probe into the brain, which has a balloon attached near the tip. With the probe inserted, a pneumatic device creates a pressure impulse to rapidly inflate and deflate the balloon within the brain. The result of the balloon expansion is to compress the surrounding

tissue, similar to the action of the temporary cavity in a ballistic injury. Although the model does not recreate certain features of the clinical injury, such as retained bone fragments or subsequent infectious processes, it is useful for studying other characteristics of the injury and for creation of a standardized cavitary defect in the brain.

4.2.3 Collagen Scaffold Fabrication and sNgR Loading

Type I collagen scaffolds (1.0% weight:volume) were fabricated from medical grade porcine microfibrillar collagen (Geistlich Biomaterials, Wolhusen, Switzerland). A suspension of the collagen was made in 0.001 N HCl, brought to pH 3, and mixed for 20 minutes. The slurry was blended at 15,000 RPM (Ultra Turrax T18 blender, IKA, Staufen, Germany) for 30 minutes at 4° C, brought again to pH 3, and blended for an additional 2 hours. The slurry was then centrifuged for 10 minutes at 5500 RPM to remove bubbles, and mixed with a pipette to ensure homogeneity. The slurry was poured in a metal mold and placed into an AdVantage Benchtop Freeze Dryer (VirTis, Gardiner, NY). The temperature was decreased at a controlled rate to -40° C over 180 minutes and held at -40° C for 60 minutes. Sublimation was conducted at 0° C and a pressure of 200 mTorr for 1020 minutes. Scaffolds were then dehydrothermally cross-linked overnight at 105° C under vacuum. Published work using similar scaffolds has determined the pore size to be approximately 100-150 μm.

The scaffolds in Group 1 were chemically cross-linked using 1-ethyl-3-(3-dimethylaminopropryl)carbodiimide hydrochloride (EDC) (Sigma-Aldrich Inc, St. Louis, MO) with addition of N-hydroxysuccinimide (NHS) to increase the reaction rate. An EDC:NHS ratio of 5:2 was used, and the scaffolds were cross-linked for 1 hour at room

temperature. EDC cross-links collagen through activation of carboxylic acid groups that react with lysine free amine groups to form amide bonds. EDC is a water soluble agent that does not remain in the collagen after the scaffolds have been thoroughly rinsed. This is advantageous for *in vivo* applications due to the fact that many cross-linking agents such as glutaraldehyde are cytotoxic. Following cross-linking, the scaffolds were freeze-dried again, soaked for 2 hours in PBS, and freeze-dried a final time. The scaffolds were eventually cut into the desired implant size with a 4 mm diameter biopsy punch. The scaffolds in the dry state were approximately 4 mm in diameter and 2 mm thick, but after full hydration measured approximately 6 mm in diameter and 3 mm in thickness.

Scaffolds in Group 2 were chemically cross-linked in the same manner, except that they were first soaked for two hours in a 1.0 mg/mL solution of sNgR. The cross-linking was expected to immobilize a small mount of sNgR on the scaffold by covalent linkage. This would provide for a some release of sNgR in the event that the scaffold degraded *in vivo* over time. In actuality, the scaffolds were not degraded *in vivo*, and any cross-linked sNgR was unlikely to have a significant effect. Following cross-linking, the scaffolds were freeze-dried, and then soaked in an 8.2 mg/mL sNgR solution. The scaffolds loaded with the sNgR solution were freeze-dried a final time and cut to the desired size for implantation.

4.2.4 Soluble Nogo Receptor

The soluble Nogo receptor is a fusion protein produced by Biogen Idec. It is developed by fusing cDNA encoding the 1st 310 amino acids of rat NgR1 with cDNA encoding the Fc region of rat IgG1, followed by expression in Chinese hamster ovary cells [161]. The

resulting protein consists of the rat IgG1 Fc region with two NgR molecules replacing the IgG1 antigen binding fragment.

4.2.5 Surgical Procedure and Animal Care

27 male Sprague-Dawley rats were used in this study. All procedures were approved by the Boston VA Healthcare System Institutional Animal Care and Use Committee.

Animals were shaved, anesthetized with isoflurane, and positioned in a stereotaxic frame where the anesthetic delivery was maintained through a nosecone. A circulating water heating pad was used to maintain body temperature throughout the surgery and also for several hours during the post-operative recovery. Heart rate and blood oxygen saturation were monitored from a probe on the foot during the procedure.

After sterilizing the skin with 13% povidone iodine solution, a midline incision was made along the top of the head to expose the skull, followed by a lateral incision extending from the posterior aspect of the midline incision and passing just anterior to the left ear. With the top of the skull and the left side of the head exposed, a portion of the left temporalis muscle was excised with care taken to avoid damaging the temporal branch of the facial nerve. With the lateral aspect of the skull exposed, a 3 mm diameter window was drilled in the skull at a position 1 mm anterior to bregma and 3 mm ventral to bregma.

The PBI probe was inserted into the brain, with the tip advanced 10 mm from the surface of the left hemisphere into the right hemisphere. The PBI balloon was inflated to a diameter of 6.3 mm to create an injury encompassing approximately 10% of the rat brain volume. It is noted that the balloon is several mm proximal to the tip of the probe,

such that the balloon inflation is predominately in the left hemisphere despite the probe tip being in the right hemisphere. This scenario mimics a projectile entering the left hemisphere and dissipating its kinetic energy before coming to rest in the right hemisphere. Following the balloon inflation, the probe was retracted from the brain and bleeding was controlled using Gelfoam. The cranial window was covered with a Bio-Gide collagen membrane (Geistlich Biomaterials, Wolhusen, Switzerland) and the surgical incision was closed with a 4-0 suture.

1 week after the injury, animals underwent a second surgery in which a second incision was made parallel to the lateral incision from the first surgery, enabling access to the defect site. After removing the collagen membrane covering the cranial window, the lesion site was exposed. In Group 5, the collagen scaffolds were hydrated with 25 uL PBS immediately prior to implantation into the defect. In Group 6 and Group 7, the scaffolds were hydrated with 25 uL of 8.26 mg/mL sNgR solution before implantation. The scaffold were implanted very shortly after hydration, such that the scaffolds had not yet expanded to their full size. The delivered dose was estimated to be between 200 and 300 ug. The cranial window in each case was covered again with a collagen membrane and the incision closed with a 5-0 suture.

Following all surgeries, animals were allowed to recover in warmed cages with additional oxygen and food and water provided at bedding level. Buprenorphine (0.05 mg/kg) was given for pain relief, while Cefazolin (20 mg/kg) was given to prevent infection.

4.2.6 Animal Sacrifice and Specimen Processing

Animals were sacrificed 4 weeks (Groups 5 and 6) or 8 weeks (Group 7) after the implantation of the collagen scaffolds. Before sacrifice, animals were deeply anesthetized with an intraperitoneal injection of sodium pentobarbital (150 mg/kg). Animals were then transcardially perfused with 150 mL cold heparanized PBS (20 units/mL) followed by 250 mL cold 4% paraformaldehyde solution (USB corporation 19943, Cleveland, OH.) Brains were extracted and immersed in 4% paraformaldehyde for 2-3 days at 4° C. Brains were processed through reagent alcohol (70% - 10 min, 80% - 90 min, 95% - 2 x 90 min, 100% - 2 x 90 min, 100% - 90 min under vacuum), xylene (3 x 90 min), and paraffin (2 x 180 min under vacuum, 58° C). Samples were then embedded in paraffin and sectioned on a mictrome at 5 μm. Sections were taken at approximately 1 mm intervals spanning the lesion. Slides were dried on a warmer at 60° C for several hours.

4.2.7 Histology and Immunohistochemistry

Sections were stained with hematoxylin and eosin for histomorphometric analysis and for general histologic observation of the injury.

The fluorescent dye Fluoro-Jade C (Millipore AG325) was used for visualization of degenerating neurons in the thalamus. Sections from approximately 2.5 mm posterior to bregma were deparrafinized and rehydrated prior to incubation in 0.06% $KMnO_4$ (Sigma 223468) for 20 minutes. After 3 rinses in deionized water, slides were then stained with 0.00015% Fluoro-Jade C solution for 20 minutes and rinsed 3 more times in water. Slides were dried on a warmer at 60° C for 10 minutes, placed in xylene for several minutes, and coverslipped with Cytoseal mounting medium.

Antibodies, dilution factors, and antigen retrieval methods used for immunohistochemistry are summarized in Table 4. The staining procedure was conducted at room temperature. Following deparrafization, rehydration, and antigen retrieval, slides were rinsed with wash buffer (Dako S3006) containing TBS and 0.05% Tween 20. Slides were blocked for 2 hours with Dako protein block (Dako X0909) prior to addition of the primary antibody for 2 hours. Following 3 rinses with wash buffer, the secondary antibody was added for 1 hour. After 3 more rinses, a 100 ng/mL solution of the fluorescent DNA stain 4',6-diamidino-2-phenylindole (DAPI) was added for 30 minutes. 3 final rinses with wash buffer were performed and the slides were then placed in TBS for 3 minutes. The slides were transferred to a 0.1% solution of Sudan Black (Sigma 199664) dye for 20 minutes in to reduce tissue autofluorescence. Following 3 rinses in TBS, slides were coverslipped with Immu-mount aqueous mounting medium (Thermo Scientific 9990402).

Table 4 Immunohistochemistry reagents (Abbreviations: rb (rabbit), ms (mouse), gt (goat)

1° Antibody	Source	Retrieval	Dilution	2° Antibody
GFAP (rabbit polyclonal)	Dako (Z0334)	0.1% Protease XIV 25 min (Sigma P5147)	1:500	Dylight 488 donkey anti-rabbit IgG (Jackson ImmunoResearch 711-485-152)
Von Willebrand Factor (rabbit polyclonal)	Dako (A0082)	0.1% Protease XIV 40 min (Sigma P5147)	1:100	Dylight 488 donkey anti-rabbit IgG (Jackson ImmunoResearch 711-485-152)
Doublecortin (goat polyclonal)	Santa Cruz (sc-8066)	Citrate buffer pH 6, 2 min 120° C (Dako S1699)	1:100	Dylight 488 donkey anti-goat IgG (Jackson ImmunoResearch 705-485-003)
CD68 (mouse	Serotec	0.1% Protease	1:200	Dylight 549 donkey

monoclonal IgG)	(MCA341R)	XIV 20 min (Sigma P5147)		anti-mouse IgG (Jackson ImmunoResearch 715-505-150)
NeuN (mouse monoclonal IgG)	Millipore (MAB 377)	Citrate buffer pH 6, 1 min 120° C (Dako S1699)	1:200	Dylight 549 donkey anti-mouse IgG (Jackson ImmunoResearch 715-505-150)
CNPase (mouse monoclonal IgG)	Abcam (ab6319)	Citrate buffer pH 6, 20 min 95° C (Dako S1699)	1:500	Dylight 549 donkey anti-mouse IgG (Jackson ImmunoResearch 715-505-150)
CS56 (mouse monoclonal IgM)	Sigma (C8035)	0.1% Protease XIV 40 min (Sigma P5147)	1:100	Rhodamine donkey anti-mouse IgM (Jackson ImmunoResearch 715-025-020)
Neurofilament (mouse monoclonal IgG)	Abcam (ab24570)	None	1:150	Dylight 549 donkey anti-mouse IgG (Jackson ImmunoResearch 715-505-150)
Tau-1 (mouse monoclonal IgG)	Millipore (IHCR1015-6)	Citrate buffer pH 6, 2 min 120° C (Dako S1699)	Prediluted	Dylight 549 donkey anti-mouse IgG (Jackson ImmunoResearch 715-505-150)
MAP1b (mouse monoclonal IgG)	Abcam (ab3095)	Citrate buffer pH 6, 10 min 95° C	1:100	Dylight 488 donkey anti-mouse IgG (Jackson ImmunoResearch 715-485-150)

4.2.8 Imaging

Light microscope images were taken with an Olympus camera interfaced with a Olympus BX51 microscope, while fluorescent images were captured an Olympus DP71 camera interfaced with an Olympus BX60 microscope. Adobe Photoshop CS3 was used for

minor image processing procedures such as cropping and adjustment of levels to reduce background.

4.2.9 Histomorphometric Analysis and Cell Counts

Lesion area was demarcated in hematoxylin and eosin stained sections at approximately 1 mm intervals spanning the lesion. The lesion was defined by areas of obvious necrosis with lack of cellularity, along with regions of dense macrophage infiltration, hemorrhage, gliosis, and vacuolization. A linear interpolation was used to reconstruct an approximate volume, with the volume between sections being equal to the average of the areas multiplied by the distance between them. Cell density was determined by counting the number of cells within the scaffold and normalizing by diving by the scaffold area.

4.2.10 Statistics

Numerical values are reported at mean ± standard error, and all statistical analysis was performed using Statview (version 5.0.01, SAS Institute Inc., Cary, NC). Unpaired t-tests were used to compare differences between experimental groups, with a p-value of 0.05 used for determining statistical significance.

4.3 Results

4.3.1 Animal Survival, Recovery, and Qualitative Behavioral Observations

22 out of 27 animals survived, with all deaths occurring after the first surgery. No obvious differences were noted in the animal recovery or behavior in the three groups.

Similarly, the response to the injury was generally the same as has been observed in previous work. In particular, the rats had right forelimb deficits that improved several days after the injury. It is noted that all of the animals survived the implantation of the scaffold at 1 week post-injury and appeared not to suffer any deleterious effects from it. This establishes that implantation of large scaffolds 1 week after the injury is technically feasible in the rat model and is safe for the animals over several weeks. Animals generally lost weight over the first 2 days after the injury before resuming weight gain. Following the implantation surgery, animals generally maintained their weight (Figure 4.1, Figure 4.2, and Figure 4.3).

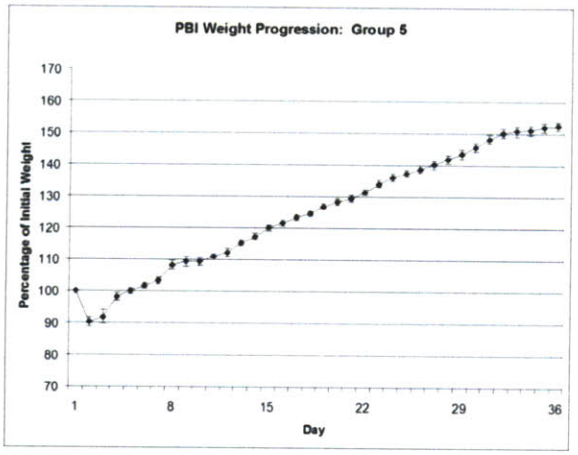

Figure 4.1. Group 5 Weight Progression Following PBI and Scaffold Implantation

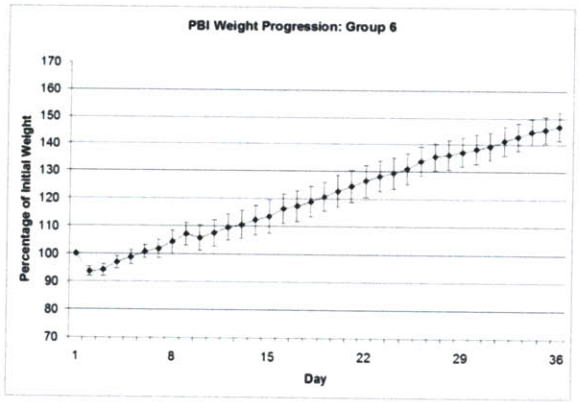

Figure 4.2. Group 6 Weight Progression Following PBI and Scaffold Implantation

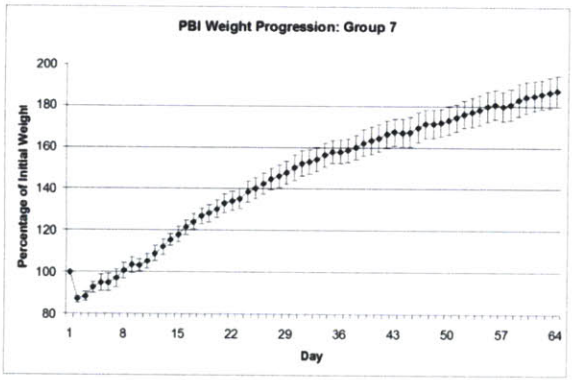

Figure 4.3. Group 7 Weight Progression Following PBI and Scaffold Implantation

4.3.2 Lesion Volume and Scaffold-Brain Histological Observations

The volume of the lesion in Group 5 was found to be 84.2 ± 5.2 mm^3, while the lesion in Groups 6 and 7 were 72.8 ± 5.3 mm^3 and 93.8 ± 11.2 mm^3, respectively. The lesion in Group 7 was significantly larger than in Group 6 (p=0.009), but was not significantly different from Group 5 (Figure 4.4). Group 5 and Group 6 were not significantly different.

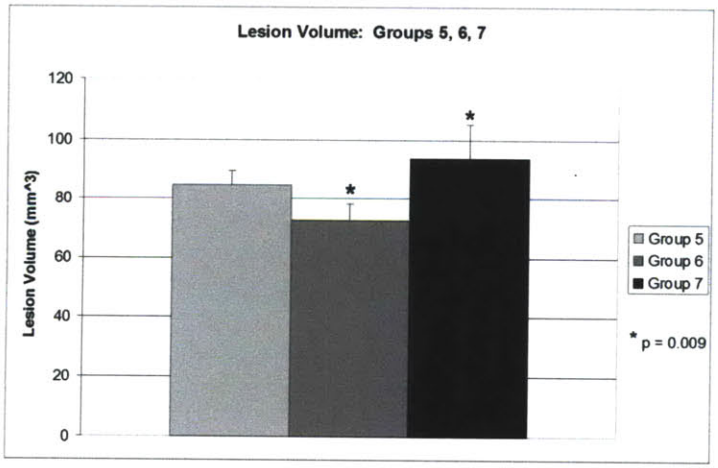

Figure 4.4. Lesion Volume for Groups 5, 6, and 7. Lesion volume in Group 7 was significantly larger than that of Group 6 (p=0.009).

Scaffolds in Group 5 appeared to mostly fill the lesion, with some cellular infiltration (Figure 4.5). The scaffold pores remained open, and no signs of degradation were evident. Scaffolds in Group 6 similarly filled the lesion, but appeared to be much more integrated with the surrounding tissue (Figure 4.6). One could find in some cases a dense cellular infiltrate with deposition of extracellular matrix inside the scaffold. Additionally, cells of varying morphology could be seen, suggesting the infiltrate was not restricted to a single cell type (Figure 4.6c). Among the visible cells were what appear to be numerous macrophages, including several multinucleated giant cells. Endothelial cells lining small blood vessels were apparent within the scaffolds of Group 6 based. Other phenotypes possible for such cells with elongated nuclei include microglia, endothelial cells, or less likely fibroblasts. Group 5 scaffolds had some cells with similar morphology, but few foreign body giant cells were observed. Additionally, very little extracellular matrix could be detected within the Group 5 scaffold in comparison to Group 6. Group 7 scaffolds were qualitatively similar to those of Group 6, with some samples showing a robust infiltration of cells (Figure 4.7). The Group 7 scaffolds appeared to be intact and undegraded.

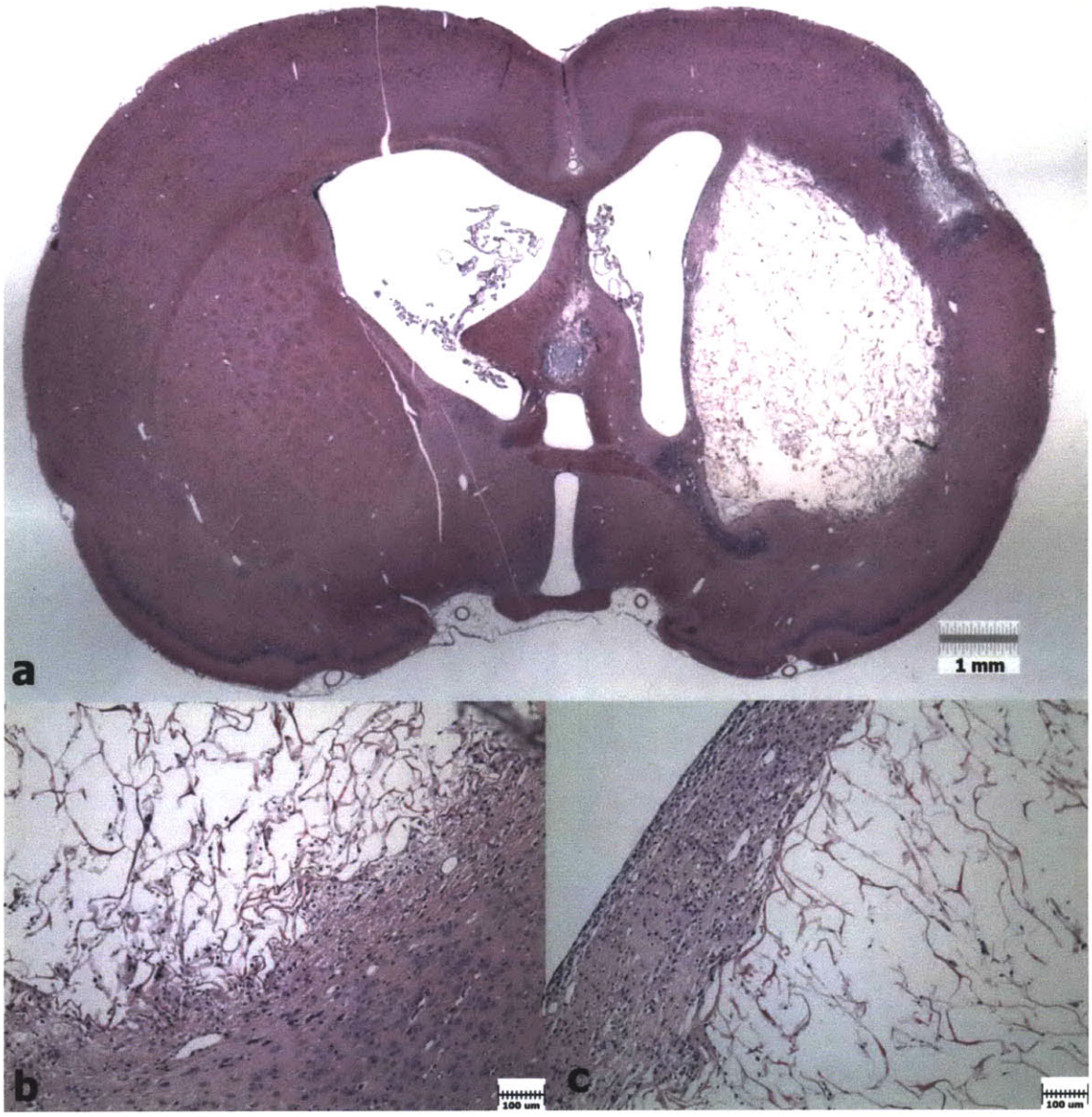

Figure 4.5. H&E Histology 4 Weeks after Scaffold Implantation (Group 5). a) H&E image showing a scaffold filling the defect in Group 5, 4 weeks after implantation. b) Cellular infiltration at the inferior border of the scaffold. c) Sparse cellular infiltration near the superior medial border of the lesion cavity.

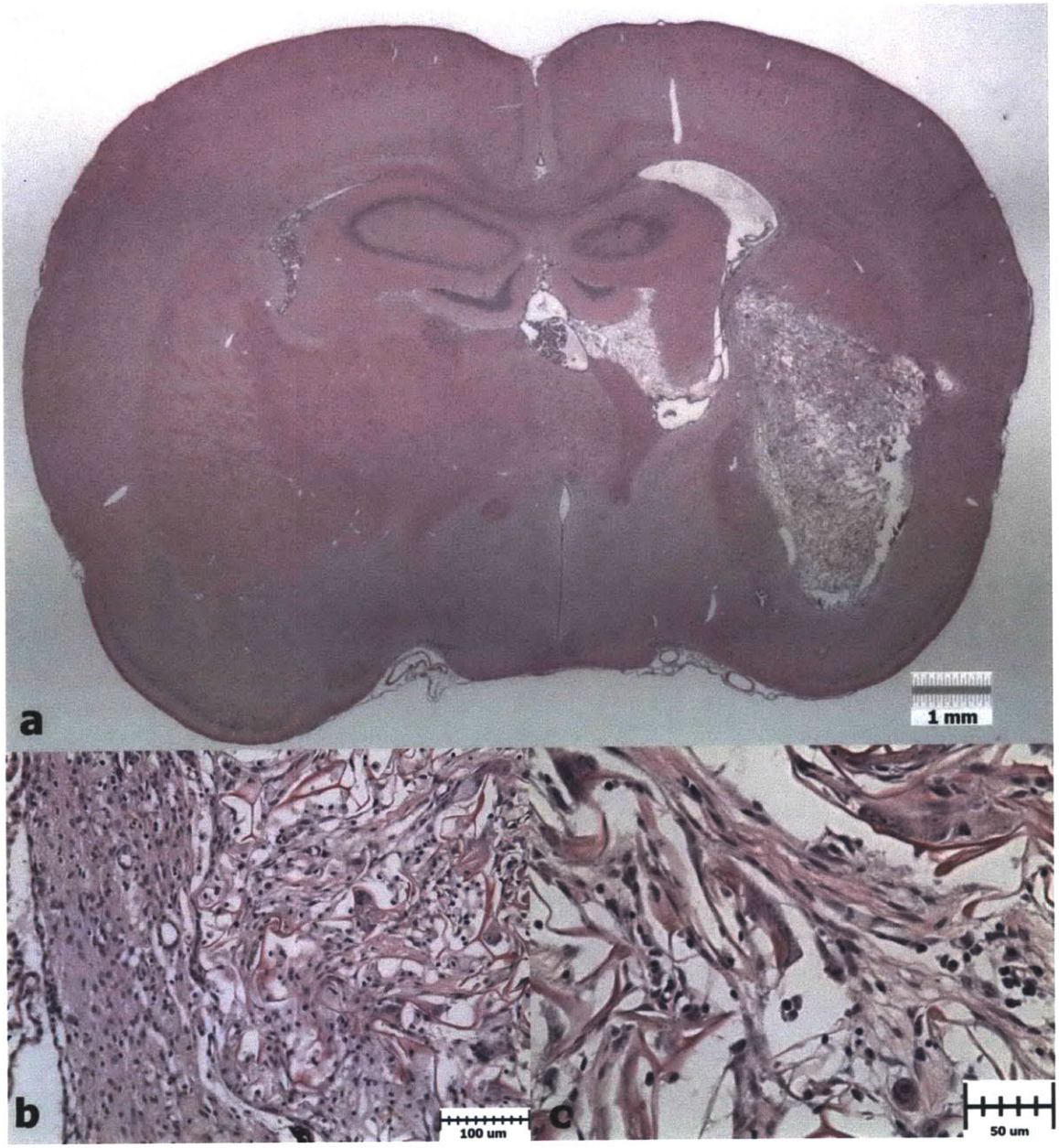

Figure 4.6. H&E Histology 4 Weeks after Implantation of an sNgR-loaded Scaffold (Group 6). a) H&E image of the PBI lesion with an sNgR loaded scaffold filling the defect. The cellular infiltrate can be seen even at low magnification. b) Dense cellular infiltration near the medial border of the scaffold. c) Cellular infiltrate with cells of varying morphology apparent.

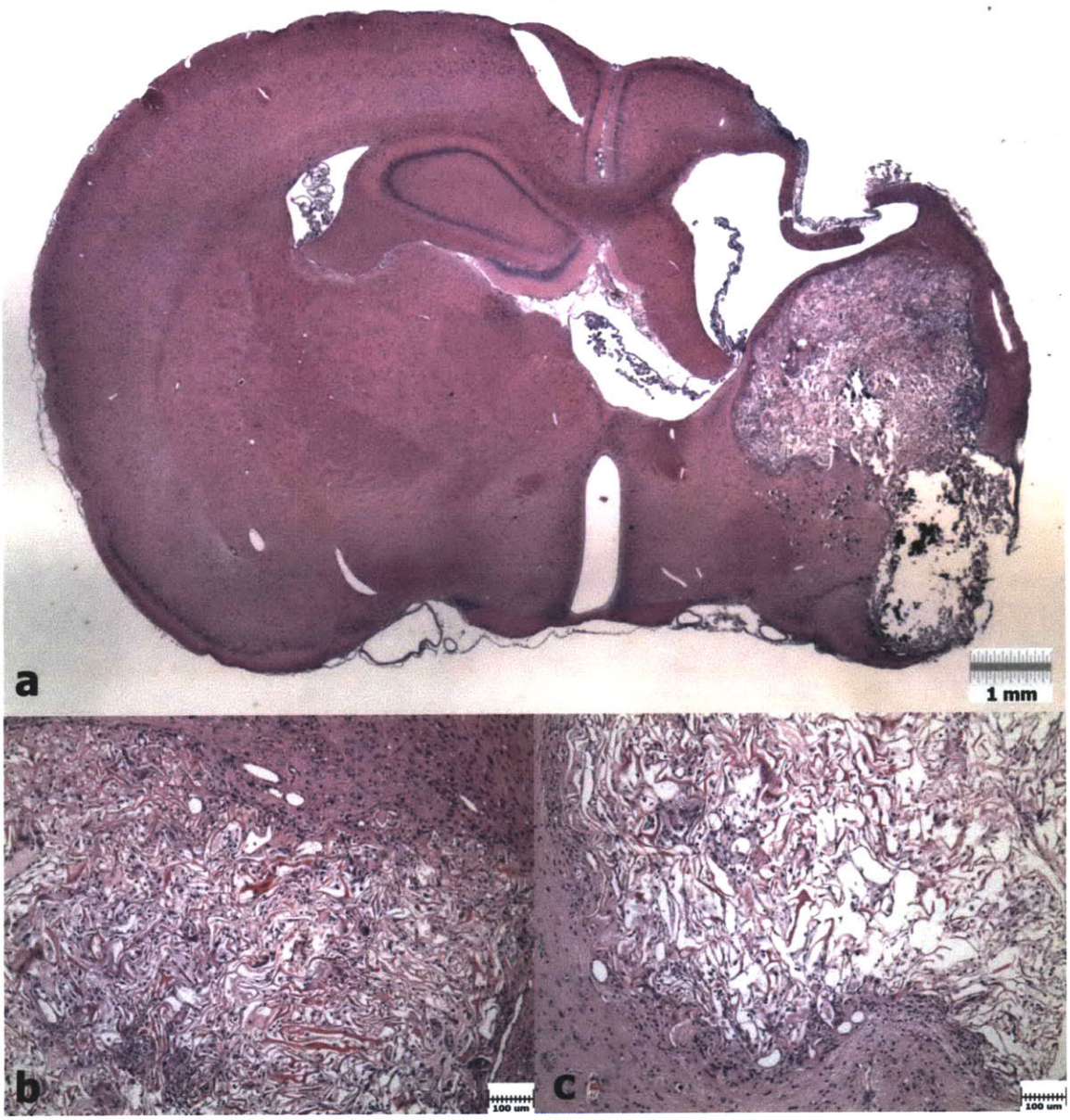

Figure 4.7. H&E Histology 8 Weeks after Implantation of an sNgR-loaded Scaffold (Group 7). a) H&E image of a PBI lesion with an sNgR scaffold filling much of the defect 8 weeks after implantation. b) Dense cellular infiltrate near the superior border of the lesion. c) Cellular infiltrate near the inferior border of the scaffold.

4.3.3 Glial Scarring and Inflammation: GFAP and CD68

Intense GFAP staining was observed surrounding the lesion boundary in Groups 5, 6, and 7. A transition was observed in astrocyte morphology when moving closer to

the lesion. The normal astrocytes showed distinct processes and the typical star-like morphology. However, closer to the lesion the astrocyte processes were no longer distinct, and instead stained as a nearly uniform band. The amount of GFAP staining within the scaffolds was generally low relative to the surrounding tissue (Figure 4.8, Figure 4.9, and Figure 4.10.

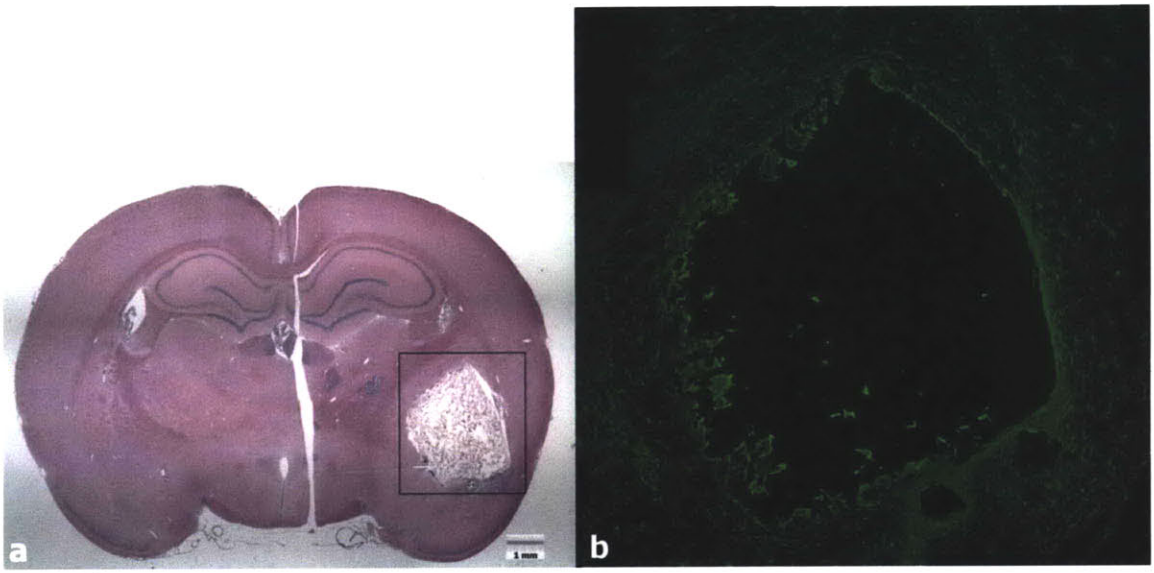

Figure 4.8. GFAP Staining Near the Implanted Scaffold after 4 weeks (Group 5). a) H&E image of a PBI lesion with an implanted scaffold. b) GFAP staining surrounding the scaffold, with some scattered staining within the scaffold.

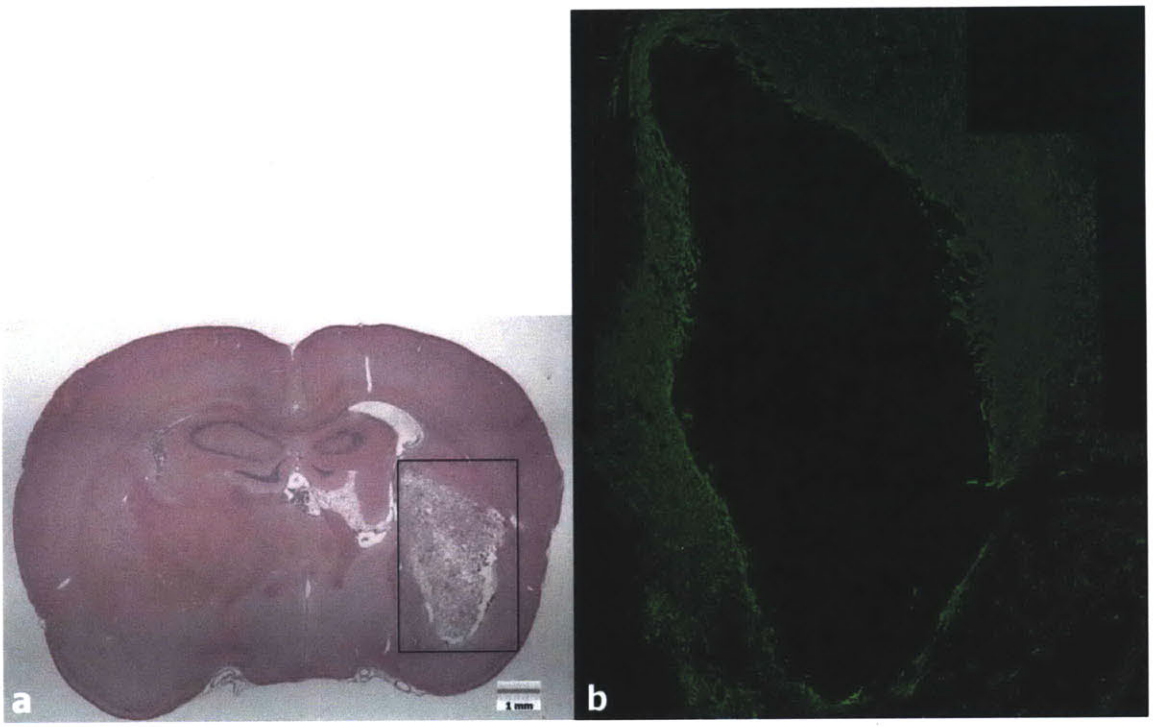

Figure 4.9. GFAP Staining Near an sNgR-loaded Scaffold after 4 weeks (Group 6). a) H&E image of an sNgR loaded scaffold within a PBI lesion. b) Dense GFAP staining surrounding the scaffold, with a little staining within the scaffold

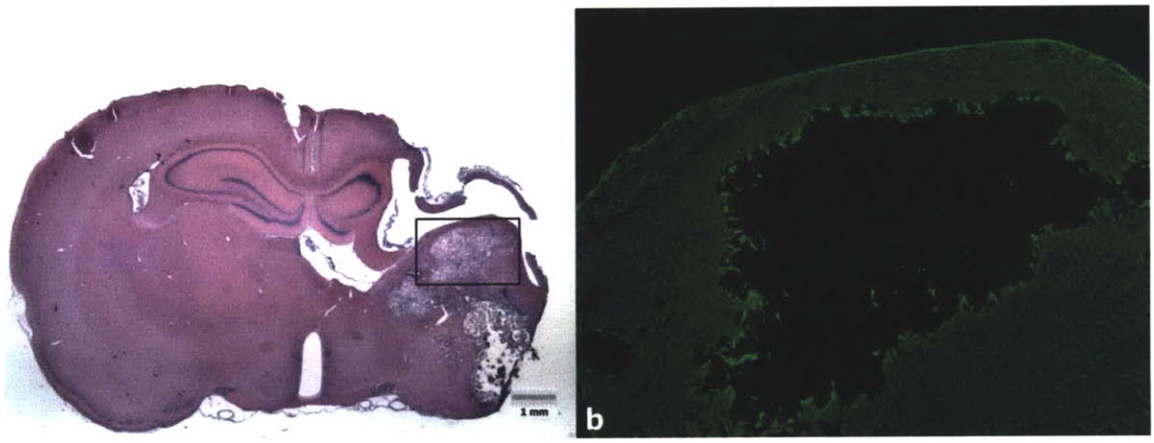

Figure 4.10. GFAP Staining Near an sNgR-loaded scaffold after 8 weeks (Group 7). a) H&E image of an sNgR scaffold with a PBI lesion. b) GFAP staining surrounding the scaffold, with a some staining also seen within the scaffold.

The density of astrocytes within the collagen scaffolds was found to be 9.2 ± 2.1, 10.7 ± 2.9, and 30.1 ± 4.5 cells/mm^2 for Groups 5, 6, and 7, respectively. The astrocyte density in Group 7 was significantly greater that that in Group 5 and 6 ($p=0.001$ and

p=0.004, respectively), while Groups 5 and 6 were not significantly different (Figure 4.11).

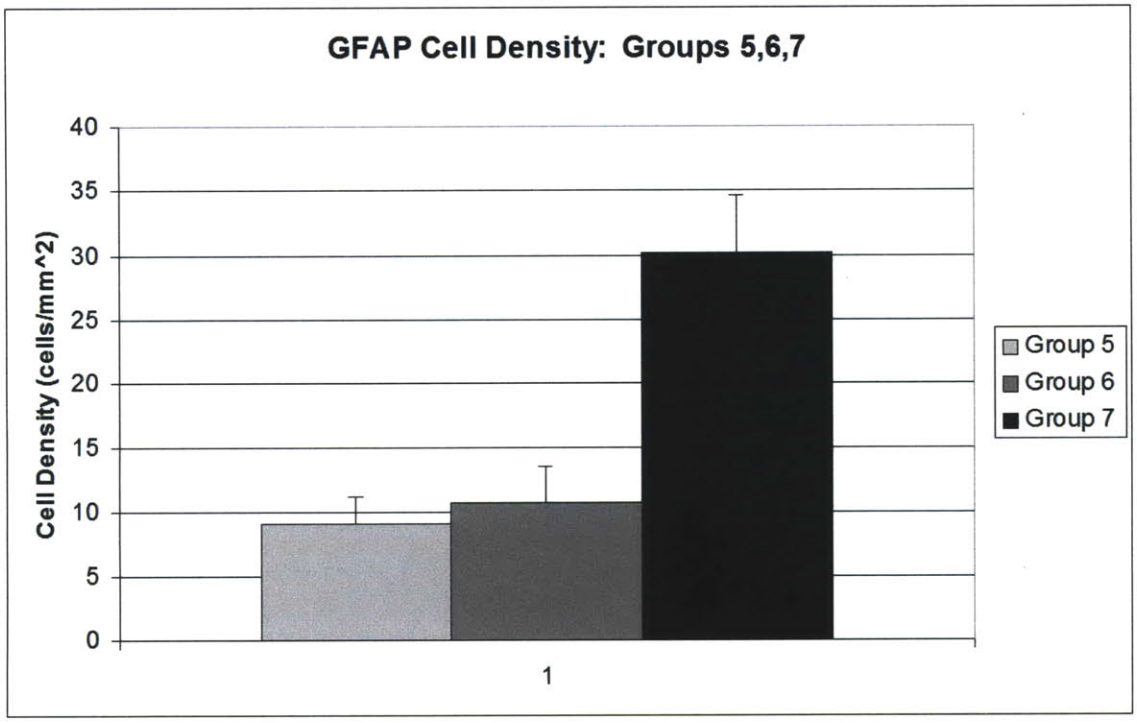

Figure 4.11. GFAP cell density within collagen scaffolds (Groups 5, 6, 7). GFAP cell density in Group 7 scaffolds was significantly higher than in Group 5 (p=0.001) and Group 6 (p=0.004).

The cellular infiltration of the scaffold appeared to consist predominantly of macrophages in most cases. Many CD68-positive macrophages were observed around the lesion and within the scaffolds of all groups (Figure 4.12, Figure 4.13, Figure 4.14).

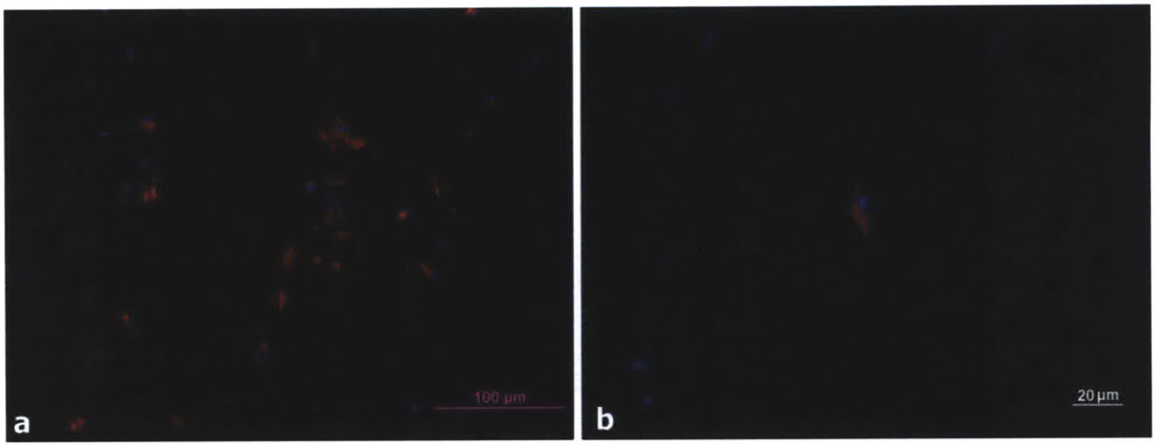

Figure 4.12. CD68-positive macrophages within a collagen scaffold after 4 weeks (Group 5). a) 20x magnification image showing numerous macrophages within a scaffold. b) High magnification image showing a macrophage along a scaffold strut. (Red: CD68, Blue: DAPI)

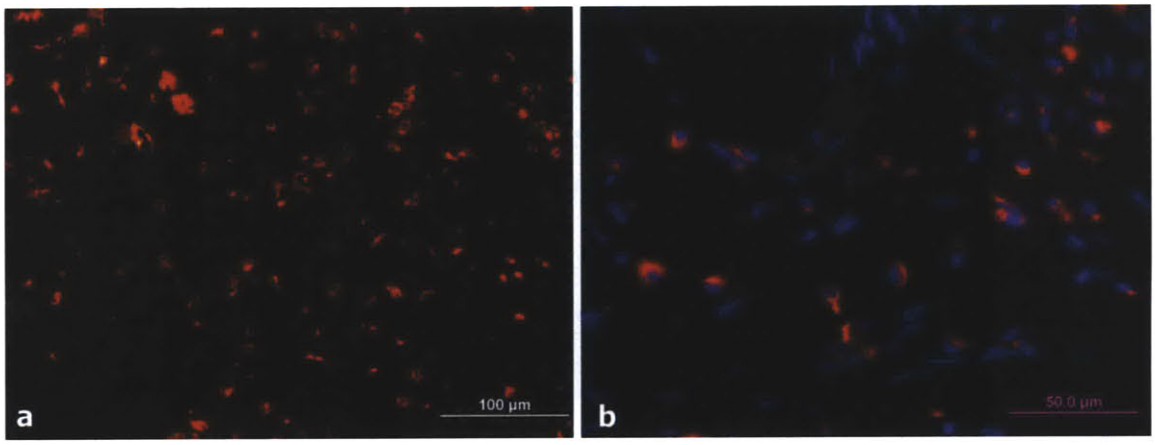

Figure 4.13. CD68-positive macrophages within an sNgR-loaded scaffold after 4 weeks (Group 6). a) 20x magnification image showing a very dense macrophage infiltrate within a scaffold. b) 40x image showing macrophages among cells of other phenotypes within the scaffold. (Red: CD68, Blue: DAPI)

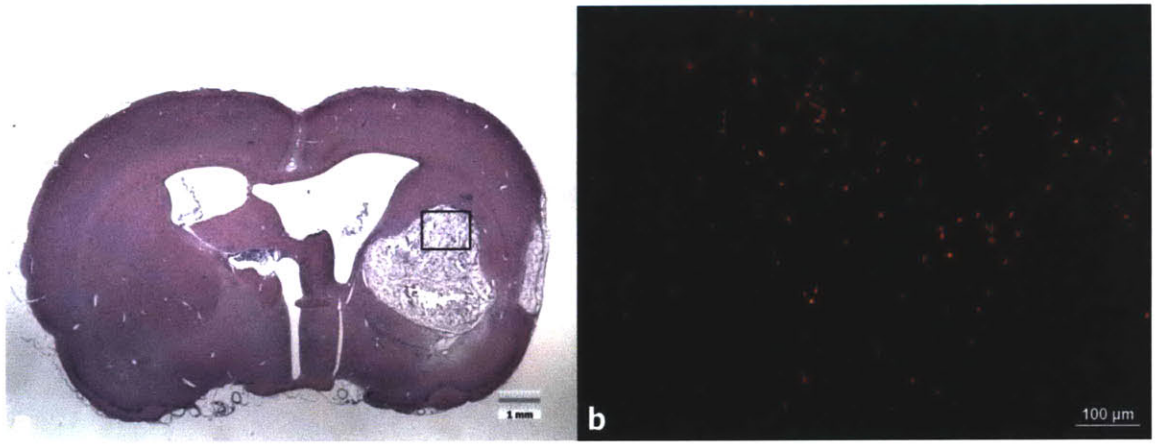

Figure 4.14. CD68 positive macrophages within an sNgR-loaded scaffold after 8 weeks (Group 7). a) H&E image of a scaffold within a PBI lesion. b) Macrophages within the scaffold.

The density of CD68-positive macrophages within the collagen scaffolds was 27.6 ± 6.3, 218.7 ± 51.9, and 57.0 ± 7.0 cells/mm^2 for Groups 5, 6, and 7, respectively (Figure 4.15). The Group 6 density was significantly higher than that of both Group 5 and 7 (p=0.003 and p=0.009, respectively). The Group 7 density was also significantly higher than that of Group 5 (p=0.009).

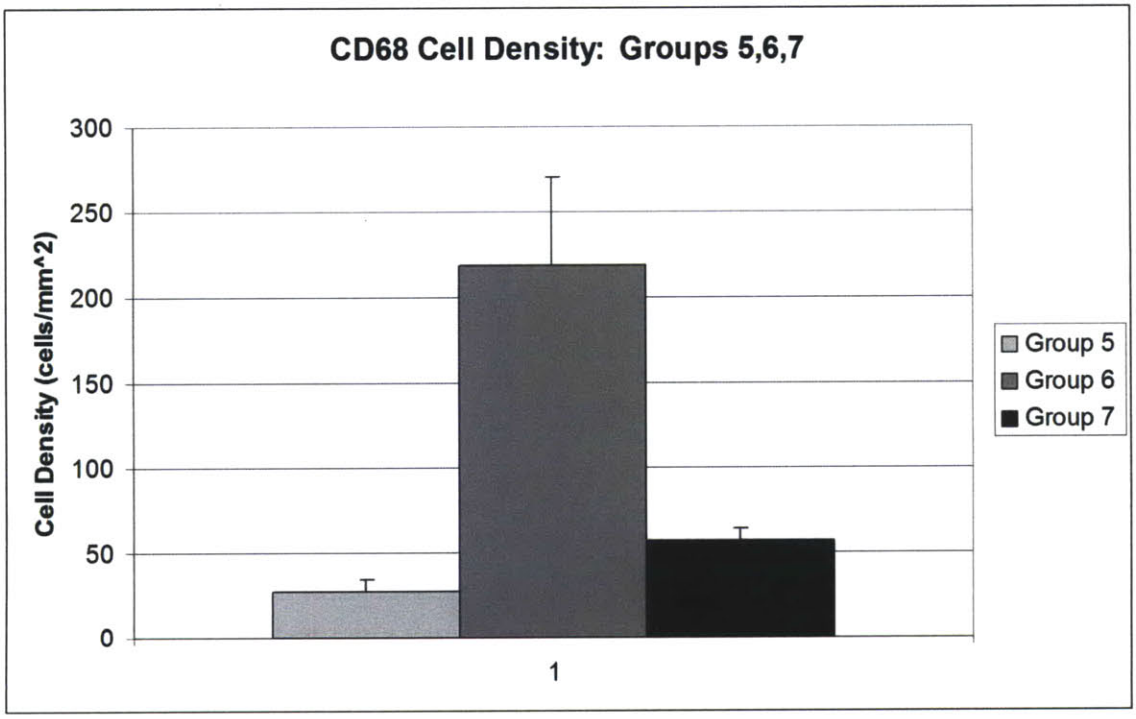

Figure 4.15. CD68 Cell Density Within Collagen Scaffolds (Groups 5, 6, and 7). Group 6 had a significantly higher density of macrophages in the scaffold than Group 5 (p=0.003) and Group 7 (p=0.009). Group 7 also had a higher density than Group 5 (p=0.009).

4.3.4 Fluorojade C Staining for Degenerating Neurons

By 5 weeks and 8 weeks post-injury, very few fluorojade-positive neurons could be detected in the thalamus or cortex. There was, however, persistent white matter reactivity in the corpus callosum, external capsule, and internal capsule.

4.3.5 Von Willebrand Factor Staining for Endothelial Cells

Numerous blood vessels were observed surrounding the lesion, including both small capillaries and some larger vessels. A few blood vessels were detected within the scaffolds of Group 5 (Figure 4.16), while considerably more were seen in Group 6 (Figure 4.17) and Group 7 (Figure 4.18) scaffolds. An average density of 6.1 ± 1.1 vessels/mm^2 were counted in Group 5 scaffolds (Figure 4.19), which was significantly less than the 26.1 ± 4.5 vessels/mm^2 in Group 6 ($p=0.001$) and 15.9 ± 3.4 vessels/mm^2 in Group 7 ($p=0.018$).

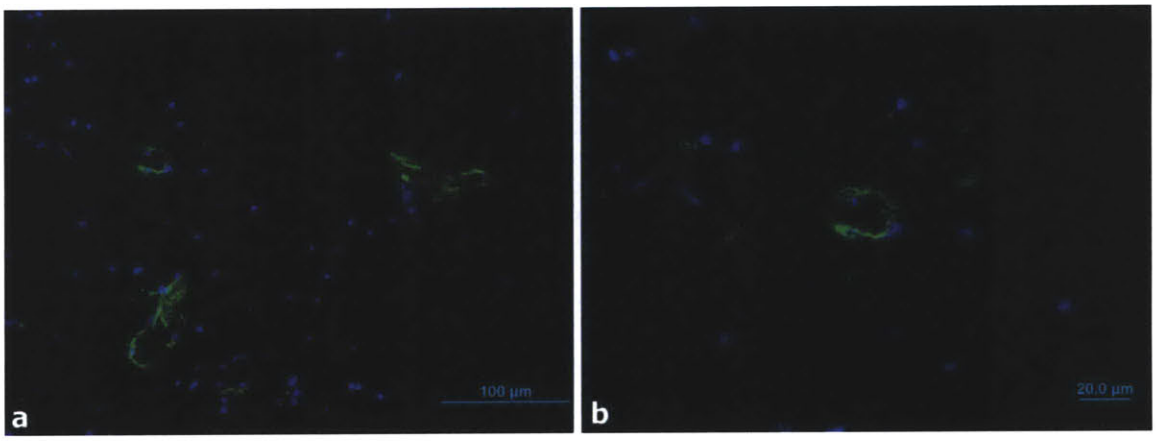

Figure 4.16. VWF positive cells/vessels in a collagen scaffold after 4 weeks (Group 5). a) VWF positive cells/vessels within a scaffold. b) 40x magnification of VWF positive cell/vessel. (Green: VWF, Blue: DAPI)

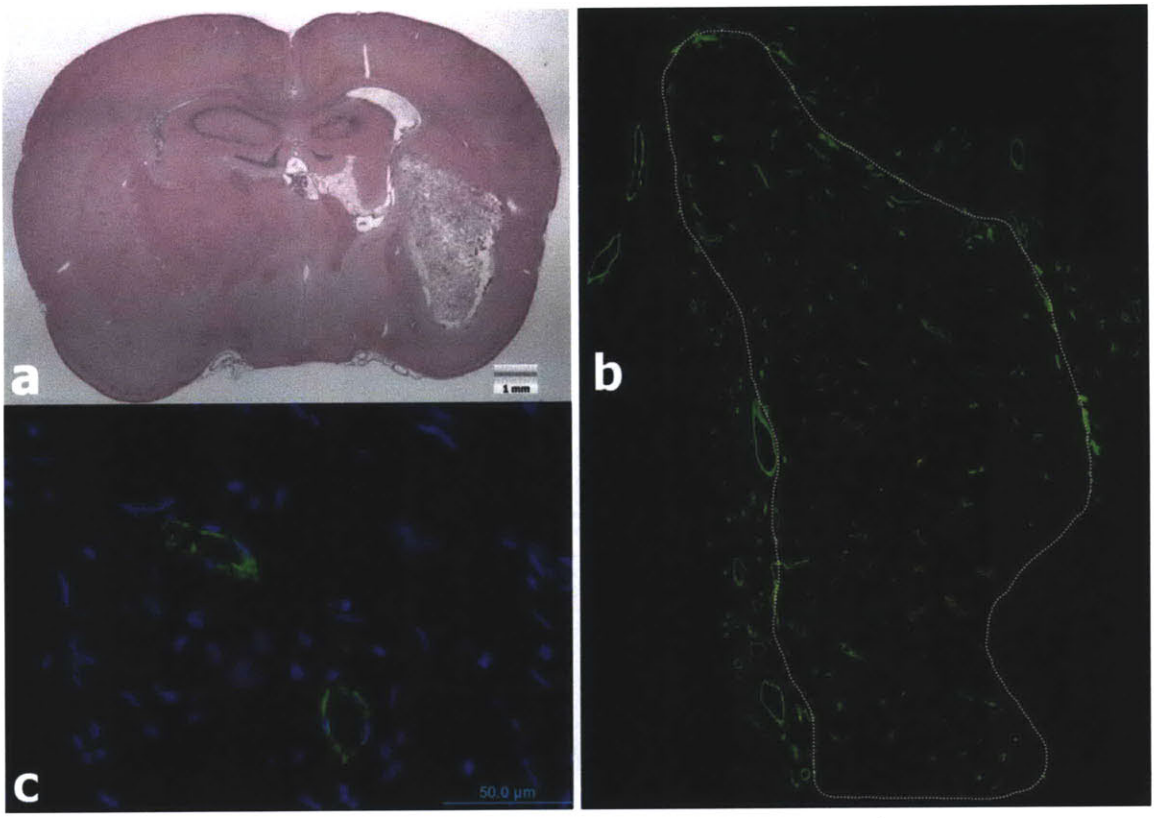

Figure 4.17. VWF positive cells/vessels in a sNgR loaded scaffold after 4 weeks (Group 6). a) H&E image of a scaffold within a PBI lesion. b) VWF positive cells/vessels distributed throughout the collagen scaffold (white line indicates approximate scaffold border). c) 40x magnification of VWF positive cells/vessels. (Green: VWF, Blue: DAPI)

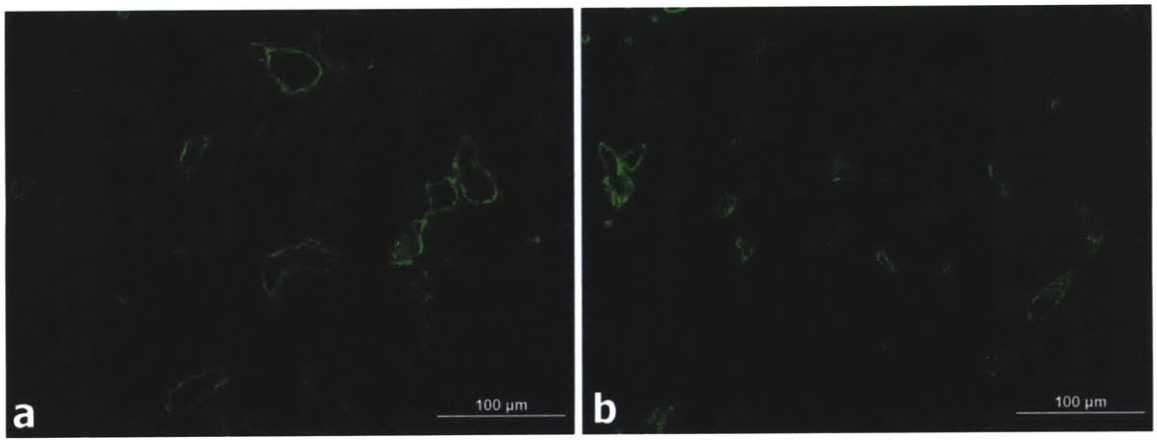

Figure 4.18. VWF positive cells/vessels in a sNgR loaded scaffold after 8 weeks (Group 7). a) VWF positive cells/vessels within a collagen scaffold. b) Additional VWF positive cells/vessels with a scaffold.

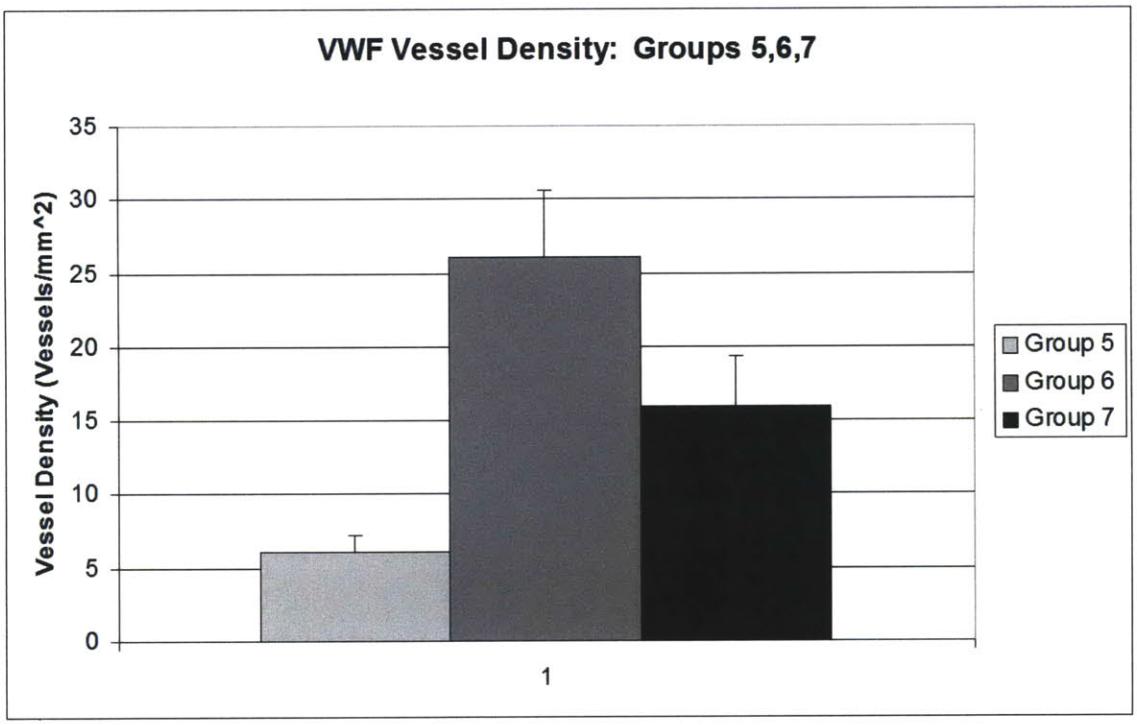

Figure 4.19. VWF Cell/Vessel Density within collagen scaffolds. The density of cells/vessels in Group 6 and Group 7 was significantly greater than in Group 5 (p=0.001 and p=0.018, respectively).

4.3.6 CNPase Staining for Oligodendrocytes

CNPase staining revealed myelinated axons of the corpus callosum and internal capsule near the lesion site. CNPase oligodendrocytes could be observed near the edge of the scaffolds in each group and occasionally they were seen in contact with scaffolds (Figure 4.20, Figure 4.21, and Figure 4.22. Oligodendrocytes were not, however, found at distances within the scaffolds beyond 100-200 μm.

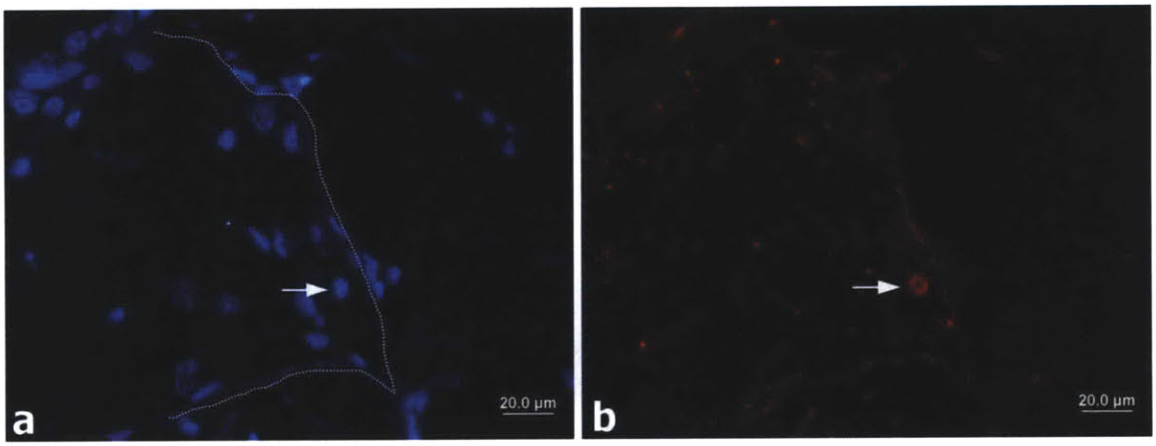

Figure 4.20. CNPase staining near the border of a collagen scaffold after 4 weeks (Group 5). a) DAPI stain showing cells in close proximity or in contact with a collagen scaffold (white lines show scaffold struts). b) A CNPase positive oligodendrocyte (white arrow) slightly within the border of the scaffold.

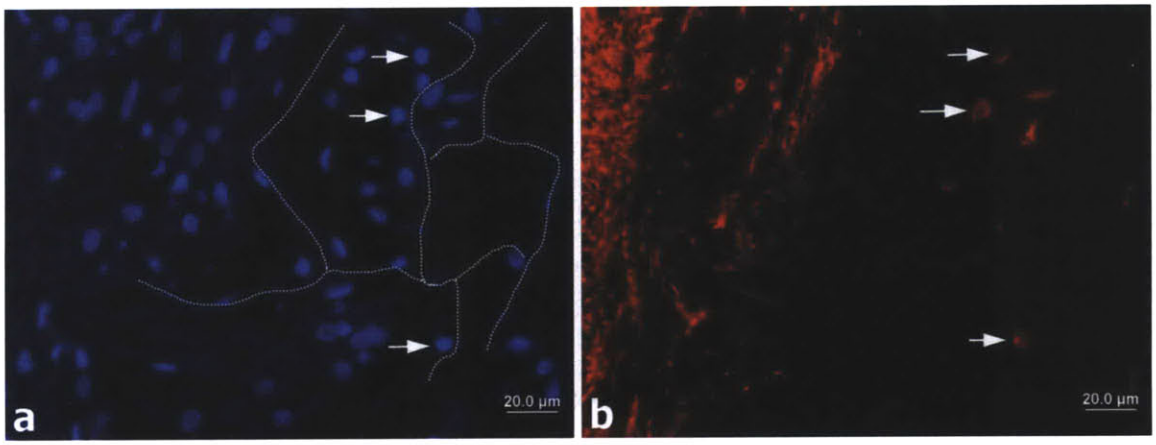

Figure 4.21. CNPase staining near the border of an sNgR loaded scaffold after 4 weeks (Group 6). a) DAPI staining showing cells within the scaffold, near its border. White lines indicate scaffold struts. b) CNPase positive oligodendrocytes (white arrows) slightly within the scaffold border.

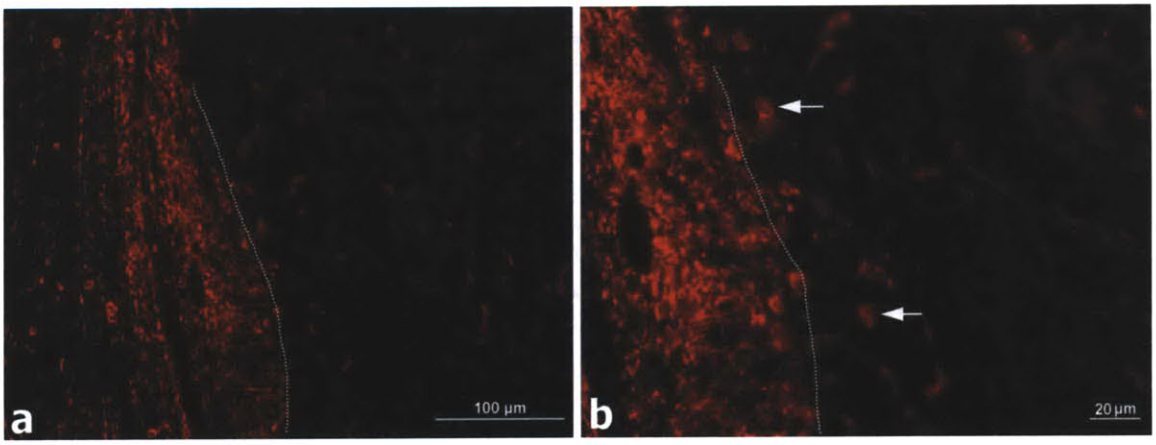

Figure 4.22. CNPase staining near the border of an sNgR loaded scaffold after 8 weeks (Group 7). a) CNPase staining showing myelinated axons near the scaffold border (white line) b) CNPase staining

showing myelinated axons and a few oligodendrocytes (white arrows) in contact with the scaffold edge

4.3.7 NeuN Staining for Mature Neurons

NeuN-positive neurons were found surrounding the lesion site and in close proximity to the scaffold. In each group, isolated areas could be identified in which neurons were within the scaffold borders (Figure 4.23, Figure 4.24, and Figure 4.25). In some cases, neurons could be observed directly in contact with the scaffold struts. Similar to the distribution of oligodendrocytes, neurons were not observed deep within the scaffolds.

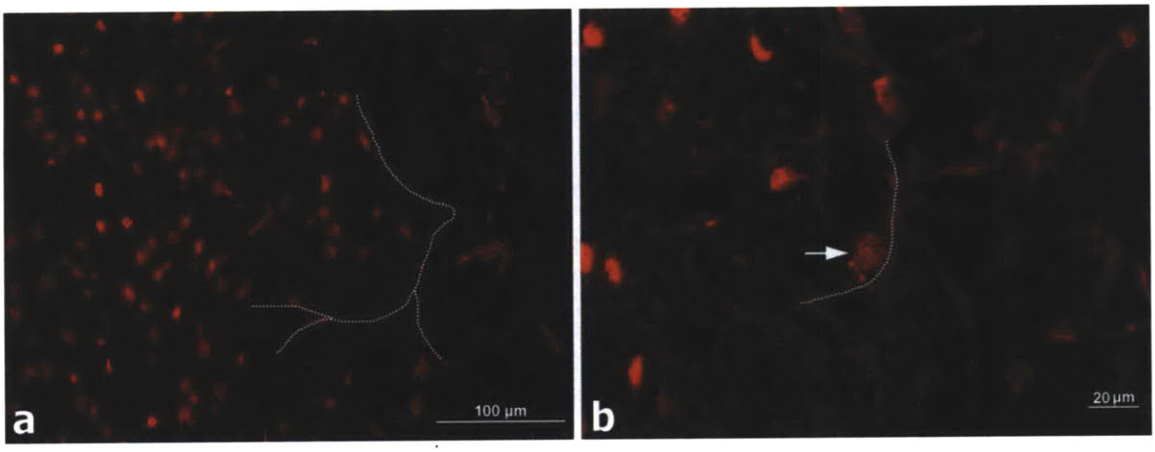

Figure 4.23. NeuN staining near the border of a collagen scaffold after 4 weeks (Group 5). a) NeuN positive neurons in viable brain near the scaffold edge. White lines indicate the approximate location of scaffold struts b) A few NeuN positive cells (white arrow) within the scaffold

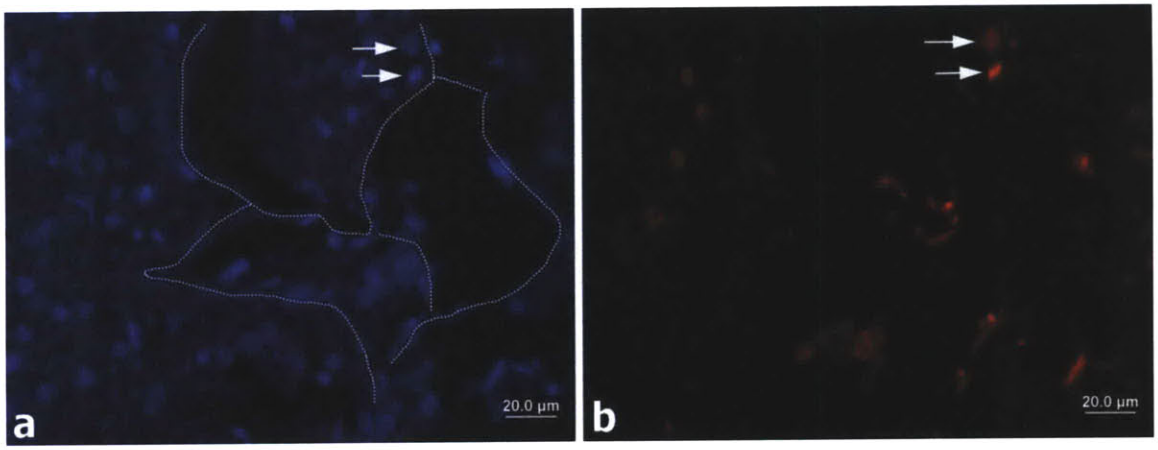

Figure 4.24. NeuN staining near the border of an sNgR loaded scaffold after 4 weeks (Group 6). a) DAPI staining showing cells slightly within the scaffold border. Scaffold struts are indicated with white lines b) NeuN staining showing a few neurons (white arrows) within the scaffold.

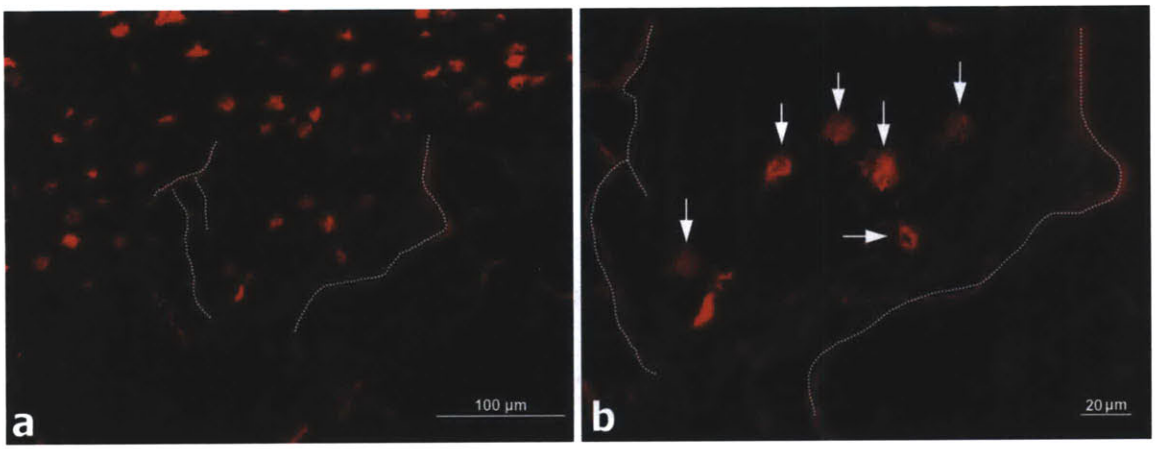

Figure 4.25. NeuN staining near the border of an sNgR loaded scaffold after 8 weeks (Group 7). a) NeuN staining showing a few neurons within the scaffold, near the superior border. White lines indicate scaffold struts b) 40 x magnification of the neurons (white arrows), surrounded by scaffold struts.

4.3.8 Doublecortin Staining for Neural Progenitors

Cells staining positive for DCX were found in the subventricular zone and subgranular zone of the dentate gyrus, similar to what one would find in uninjured brain. In sections where the lesion was in proximity to the subventricular zone, DCX positive cells appeared to have migrated to areas surrounding the lesion. It appeared possible that the cells may have proliferated relative to the staining seen in normal brains. While some DCX positive cells were occasionally found close to the scaffolds, no such cells were observed within the scaffolds of either group.

4.3.9 Tau-1, Neurofilament, and MAP1b Staining for Axons

Antibody staining for markers Tau-1, Neurofilament, and MAP1b revealed axons generally coursing around the lesion, often in close proximity to the borders of collagen

scaffolds. The pattern of Neurofilament staining was similar among the three groups, with an absence of axon staining at significant distances within the scaffold. While axons may have contacted the edge of the scaffold in some cases, they mostly traversed outside of the border along lesion periphery (Figure 4.26, Figure 4.27, and Figure 4.28).

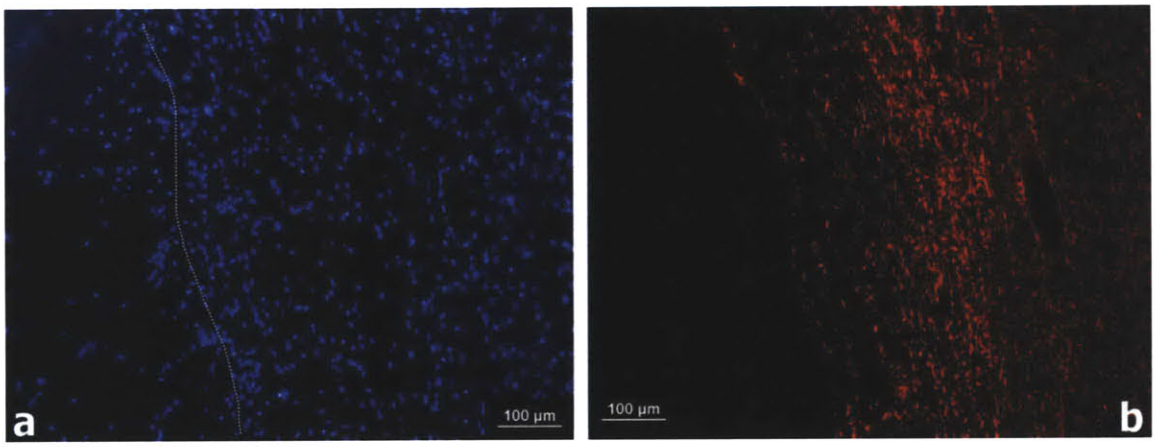

Figure 4.26. Neurofilament staining bordering a collagen scaffold after 4 weeks (Group 5). a) DAPI staining showing cells along and within the scaffold border (white line). b) Neurofilament staining of axons running alongside the scaffold, but not within it.

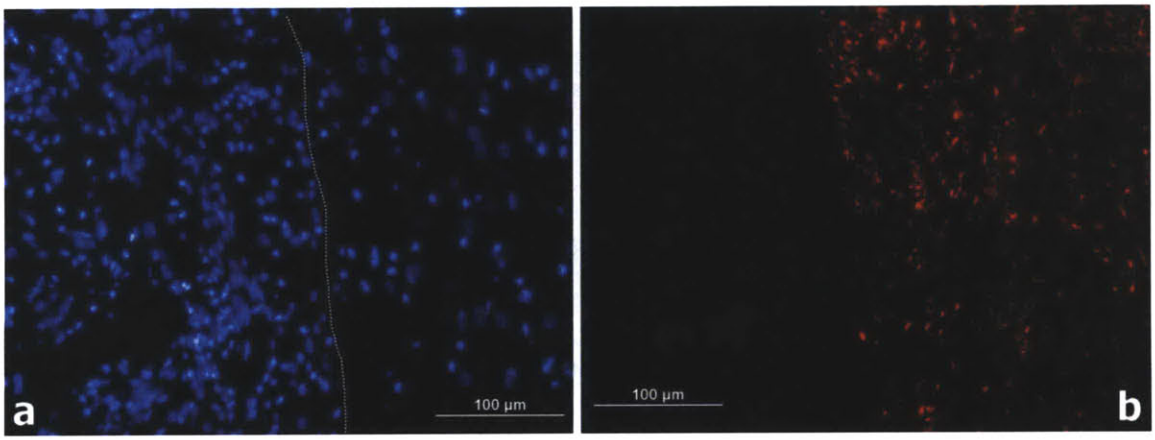

Figure 4.27. Neurofilament staining bordering an sNgR loaded scaffold after 4 weeks (Group 6). a) DAPI staining showing cells bordering the scaffold and a dense infiltrate into the scaffold. b) Neurofilament staining along the scaffold border, but not within the scaffold.

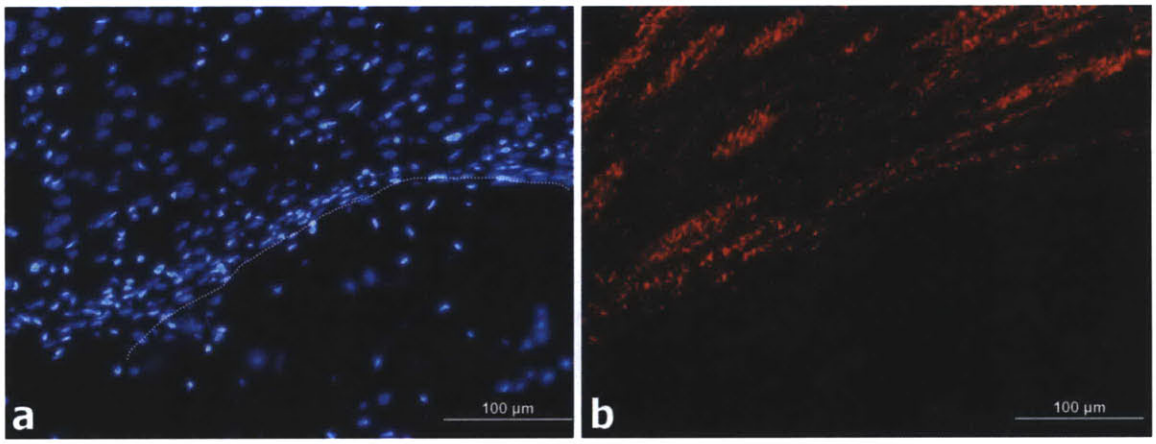

Figure 4.28. Neurofilament staining bordering an sNgR loaded scaffold after 8 weeks (Group 7). a) DAPI staining showing cells along and within the scaffold border (white line). b) Neurofilament staining showing axons passing adjacent to the scaffold.

Staining for Tau-1 was somewhat similar to neurofilament, but showed more staining of axons in gray matter. Many oligodendrocytes were also found to stain positive for Tau-1, which has been reported previously [171-175]. Tau-1 positive staining generally bordered the scaffold (Figure 4.29), but in isolated cases was seen to encroach slightly within the scaffold margins (Figure 4.30 and Figure 4.31).

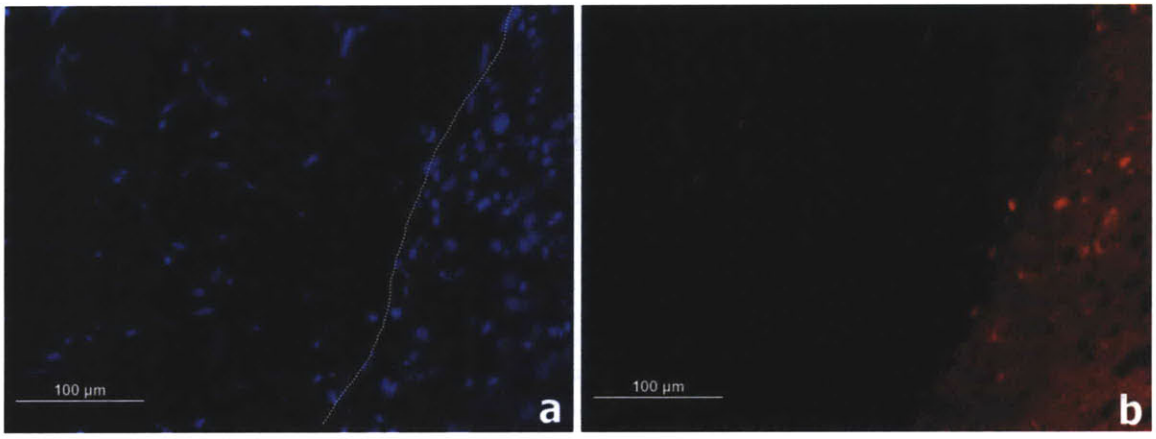

Figure 4.29. Tau-1 staining bordering a collagen scaffold after 4 weeks (Group 5). a) DAPI staining showing cells bordering and within the scaffold. The white line indicates the scaffold border. b) Tau-1 staining showing axons bordering the scaffold, but not entering it.

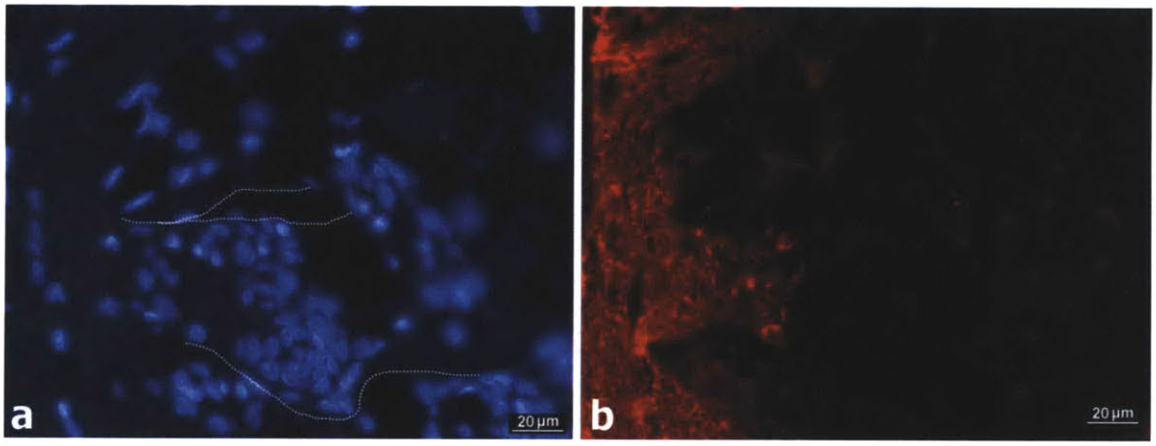

Figure 4.30. Tau-1 staining near the border of an sNgR loaded scaffold after 4 weeks (Group 6). a) DAPI staining showing cells near the scaffold border and slightly within it. White lines indicate scaffold struts. b) Tau-1 staining which comes in contact with the scaffold near the lesion border.

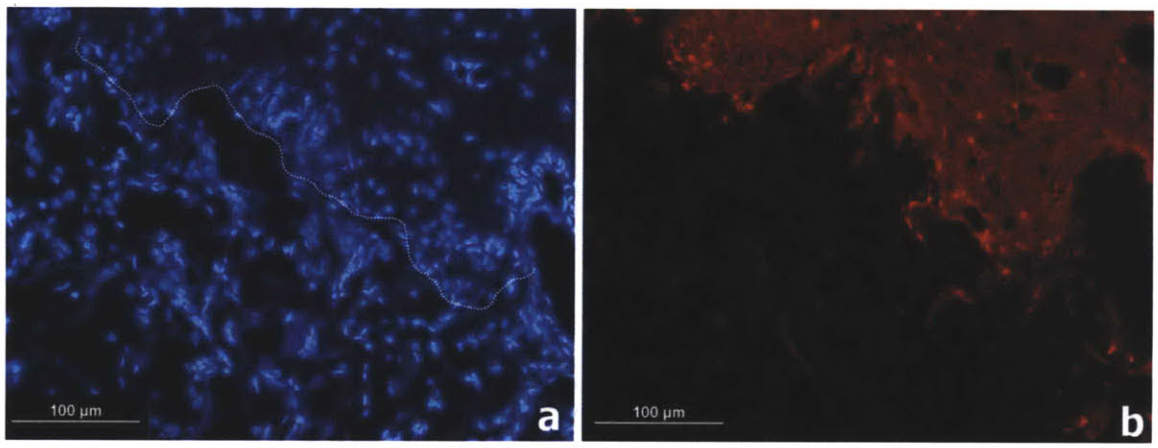

Figure 4.31. Tau-1 staining near the border of an sNgR loaded scaffold after 8 weeks (Group 7). a) DAPI staining showing a dense cellular infiltrate into the collagen scaffold. The scaffold border is indicated by the white line. b) Tau-1 staining showing axons in contact with the scaffold border, but not extending far within the scaffold.

4.4 Discussion

The procedure for preparing and implanting the collagen scaffolds resulted in the lesion cavities being mostly filled several weeks after implantation. Knowledge of the approximate size of the defect after 1 week, and later after 5 weeks allowed for a reasonably appropriate choice of scaffold size. While there are areas for improvement to

ensure that viable tissue is not injured during the implantation, several principles can be taken away from this study and previous work to plan future experiments with the PBI model. First, previous work implanting dry scaffolds seemed to have produced variability in terms of the amount of bleeding induced and the final volume of the lesion after 4 weeks. Here, we have taken the approach of hydrating the scaffold prior to implantation, resulting in a softer material of stiffness similar to that of the brain. For scaffolds loaded with protein or having undergone multiple freeze-drying cycles, hydration is also crucial for expanding the material and opening the pores. The timing of this expansion is of importance due to the limited size of the cranial window through which the material is implanted. A fully expanded scaffold of 6 mm diameter is considerably larger than the cranial window, which measures only 3-4 mm. By hydrating the scaffold immediately prior to implantation, the scaffold can be inserted through the window before it has fully expanded. The scaffold is thus easier to insert, but will expand *in vivo* to come in contact with the border of the cavity. By designing the scaffold to have mechanical properties reasonably similar to brain, it can safely rest within the tissue in a slightly compressed state after the initial implantation. Additionally, it appears from our observations that the scaffold will continue to expand as the lesion cavity grows over several weeks. The size of the scaffold should thus be carefully chosen, as a scaffold that is too large may cause tissue damage, while an undersized scaffold will fail to fill the defect. The scaffolds used in Group 5 may have been slightly too large, as the size of the lesion was somewhat greater than in lesions without scaffold implantation. It is noted that the implantation procedure can be simplified by increasing the size of the cranial window. While this is an option, we

considered it preferable to minimize the size of the craniotomy in light of the severity of the injury to be administered in the animals. One can also consider the use of injectable materials that solidify or gel after being introduced into the brain [176-179]. They have the advantage of conforming to the shape of the cavity, but are limited in terms of controlling pore size, a critical factor for cellular infiltration.

The difference in cellular infiltration between Group 5 and the sNgR groups indicates an effect of the soluble Nogo receptor, but the nature of the histological response appears somewhat complex in light of the supporting immunohistochemistry. The pattern of GFAP staining suggests that the neither the scaffold, nor the sNgR, have an effect on the glial scar. The dense gliosis surrounding the lesion was also notable in that it generally did not extend to within the scaffold, though we did observe more astrocytes after 8 weeks relative to 4 weeks. Previous studies have reported that scaffolds of varying composition seem to promote astocyte infiltration [130, 135], with potential disruption of the glial scar [134]. Given that the densities of GFAP positive cells was relativelylow, it appears that astrocytes do not have a strong affinity for migrating into collagen scaffolds *in vivo*. This is consistent with our previous results using smaller scaffolds, although the degree of cellular infiltration was less in those cases. The lack of astrocytes within the scaffolds in this study was somewhat surprising in consideration of the fact that multiple other cell types were present. While astrocytes are a source of chondroitin sulfate proteoglycans that contribute to the glial scar [180, 181], it appears that the dense extracellular matrix within the scaffolds in Group 6 was not deposited by astrocytes. Rather, it is likely that the macrophages/microglia within the scaffolds were responsible for the extracellular matrix.

The CD68 positive macrophages were the most common cell type identified in the scaffolds of all groups. This is an expected result due to the persistence of the biomaterial at 5 weeks, as virtually any implant will elicit some degree of a foreign body reaction. There was a difference, however, in that the scaffolds containing sNgR had more macrophages in them and also displayed more multinucleated giant cells. There are a number of possible explanations for these observations. First, it is possible that the sNgR molecule itself was recognized as being foreign, thus stimulating an immune response to eliminate it. This seems unlikely due to the fact that the NgR molecule and the Fc region it is fused to are both of rat origin. Further, the sNgR molecule has been used in a number of other studies without evidence of an immune response. However, the presence of the Fc region itself might be the initiator of the immune response due to complement binding. Another possibility is that the amount of protein delivered, rather than the identity of protein, promoted a macrophage response. In contrast to other studies that delivered continuous small doses of sNgR over long time periods, the implanted scaffold contained the entire dose of sNgR. The introduction of several hundred micrograms of protein at once might have induced a macrophage response, possibly through binding of complement. It is possible that sNgR with bound myelin proteins might also promote complement binding and a subsequent macrophage infiltration to clear the complexes. The presence of the multinucleated giant cells throughout the scaffold suggests that perhaps the cross-linking procedure in the sNgR group affected the antigenicity of the scaffolds. This would imply that the sNgR cross-linked to the scaffold enhanced the foreign body response to the material. This, however, also seems unlikely due to the small amount of sNgR that could be cross-linked and the fact that the cross-

linked sNgR would not be appreciably different from the free sNgR loaded in the scaffold. While the cross-linking might disrupt certain epitopes of the protein, there is no particular reason to believe that this would affect the response by macrophages. If the cross-linked sNgR had bound and immobilized myeling proteins, complement binding might then induce a macrophage response directed against the scaffold-sNgR-myelin complex. A simpler explanation would be that the presence of the protein simply increased the degree of cross-linking of the scaffold. A more highly cross-linked scaffold might thus be more likely to induce a robust foreign body reaction. It has been shown that the addition of the lysine amino acid increases the stability of collagen cross-linked by carbodiimide treatment [182] . This explanation potentially falls short due to the fact that the cross-linking procedure in Group 1 was expected to rather thoroughly cross-link the collagen even in the absence of an additional protein. Based on previous work, one would expect a high degree of cross-linking after a 1 hour reaction with an EDC:NHS ratio of 5:2 [96]. Thus, any additional cross-linking due to the sNgR would be unlikely to change the chemical structure of scaffold to a large extent.

A somewhat intriguing idea relates to recent discoveries that some macrophages actually express the Nogo receptor [183-186]. In one study examining clearance of macrophages from peripheral nerve injuries, it was found that the presence of myelin seemed to promote macrophage efflux from the injury site [184]. Blocking the action of myelin proteins via NgR knockouts, siRNA knockdowns of NgR, or intracellular Rho/ROCK inhibition reversed the effect and resulted in macrophages persisting in the lesion site. It was suggested that similar effects might be present in the central nervous system such that myelin proteins act as repulsive agents to keep macrophages from

spreading beyond the injury site and also act as a cue for macrophage efflux as the inflammatory response dies down [183]. As a result, it was hypothesized that blocking NgR signaling might result in the persistence of macrophages at CNS lesion sites. It is noted, however, that in such a scenario there must be a balance between myelin proteins instructing macrophages to migrate away and the presence of necrotic debris with cytokines etc. telling macrophages to migrate towards the injury. The distinction between myelin proteins within a necrotic region of the CNS that must be cleared, and those within intact axonal myelin causing macrophage clearance is not clear. While further study would be required to elucidate the mechanism, it does appear that the delivered sNgR had some effect on promoting macrophage infiltration of the scaffolds. The increased macrophage density in Group 6 relative to Group 7 does not have an obvious explanation, but it could simply be the result of variation in the animals groups and scaffold preparation.

The presence of significant vascularity within the scaffolds of Groups 6 and 7 provides a potential framework for future regenerative therapies. Untreated defects of this kind typically result in a large cavity, free of any cellular or extracellular matrix components. In order for any regeneration to take place, the void must be filled with a physical substrate for cell and axon growth, but also must have a source of oxygen for cell survival. By demonstrating the formation of vessels throughout a portion of the scaffold filling the defect, the possibility for survival of endogenous or transplanted neural cells is greatly enhanced. While the infiltrating cells in the scaffold are clearly viable, one can foresee a therapy in which exogenous cells might be delivered to the

lesion site after allowing a sufficient time for vacularization and extracellular matrix formation within a scaffold.

Given that Group 5 had fewer vessels within the boundary of the scaffolds, the sNgR receptor appears to have had an indirect effect on vascular proliferation. It appears likely that the increase in macrophage infiltration in Groups 5 and 6 also served to increase recruitment of endothelial cells for vessel formation. Further, the extracellular matrix deposited by the macrophages was likely important for small vessel formation due to the relatively large pore size of the scaffolds. Macrophages and endothelial cells infiltrating have been observed to infiltrate biomaterials implanted in the brain in other studies [33, 126, 129, 132].

The isolated areas in which neurons and oligodendrocytes were observed within the scaffold border are likely not indicative of any significant regenerative response. Rather, these areas demonstrate that there the collagen scaffold can integrate with viable brain tissue in particular areas. This may be related to variability in the glial scarring, making some regions more conducive to interaction of neurons and oligodendrocytes with the biomaterial. The sNgR molecule was intended as a therapy to bind myelin proteins in the injury site, thus permitting an increased degree of axonal regeneration. If regenerating axons did indeed infiltrate into the scaffold, it would be reasonable to assume that oligodendrocyte might also migrate to the lesion to myelinate the axons. However, we were unable to observe significant ingrowth of axons into the scaffold beyond isolated peripheral areas. A smaller injury with a smaller scaffold would be helpful in better understanding whether the areas of tissue integration we have observed may have any therapeutic potential. In future work, antibody staining for GAP-43 may

also be of benefit for visualizing axons that may be regenerating even if they are not in the scaffold.

The role of the macrophages in and around the scaffold may be both beneficial and harmful for regeneration. Given that the scaffold does not appear to degrade significantly over a period of several weeks, it is possible that it could remain indefinitely. Whether or not this might have major deleterious effects is unknown. If a proliferation of giant cells persists to a greater extent, it could be harmful and lead to a loss of viable tissue [139]. Clearly, this would not be an appropriate environment for regeneration of axons and migration of neurons. Macrophages have, however, been shown to have beneficial effects in regeneration after optic nerve lesions [187]. The effects of inflammatory processes involving macrophages and their interactions with other cell types is a topic of considerable complexity. With regard to this work, it can be concluded that the presence of macrophages in the scaffold seems to have correlated with increased vascularity of the lesion site. The fact that a very large cavity can potentially be vascularized seems to be a positive development. Development of a more degradable scaffold might allow for vascularization and ECM deposition, but with an eventual resolution of the macrophage response. The lesion site might then present a more suitable environment for regenerative therapies.

Acknowledgements

We thank Daniel Lee and Paul Weinreb at Biogen Idec for generously providing the soluble Nogo receptor. We also thank Alix Weaver for assistance with hematoxylin and eosin staining.

Chapter 5: Implantation of a Collagen Scaffold Seeded with Adult Rat Hippocampal Progenitors in a Rat Model of Penetrating Brain Injury

5.1 Introduction

Pre-clinical studies of stem/progenitor cell therapies have shown promise for a number of central nervous system injuries and diseases [55, 57, 188-195]. The unique characteristics of each pathology guide the various decisions that must be made for designing an appropriate therapeutic strategy. Some of the considerations that must be taken into account include the goal of the therapy (e.g. neuroprotection vs. regeneration), the cell type to be used, the environmental conditions affecting survival, proliferation, and differentiation *in vitro* and *in vivo*, the medium for delivering the cells, the desired anatomical location for engraftment, and the timing and surgical procedure for administering the therapy. Many of these factors are not independent, and compromises must inevitably be made in choosing how to proceed.

Penetrating brain injury, commonly encountered in military conflicts due to bullets and shrapnel, represents a somewhat complicated case for cellular therapies. The injury is characterized by tissue destruction along the trajectory of the projectile, as well as damage to surrounding areas from the formation of a temporary cavity. The temporary cavity results from dissipation of the projectile's kinetic energy as it tumbles through the tissue, and may commonly be many times larger than the diameter of the projectile [39]. A combination of mechanical damage, along with hemorrhage, ischemia, and cytotoxic molecular elements, leads to a complex and often severe injury. A rat model of PBI has been developed recently that reproduces several aspects of the clinical injury without the use of actual projectile. The model involves insertion of balloon-tipped probe into the brain, followed by a rapid inflation of the balloon to mimic the temporary cavity seen in a ballistic injury [40]. While not reproducing all aspects of clinical PBI (e.g. infection and

retained fragments in the brain), this model serves as a useful tool for studying implantation of potential cellular therapies into a standardized cavitary defect.

The goals for treatment of PBI may include both neuroprotection to mitigate the extensive secondary injury, and also regeneration to replace lost neurons and glial cells. The extent to which both goals might be achieved with the same cell population remains to be elucidated as the field moves forward, but current research indicates that all available cell sources have significant limitations that would make a single cell therapy inadequate. Rather, a particular cell type might be suitable for addressing some of the elements of the larger problem, while a combination of delivered cell types might be necessary for a more complete therapy. In PBI, several different regions of the brain may be affected, each with a variety of different cell types and subtypes. An attempt at replacing or rebuilding part of a lost brain structure would likely require a comprehensive multifactorial approach targeting inflammation, cytotoxic elements, inhibitory factors, growth states of endogenous cells, implantation of large numbers of exogenous replacement cells, and appropriate control mechanisms for differentiation and anatomical localization for the delivered cells.

Addressing the multitude of obstacles that prevent full regeneration after brain injury remains a goal for the future. At present, we focus on a few important features of PBI in consideration of how cellular therapy might be of potential benefit. The injury environment immediately after PBI is likely to be highly inhospitable for implanted cells. Hemoglobin and glutamate toxicity, along with ionic imbalances and regions of ischemia are likely to kill exogenous and endogenous cells alike [41]. It would logically be advantageous from a cell-survival standpoint to wait until the acute phase of the injury

has resolved before performing an implantation . We have thus chosen for this study to wait 1 week after injury before delivering cells to the injury site.

While neural progenitor cells of varying origin have been implanted in traumatic brain lesions [177, 178, 196-215], we have chosen to use a population of adult hippocampal neural progenitors [216, 217]. The cells have been demonstrated to survive and differentiate into neurons, astrocytes, and oligodendrocytes both *in vitro* and *in vivo* when implanted into the uninjured brain [216]. Further, *in vitro* experiments have demonstrated that the cells can differentiate into neurons with various neurotransmitter phenotypes [218]. This particular population of cells, which has been well-characterized [216-223], does not appear to have been previously implanted in a model of traumatic brain injury. In this work, we have evaluated the survival and differentiation of these cells in the rat model of PBI.

The histological response to PBI involves the eventual clearance of necrotic debris, resulting in the formation of a large cavity in the brain. This cavity, surrounded by a glial scar, remains unfilled and essentially precludes the possibility of any significant regeneration within the lesion. Filling the cavity with a biomaterial can provide mechanical continuity across the lesion, while also serving as a delivery vehicle for cells. In this work, we implanted a pre-formed collagen scaffold seeded with BrdU-labeled undifferentiated neural progenitors. Survival and differentiation were then analysized with immunohistochemical methods.

5.2 Materials and Methods

5.2.1 Experimental Design

6 male Sprague-Dawley rats underwent a bilateral penetrating brain injury involving insertion of a balloon-tipped probe, followed by inflation of the PBI balloon to a volume approximately equal to 10% of that of the rat brain. 1 week later, the animals underwent a second surgery in which they were implanted with a collagen scaffold seeded with BrdU-labeled adult hippocampal neural progenitors. Animals were sacrificed 4 weeks later (5 weeks post-injury).

5.2.2 Penetrating Brain Injury Apparatus

The PBI model was developed at the Walter Reed Army Institute of Research and has been used in several published studies to date [40, 42, 43, 122]. The model aims to simulate damage to the brain caused by a projectile by mimicking both the destruction of tissue along the projectile path, as well as the temporary cavity formed by dissipation of the projectile's kinetic energy. The injury is created by inserting a probe into the brain, which has a balloon attached near the tip. With the probe inserted, a pneumatic device creates a pressure impulse to rapidly inflate and deflate the balloon within the brain. The result of the balloon expansion is to compress the surrounding tissue, similar to the action of the temporary cavity in a ballistic injury. Although the model does not recreate certain features of the clinical injury, such as retained bone fragments or subsequent infectious processes, it is useful for studying other characteristics of the injury and for creation of a standardized cavitary defect in the brain.

5.2.3 Collagen Scaffold Fabrication

Type I collagen scaffolds (1.0% weight:volume) were fabricated from medical grade porcine microfibrillar collagen (Geistlich Biomaterials, Wolhusen, Switzerland). A suspension of the collagen was made in 0.001 N HCl, brought to pH 3, and mixed for 20 minutes. The slurry was blended at 15,000 RPM (Ultra Turrax T18 blender, IKA, Staufen, Germany) for 30 minutes at 4° C, brought again to pH 3, and blended for an additional 2 hours. The slurry was then centrifuged for 10 minutes at 5500 RPM to remove bubbles, and mixed with a pipette to ensure homogeneity. The slurry was poured in a metal mold and placed into an AdVantage Benchtop Freeze Dryer (VirTis, Gardiner, NY). The temperature was decreased at a controlled rate to -40° C over 180 minutes and held at -40° C for 60 minutes. Sublimation was conducted at 0° C and a pressure of 200 mTorr for 1020 minutes. Scaffolds were then dehydrothermally sterilized and cross-linked overnight at 105° C under vacuum. Published work using similar scaffolds has determined the pore size to be approximately 100-150 μm.

5.2.4 Cell Culture and Scaffold Seeding of Adult Hippocampal Neural Progenitors

T-150 cell culture flasks were coated overnight with 10 μg/mL poly-L-ornithine, rinsed twice with sterile water, and coated again overnight with 5 ug/mL mouse laminin. Frozen cells were thawed and plated at a density of approximately 10,000 cells/cm^2. The cells were plated and expanded in DMEM/F12 high glucose medium containing L-glutamine, 1% penicillin, 1% streptomycin, 1% N2 supplement, and 20 ng/mL FGF-2. The medium was changed every 2-3 days. At the time of the first medium change, 2.5 μM BrdU was added and maintained throughout the culture period. On the morning of

the implantation surgery the cells were detached using Accutase, counted, and resuspended in medium at a density of approximately 20 million cells/mL.

Collagen scaffolds approximately 6 mm in diameter and 3 mm in thickness were placed in a 96-well plate to immobilize them for cell-seeding. A total of 60 μL of the cell suspension was pipetted onto the scaffold in each well in 3 increments of 20 μL. The 6 mm scaffolds were larger than desired for implantation, so a 4 mm biopsy punch was used to obtain the desired 4 mm scaffolds. The number of cells in the 4 mm diameter scaffolds was not known precisely, but was estimated to be around 4-5 million based on the density of the cell suspension and the volume of the scaffold. After seeding, the scaffolds were kept in an incubator until the time of surgical implantation.

5.2.5 Surgical Procedure and Animal Care

6 male Sprague-Dawley rats were used in this study. All procedures were approved by the Boston VA Healthcare System Institutional Animal Care and Use Committee.

Animals were shaved, anesthetized with isoflurane, and positioned in a stereotaxic frame where the anesthetic delivery was maintained through a nosecone. A circulating water heating pad was used to maintain body temperature throughout the surgery and also for several hours during the post-operative recovery. Heart rate and blood oxygen saturation were monitored from a probe on the foot during the procedure.

After sterilizing the skin with 13% povidone iodine solution, a midline incision was made along the top of the head to expose the skull, followed by a lateral incision extending from the posterior aspect of the midline incision and passing just anterior to the left ear. With the top of the skull and the left side of the head exposed, a portion of the

left temporalis muscle was excised with care taken to avoid damaging the temporal branch of the facial nerve. With the lateral aspect of the skull exposed, a 3 mm diameter window was drilled in the skull at a position 1 mm anterior to bregma and 3 mm ventral to bregma.

The PBI probe was inserted into the brain, with the tip advanced 10 mm from the surface of the left hemisphere into the right hemisphere. The PBI balloon was inflated to a diameter of 6.3 mm to create an injury encompassing approximately 10% of the rat brain volume. It is noted that the balloon is several mm proximal to the tip of the probe, such that the balloon inflation is predominately in the left hemisphere despite the probe tip being in the right hemisphere. This scenario mimics a projectile entering the left hemisphere and dissipating its kinetic energy before coming to rest in the right hemisphere. Following the balloon inflation, the probe was retracted from the brain and bleeding was controlled using Gelfoam. The cranial window was covered with a Bio-Gide collagen membrane (Geistlich Biomaterials, Wolhusen, Switzerland) and the surgical incision was closed with a 4-0 suture.

1 week after the injury, animals underwent a second surgery in which a second incision was made parallel to the lateral incision from the first surgery, enabling access to the defect site. After removing the collagen membrane covering the cranial window, the lesion site was exposed. A cell-seeded collagen scaffold was then implanted into the lesion site. The cranial window was covered again with a collagen membrane and the incision closed with a 5-0 suture.

Following all surgeries, animals were allowed to recover in warmed cages with additional oxygen and food and water provided at bedding level. Buprenorphine (0.05

mg/kg) was given for pain relief, while Cefazolin (20 mg/kg) was given to prevent infection.

5.2.6 *Animal Sacrifice and Specimen Processing*

Animals were sacrificed 4 weeks after the implantation of the collagen scaffolds (5 weeks post-injury). Before sacrifice, animals were deeply anesthetized with an intraperitoneal injection of sodium pentobarbital (150 mg/kg). Animals were then transcardially perfused with 150 mL cold heparanized PBS (20 units/mL) followed by 250 mL cold 4% paraformaldehyde solution (USB corporation 19943, Cleveland, OH.) Brains were extracted and immersed in 4% paraformaldehyde for 2-3 days at 4° C. Brains were processed through reagent alcohol (70% - 10 min, 80% - 90 min, 95% - 2 x 90 min, 100% - 2 x 90 min, 100% - 90 min under vacuum), xylene (3 x 90 min), and paraffin (2 x 180 min under vacuum, 58° C). Samples were then embedded in paraffin and sectioned on a mictrome at 5 μm. Sections were taken at approximately 1 mm intervals spanning the lesion. Slides were dried on a warmer at 60° C for several hours.

5.2.7 *Histology and Immunohistochemistry*

Sections were stained with hematoxylin and eosin for histomorphometric analysis and for general histologic observation of the injury.

The fluorescent dye Fluoro-Jade C (Millipore AG325) was used for visualization of degenerating neurons near the lesion and remotely in the thalamus. Sections from approximately 1 mm anterior to bregma and 2.5 mm posterior bregma were deparrafinized and rehydrated prior to incubation in 0.06% $KMnO_4$ (Sigma 223468) for

20 minutes. After 3 rinses in deionized water, slides were then stained with 0.00015% Fluoro-Jade C solution for 20 minutes and rinsed 3 more times in water. Slides were dried on a warmer at 60° C for 10 minutes, placed in xylene for several minutes, and coverslipped with Cytoseal mounting medium.

Antibodies, dilution factors, and antigen retrieval methods used for immunohistochemistry without BrdU staining are summarized in Table 4. The staining procedure was conducted at room temperature. Following deparrafization, rehydration, and antigen retrieval, slides were rinsed with wash buffer (Dako S3006) containing TBS and 0.05% Tween 20. Slides were blocked for 2 hours with Dako protein block (Dako X0909) prior to addition of the primary antibody for 2 hours. Following 3 rinses with wash buffer, the secondary antibody was added for 1 hour. After 3 more rinses, a 100 ng/mL solution of the fluorescent DNA stain 4',6-diamidino-2-phenylindole (DAPI) was added for 30 minutes. 3 final rinses with wash buffer were performed and the slides were then placed in TBS for 3 minutes. The slides were transferred to a 0.1% solution of Sudan Black (Sigma 199664) dye for 20 minutes in to reduce tissue autofluorescence. Following 3 rinses in TBS, slides were coverslipped with Immu-mount aqueous mounting medium (Thermo Scientific 9990402).

For BrdU double-labeling, the slides underwent antigen retrieval in citrate buffer at 120° for 1 min, but for GFAP and CD68 staining there was no protease treatment. Von Willebrand factor slides had additional protease treatment for 20 minutes. It was observed that the protease treatment caused degradation of the scaffolds, and thus most of the cells observed were in the surrounding brain tissue. For the BrdU staining, 10% donkey serum was used for the blocking step, while the Dako wash buffer was used to

dilute the antibodies. Reagents containing bovine serum albumin were avoided due to potential cross-reactivity of bovine IgG with the anti-goat secondary antibody. Double labeling was conducted sequentially, rather than simultaneously.

Table 5 Immunohistochemistry reagents (Abbreviations: rb (rabbit), ms (mouse), gt (goat)

1° Antibody	Source	Retrieval	Dilution	2° Antibody
GFAP (rabbit polyclonal)	Dako (Z0334)	0.1% Protease XIV 25 min (Sigma P5147)	1:500	Dylight 488 donkey anti-rabbit IgG (Jackson ImmunoResearch 711-485-152)
Von Willebrand Factor (rabbit polyclonal)	Dako (A0082)	0.1% Protease XIV 40 min (Sigma P5147)	1:100	Dylight 488 donkey anti-rabbit IgG (Jackson ImmunoResearch 711-485-152)
Doublecortin (goat polyclonal)	Santa Cruz (sc-8066)	Citrate buffer pH 6, 2 min 120° C (Dako S1699)	1:100	Dylight 488 donkey anti-goat IgG (Jackson ImmunoResearch 705-485-003)
CD68 (mouse monoclonal IgG)	Serotec (MCA341R)	0.1% Protease XIV 20 min (Sigma P5147)	1:200	Dylight 549 donkey anti-mouse IgG (Jackson ImmunoResearch 715-505-150)
NeuN (mouse monoclonal IgG)	Millipore (MAB 377)	Citrate buffer pH 6, 1 min 120° C (Dako S1699)	1:200	Dylight 549 donkey anti-mouse IgG (Jackson ImmunoResearch 715-505-150)
MAP1b (mouse monoclonal IgG)	Abcam (ab3095)	Citrate buffer pH 6, 1 min 120° C (Dako S1699)	1:100	Dylight 488 donkey anti-mouse IgG (Jackson ImmunoResearch 715-485-150)
CNPase (mouse monoclonal IgG)	Abcam (ab6319)	Citrate buffer pH 6, 20 min 95° C (Dako S1699)	1:500	Dylight 549 donkey anti-mouse IgG (Jackson ImmunoResearch 715-505-150)
BrdU (sheep polyclonal)	Abcam (ab1893)	Citrate buffer pH 6, 1 min 120° C (Dako S1699)	1:200	Dylight 549 donkey anti-sheep IgG (Jackson ImmunoResearch 713-

				505-147)

5.2.8 Imaging

Light microscope images were taken with an Olympus camera interfaced with a Olympus BX51 microscope, while fluorescent images were captured an Olympus DP71 camera interfaced with an Olympus BX60 microscope. Adobe Photoshop CS3 was used for minor image processing procedures such as cropping and adjustment of levels to reduce background.

5.2.9 Histomorphometric Analysis and Cell Counts

Lesion area was demarcated in hematoxylin and eosin stained sections at approximately 1 mm intervals spanning the lesion. The lesion was defined by areas of obvious necrosis with lack of cellularity, along with regions of dense macrophage infiltration, hemorrhage, gliosis, and vacuolization. A linear interpolation was used to reconstruct an approximate volume, with the volume between sections being equal to the average of the areas multiplied by the distance between them. Cell density was determined by counting the number of cells within the scaffold and normalizing by diving by the scaffold area.

5.2.10 Statistics

Numerical values are reported as mean ± standard error, and all statistical analysis was performed using Statview (version 5.0.01, SAS Institute Inc., Cary, NC). Unpaired t-tests were used to compare differences between experimental groups, with a p-value of 0.05 used for determining statistical significance.

5.3 Results

5.3.1 Animal Survival, Recovery, and Qualitative Behavioral Observation

Qualitatively, the animals in this work did not show obvious behavioral differences relative to our previous work. Similar to other groups, there was some weight loss over the first couple days after the injury which was subsequently regained (Figure 5.1). The rats had a deficit in their right forelimb during the first few days after injury, which was notable mainly when they were grasping food. The weakness and/or lack of coordination improved over the first week such that they eventually were able to grasp food normally with both forelimbs. It is possible that minor improvements in forelimb function might have been present as a result of implanted cells, but sensitive behavioral tests would have been necessary for detection. We do note that the animals appeared to suffer no deleterious effects as a result of the implanted cells. All animals undergoing the implantation procedure recovered without problems and survived the duration of the study.

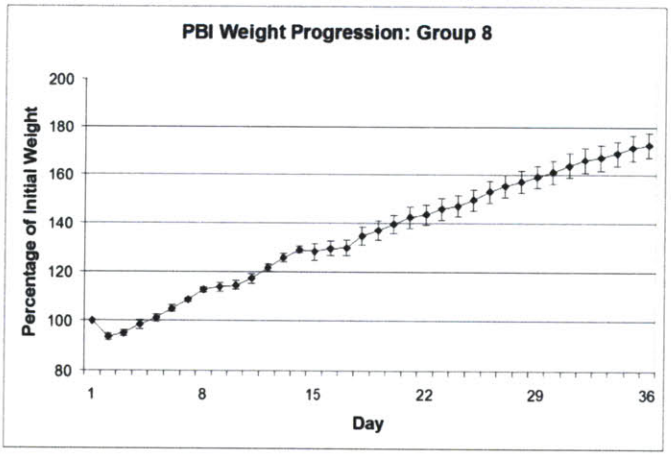

Figure 5.1. PBI Weight Progression for Group 8. Animals typically lost weight for 1-2 days after the injury, but thereafter resumed weight gain. Weight was generally maintained following the 2nd surgery to implant the cell-seeded scaffold.

5.3.2 Lesion Volume and Scaffold-Brain Histological Observations

Histology revealed that the lesion consisted of very large cavity, similar to that seen in previous studies after 5 weeks. The average volume of the entire lesion was found to be 58.0 ± 6.7 mm^3. The implanted scaffolds were present and structurally intact, but did not fill the entire cavity (Figure 5.2a). There appeared to be areas of integration between the scaffold and surrounding brain tissue, typically near the lateral aspect of the lesion (Figure 5.2b). Cells of heterogeneous morphology were present bordering and within the scaffolds (Figure 5.2c).

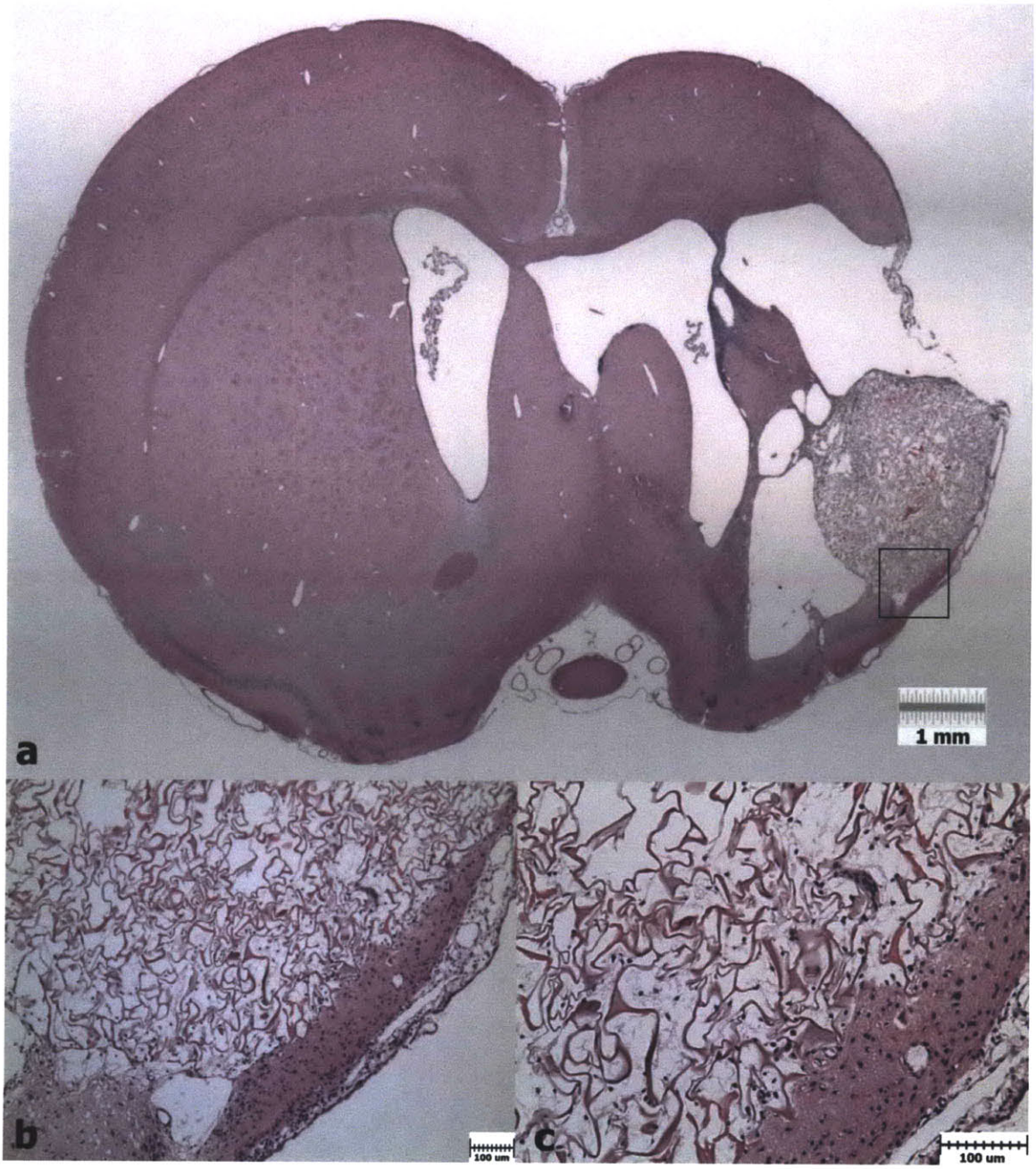

Figure 5.2. H&E Histology of a Scaffold Seeded with Neural Progenitors (Group 8). a) H&E image of a scaffold within the lesion site 4 weeks after implantation. b) Integration of the scaffold with tissue a the lateral edge of the brain. c) Cellular infiltration of the scaffold.

5.3.3 Implanted Cell-Seeded Scaffolds

At the time of seeding the collagen scaffolds for surgical implantation, additional scaffolds were seeded and processed for immunohistochemical evaluation. It was desired

to verify *in vitro* the status of the cells as being BrdU-labeled and predominantly undifferentiated. Antibody staining confirmed that nearly all of the cells were BrdU positive (Figure 5.3), while many were Nestin positive (Figure 5.4). Very few cells were GFAP positive (Figure 5.5). No positive staining could be detected for CNPase, NeuN, MAP1b, VWF, and CD68.

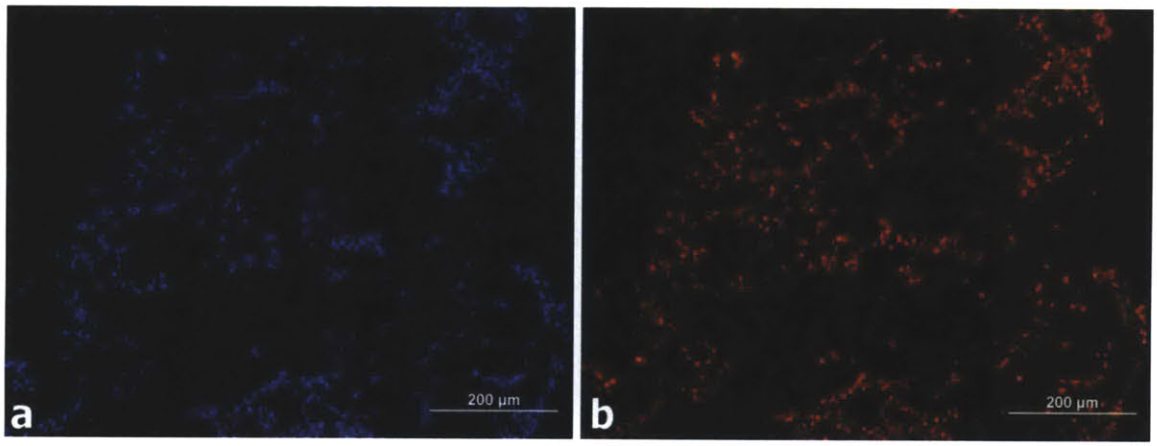

Figure 5.3. Collagen scaffold containing BrdU labeled neural progenitors (prior to implantation). a) DAPI staining showing the nuclei of cells within the scaffold. b) BrdU staining showing that nearly all of the cells within the scaffold were labeled with BrdU.

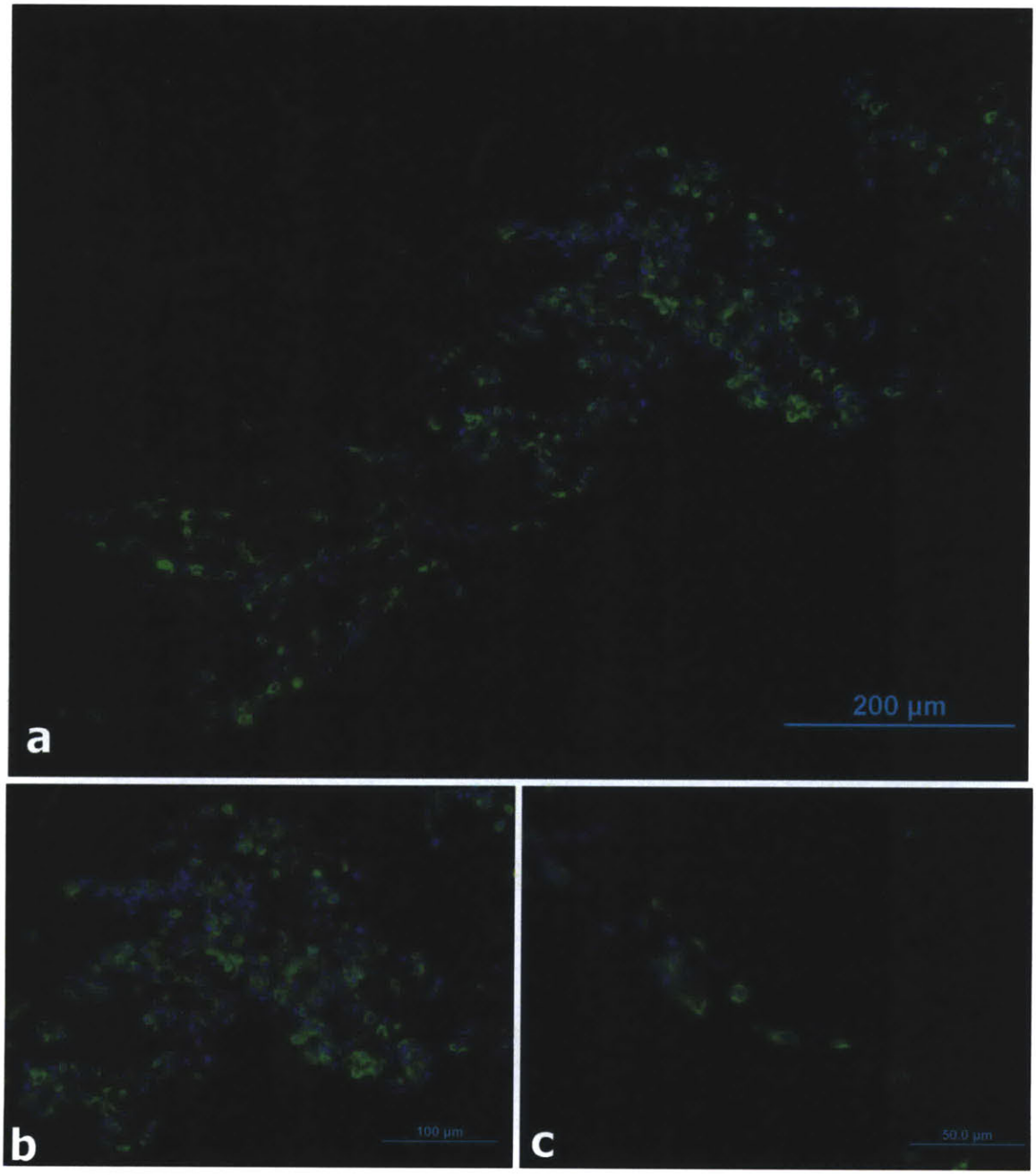

Figure 5.4. Collagen scaffold containing nestin-positive neural progenitors (prior to implantation). a) 10x magnification image showing many cells staining positive for nestin within the scaffold. b) 20x image showing a cluster of cells with most staining positive for nestin. c) 40x image of nestin positive cells along a scaffold strut. (Green: Nestin, Blue: DAPI)

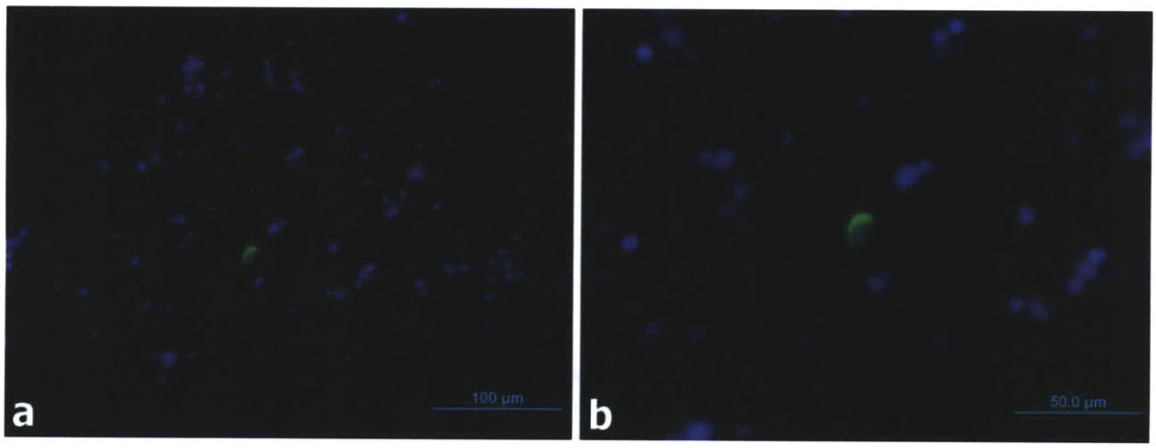

Figure 5.5. Collagen scaffold containing a GFAP positive cell (prior to implantation). a) 20x image demonstrating that very few cells in the scaffold were GFAP positive. b) 40x image of a GFAP positive cell. (Green: GFAP, Blue: DAPI)

5.3.4 Survival of Implanted Neural Progenitors

Despite the large lesion and the undersized scaffold, implanted neural progenitors were detected in brains from all of animals. The BrdU staining revealed that some of the cells had remained in the scaffold, while others had migrated into the surrounding brain tissue (Figure 5.6). BrdU labeled cells could be detected several hundred micrometers from the scaffold border, and were restricted in all cases to the ipsilateral hemisphere.

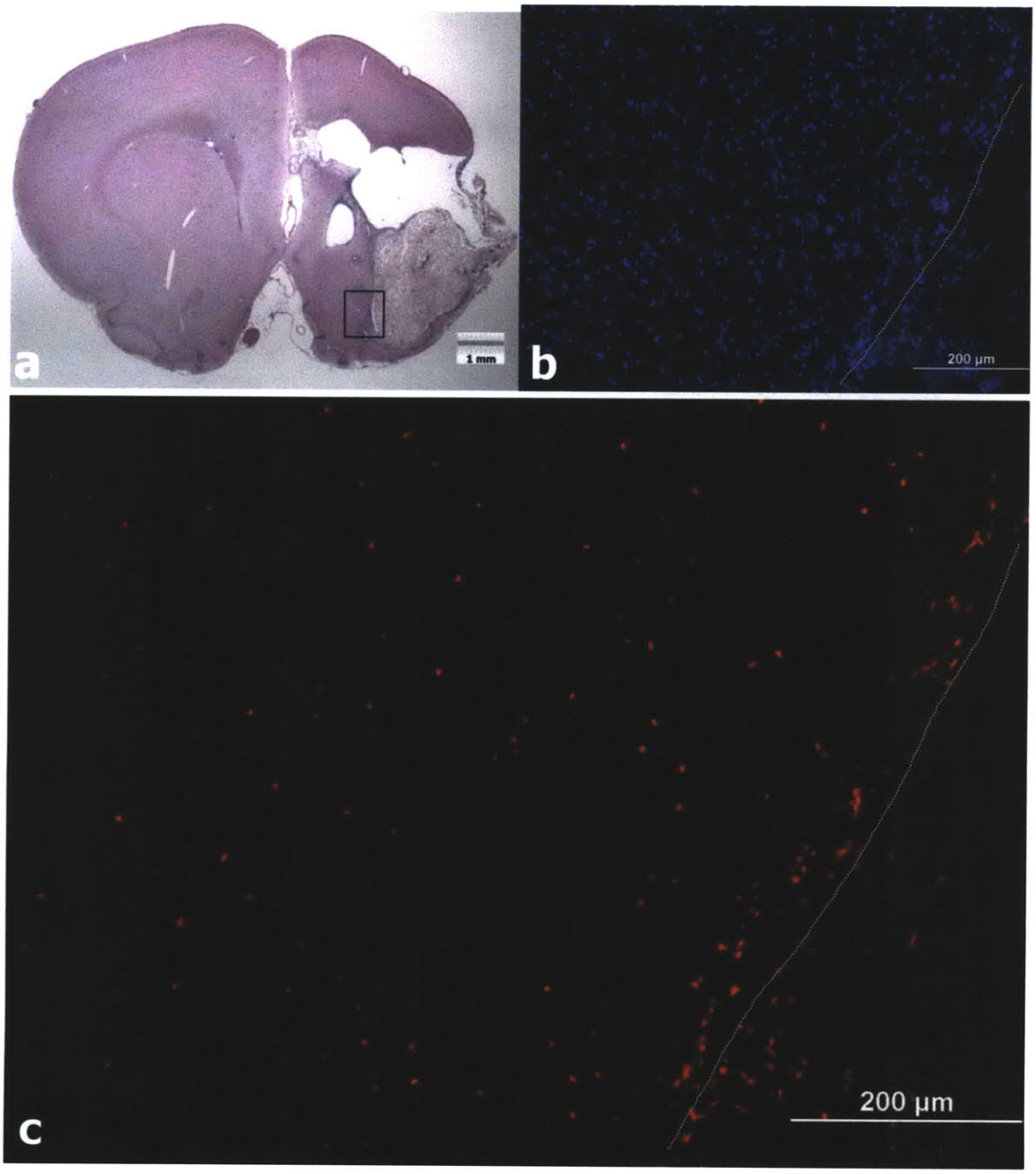

Figure 5.6. BrdU labeled neural progenitors detected *in vivo* 4 weeks after implantation. a) H&E image of a scaffold within the PBI lesion 4 weeks after implantation. b) DAPI staining (blue) showing nuclei of cells at the scaffold border (white line) and within the brain on the medial side. c) BrdU staining (red) showing implanted cells that have survived in the brain after 4 weeks.

5.3.5 Glial Scarring and Inflammation: GFAP and CD68 Staining

The typical pattern of glial scarring was observed around the lesion in the form of upregulated GFAP expression. Areas of gliosis diminished with increasing distance from the lesion, but appeared to be upregulated throughout much of the left hemisphere. A small amount of GFAP staining was present within the collagen scaffolds, though the majority of cells were negative. A number of BrdU labeled cells in the surrounding brain tissue were also found to be GFAP positive. BrdU-positive astrocytes could be detected within areas of glial scarring (Figure 5.7a) in all of the samples. In at least 4 samples, BrdU-positive astrocytes could also be found within areas of normal-appearing brain (Figure 5.7b).

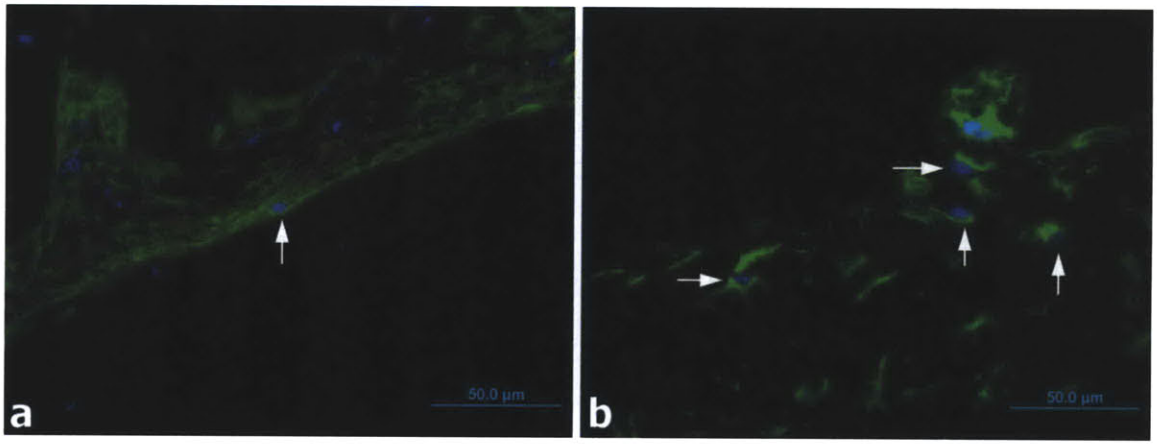

Figure 5.7. Implanted neural progenitors staining positive for BrdU and GFAP after 4 weeks. a) Double labeling for DAPI (blue) and GFAP (green) showing that some implanted cells differentiate into astrocytes (arrow) among the glial scar bordering the scaffold. b) Double labeling showing implanted cells that differentiate into astrocytes (arrows) in normal appearing brain tissue.

CD68 staining revealed the presence of many macrophages in and around the lesion site, as well as in both ipsilateral and contralateral white matter tracts. Many of the cells around and within the scaffold were CD68 positive. In at least 5 of the samples, CD68 positive macrophages in the brain which also appeared to stain positive for BrdU could be detected (Figure 5.8).

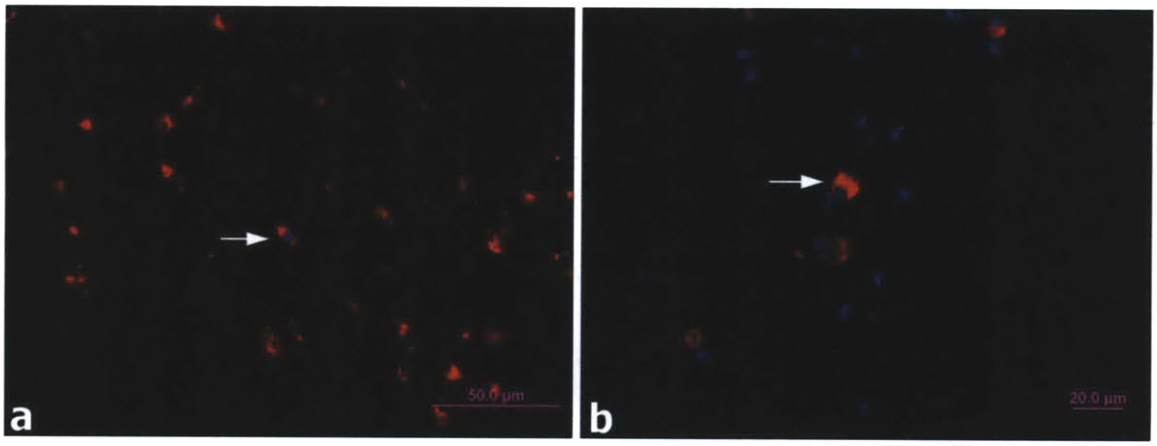

Figure 5.8. Implanted neural progenitors staining positively for CD68. a) Double labeling for BrdU (blue) and CD68 (red) showing an implanted cell (arrow) that may have differentiated into a macrophage within the brain. b). An implanted cell (arrow) from a different animal staining positively for BrdU (blue) and CD68 (red).

5.3.6 Von Willebrand Factor Staining: Blood Vessels and Endothelial Cells

Numerous blood vessels were present surrounding the lesion and in some cases around the periphery of the scaffold. Vessels were generally not found to a significant degree within the scaffold. In all samples, small vessels could be identified in the surrounding brain which included BrdU-positive endothelial cells (Figure 5.9).

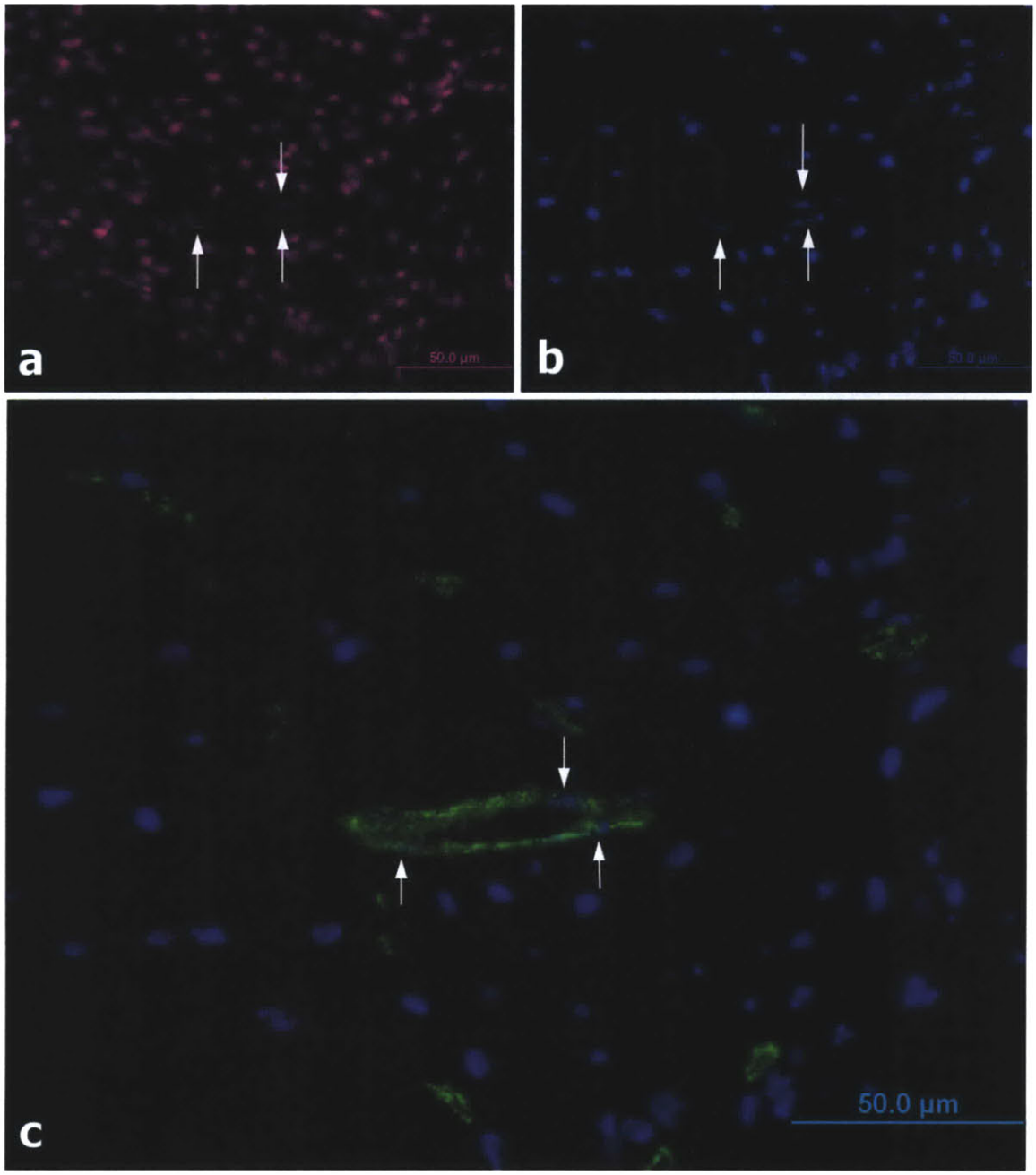

Figure 5.9. Implanted neural progenitors staining positively for VWF. a) DAPI staining (magenta) showing nuclei of all cells in the field. b) BrdU staining (blue) showing implanted cells. c) Double labeling for BrdU (blue) and VWF (green) showing a small blood vessel with three implanted cells (white arrows) that have taken on an endothelial cell phenotype.

5.3.7 CNPase Staining for Oligodendrocytes

CNPase staining revealed the presence of oligodendrocytes and myelinated axons in the vicinity of the lesion, and in some cases directly bordering the cavity. CNPase positive cells were not observed within the collagen scaffold, though there were oligodendrocytes present near the scaffold interface with surrounding brain. In all samples, cells were identified which stained positively for CNPase and BrdU. The BrdU labeled oligodendrocytes were sometimes found within regions of denser CNPase staining around clusters of other oligodendrocytes (Figure 5.10). Perineuronal oligodendrocytes were also observed near neuronal cell bodies (Figure 5.11).

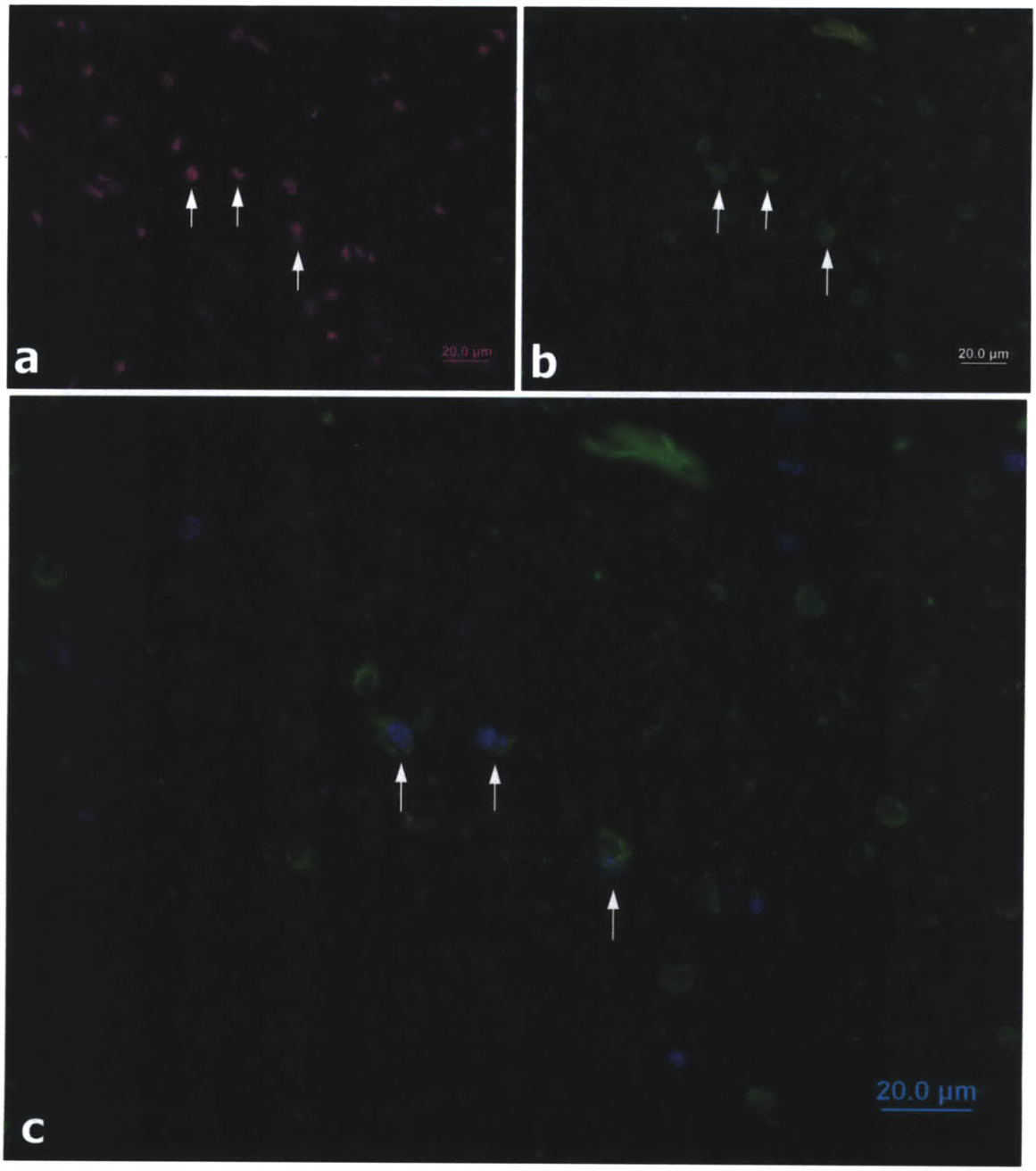

Figure 5.10. Implanted neural progenitors staining positive for CNPase. a) DAPI staining (magenta) showing nuclei of all cells in the field. b) CNPase staining (green) showing several oligodendrocytes. c) Double labeling for BrdU (blue) and CNPase (green) showing three implanted cells (arrows) that have differentiated into oligodendrocytes.

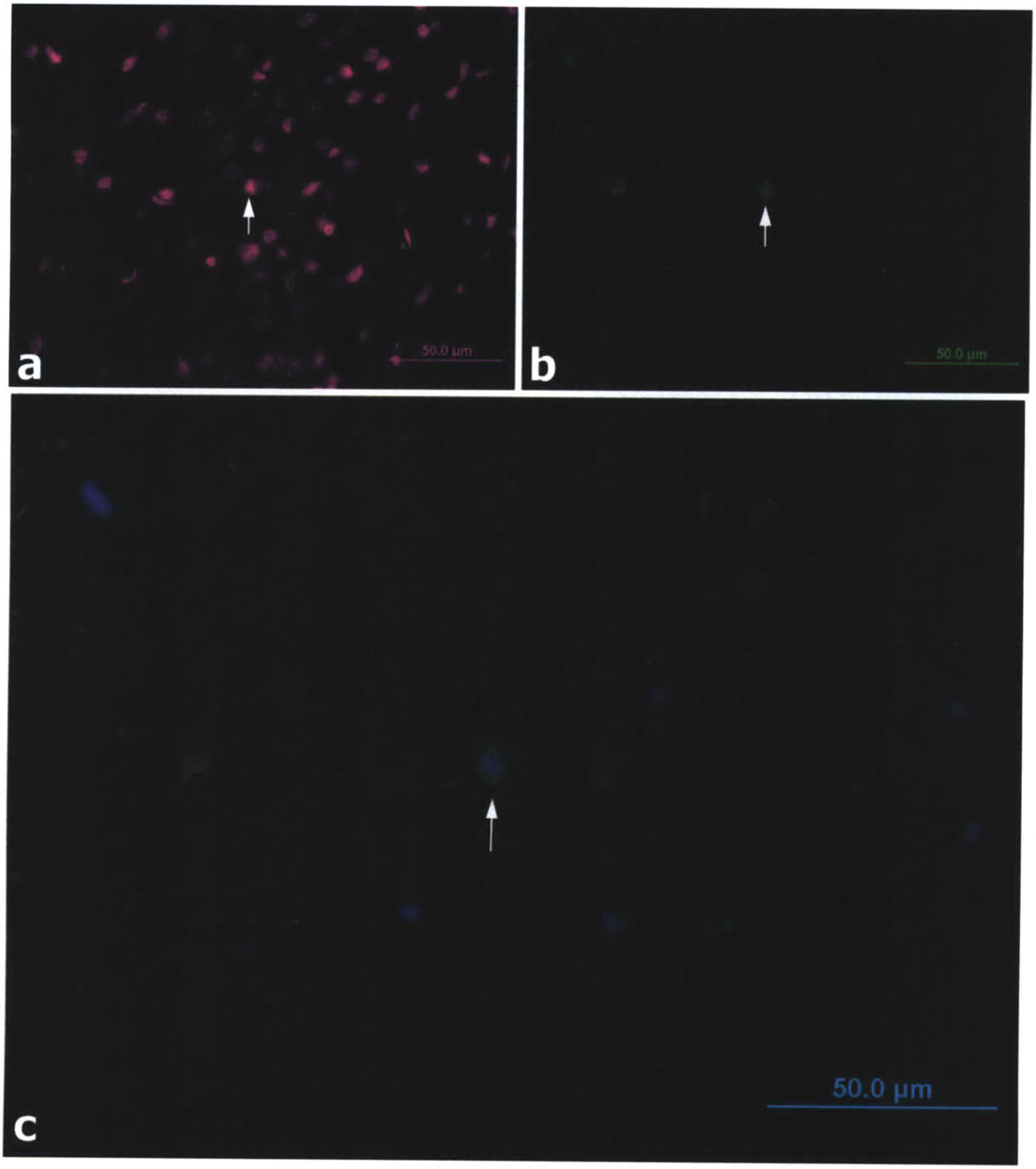

Figure 5.11. Implanted neural progenitor differentiated into a perineuronal satellite oligodendrocyte. a) DAPI staining (magenta) showing nuclei of all cells in the field. b) CNPase staining (green) showing a perineuronal satellite oligodendrocyte (white arrow). c) Double labeling for BrdU (blue) and CNPase (green) showing that the perineuronal satellite oligodendrocyte is an implanted cell.

5.3.8 NeuN Staining for Mature Neurons

While mature neurons were found in the viable brain tissue surrounding the lesion, no NeuN-positive neurons were observed within the scaffold. Very few BrdU positive cells also stained for NeuN (Figure 5.12).

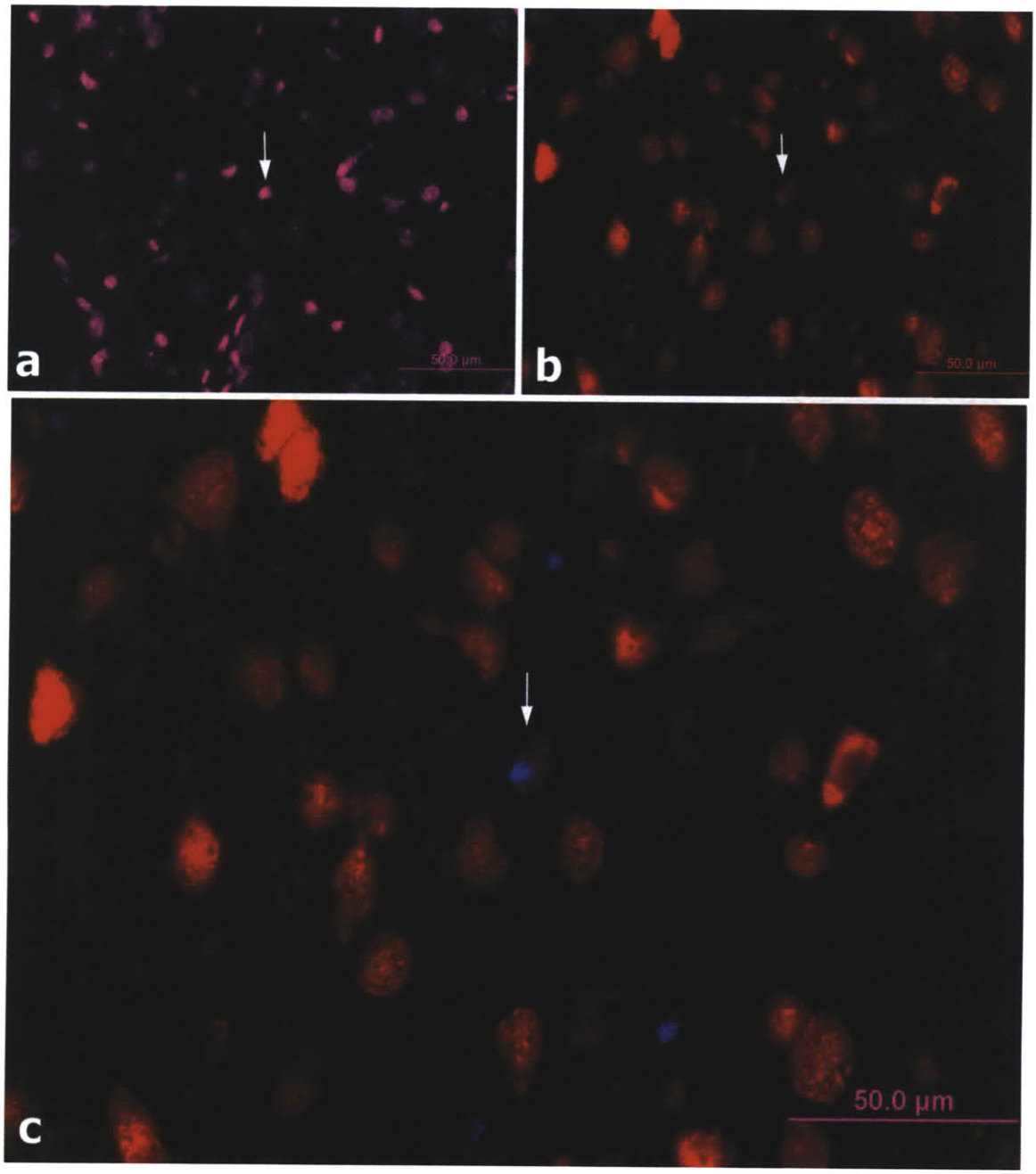

Figure 5.12. Implanted neural progenitor staining positive for NeuN. a) DAPI staining (magenta) showing nuclei of all cells in the field. b) NeuN staining (red) showing post-mitotic neurons. c)

Double labeling for BrdU (blue) and NeuN (red) showing an implanted cell (arrow) that appears to stain dimly, but positively, for NeuN.

5.3.9 MAP1b Staining for Neurons

The MAP1b did not stain cell bodies specifically enough to identify cells which might be both BrdU and MAP1b positive.

5.3.10 Doublecortin staining for Neural Progenitors

While doublecortin positive cells could be seen in and around the subventricular zone, no DCX positive cells were found in or immediately around the scaffold. Due to the lack of positive DCX cells, double-labeling was not conducted.

5.4 Discussion

The survival and recovery of the animals following the injury and the subsequent implantation surgery establishes the safety of these methods for future studies. We observed no adverse behavioral effects as a result of the implanted cells, and there were no tumors or irregular cell growths seen on histology. While electrophysiology measurements were not made, we did not observe any seizures or severe neurological abnormalities beyond the expected forelimb deficits.

Many different cell types have been used previously in studies of traumatic brain injury, including marrow derived stromal cells [224], adipose derived stromal cells [133], umbilical cord blood derived cells [225], post-mitotic neurons [208], and fetal and adult stem/progenitor cells [226]. Cell therapies have in some cases shown beneficial effects on functional recovery and lesion volume [205, 226]. However, the adult rat

hippocampal progenitors used in this study have not, to our knowledge, been used previously in models of traumatic brain injury or stroke.

The basic characteristics of the PBI cavity were similar to those of other groups, with most of the necrotic debris cleared by 5 weeks post-injury. The cavity in the brain expanded to a degree which made the implanted biomaterial somewhat undersized. A large portion of the scaffold's surface area was not in contact with the surrounding brain, but rather was simply suspended in the lesion cavity. A smaller injury would be advantageous for future work since greater proximity of the scaffold with the brain would allow more of the implanted cells to migrate out into the surrounding tissue. Similarly, one may expect more integration of endogenous cells with both the scaffold and the delivered neural progenitors. Although the average lesion volume was less than the average for injured animals without implanted scaffold, the difference was not statistically significant.

While many of neural progenitor cells survived, the 1 week time point for implantation presented some challenges. In particular, the surgical procedure involved a significant amount of bleeding due to the scar tissue that formed around the cranial window. Although it appeared that much of the bleeding was external to the skull, it was nonetheless difficult to implant the scaffold without exposing the material and cells to some bleeding. One potential solution would be to wait an additional week in order to allow for further stabilization of the vasculature both in the scar outside the skull and within the evolving brain lesion. A slightly larger cranial window may also provide the opportunity for more precise localization of the scaffold with minimization of bleeding.

The cellularity of the scaffolds appeared to consist of a combination of the exogenous implanted neural progenitors and endogenous cells that migrated into the scaffold. Despite lack of chemical cross-linking, the scaffolds did not appear to be degrading. Whether or not the scaffold might remain *in vivo* indefinitely is not clear, but the lack of a robust foreign body response suggests that it might maintain structural integrity for a period of least months.

The GFAP reactivity surrounding the lesion suggests formation of a glial scar typical for this kind of lesion. The intense staining all along the border of the cavity indicates that neither the scaffold nor the cells had a notable effect on disrupting the glial scar. Other studies have described astrocyte infiltration of scaffolds [130] and reduction in gliosis around the lesion[134]. In our work with collagen scaffolds, we have not observed any such effect. This would imply that the material composition of the scaffold is of importance for determining which cell types are likely to migrate into it. It is also not a foregone conclusion that astrocyte infiltration is a beneficial scenario, particularly if the astrocytes are of a reactive phenotype and aren't accompanied by other cell types. In this work, we did observe a relatively small number of astrocytes within the scaffold. In some cases, these appeared to be implanted progenitors that differentiated into astrocytes. Previous work has shown that stem/progenitor cells implanted into lesion sites sometimes preferentially differentiate into astrocytes. This may be a result of the same factors in the injury environment that produce gliosis among endogenous astrocytes. Although we observed progenitors that have differentiated into astrocytes, we have also observed differentiation into various other cell types. We conclude from this that the 1 week time point for implantation may be beneficial in limiting the degree of astrocyte differentiation

and allowing for differentiation into other phenotypes. After 1 week, the resolution of the acute phase of the injury may result in an environment with fewer inflammatory mediating factors [204], thus permitting the more diverse differentiation.

Macrophages observed throughout the scaffold appeared to be the most abundant cell type. Their infiltration of the scaffold was likely due in part to erythrocytes and other dead cells that accumulate during and after the implantation. While collagen is a natural material, the presence of virtually any implant stimulates macrophages to some extent. It is also noted that type I collagen is not normally found in the brain [227], which may enhance the reaction of macrophages and microglia. The observed response was not a particularly robust foreign body reaction, based on the lack of multinucleated giant cells and the fact that the interface between brain and scaffold is not particularly dense with macrophages. Interestingly, several macrophages appeared to also stain positively for BrdU. The simplest explanation for this observation would be that the macrophages phagocytosed some of the dead implanted progenitors. It may also be possible that cell fusion resulted in transfer of DNA from the BrdU labeled cells to endogenous macrophages [228]. It is noted in some cases that the BrdU staining was in a dense, well-circumscribed pattern than colocalized with the cell nucleus under visualization of the DAPI stain. This is in contrast to other double-labeled macrophages in which the BrdU staining was more disorganized and fragmented, suggesting that another cell has been phagocytosed. While it initially seems unlikely that this population of hippocampal neural progenitors would have the capability to differentiate into microglia with a macrophage phenotype, the possibility cannot be ruled out. Although microglia and macrophages are of mesodermal origin, it has been shown that mouse neural progenitors

can differentiate into endothelial cells [229], which also are generally of mesodermal origin. Careful *in vitro* experiments would be needed to establish whether or not the apparent differentiation of these neural progenitors into microglia/macrophages is a real effect.

The pattern of degeneration in the thalamus and white matter tracts was similar to that seen in previous studies. The timing of implantation may have precluded the possibility of a significant neuroprotective effect, as we have observed that by 5 weeks the number of neuronal cell bodies staining positively is low. It appears that perhaps most of the neurons die within the first week, so that an implantation time of 1 week is simply too late to have an effect. With earlier implantation and evaluation time points, it may still be worth investigating whether a neuroprotective effect might be observed [230].

The vascularization surrounding the lesion is consistent with observations from previous groups of animals. The presence of BrdU labeled cells among the blood vessel endothelial cells is an interesting finding with significant therapeutic potential. It is first acknowledged that some double-labeled endothelial cells could have been the result of fusion between implanted and endogenous cells. While we cannot definitively rule out this possibility, it has been conclusively demonstrated that mouse neural progenitor cells can differentiate into endothelial cells *in vitro* and *in vivo* [229]. It would be reasonable to expect that cells of rat origin might possess the same capability, indicating that the observed cells likely did differentiate *in vivo*. Previous work demonstrated that the presence of endothelial cells stimulated the endothelial differentiation of mouse neural progenitors. It has also been demonstrated that endothelial cells can promote

proliferation of neural progenitors, along with differentiation down neuronal and glial pathways [231]. Our work suggests that perhaps the endogenous endothelial cells involved in the robust vascularization around the lesion site influenced the implanted neural progenitors. The possibility of implanted progenitors being incorporated into newly formed blood vessels may have benefit in the recovery after brain injury. In particular, areas near the edge of an ischemic region, such as the penumbra in stroke pathology, are at risk of losing viability in the absence of reperfusion. If delivery of neural progenitors can accelerate or enhance the vascularization of these regions, functional tissue might be spared, leading to an improved outcome. It may also be possible to differentiate the cells into an endothelial phenotype prior to implantation. The presence of additional endothelial cells may have a beneficial effect on both endogenous and exogenous neural progenitors that might contribute to functional repair and recovery through neuronal or glial differentiation.

CNPase staining allowed for visualization of myelinated axons in white matter, but also individual oligodendrocyte cell bodies. The absence of oligodendrocytes within the collagen scaffold is not surprising, given the large size of the lesion and the relatively small scaffold. With a smaller injury, one might ideally expect the possibility of axons growing through the scaffold to establish continuity across the defect, potentially followed by myelination by oligodendrocytes. While that did not occur in this case, there did appear to be BrdU-labeled cells that also stained positive for CNPase. As in the other cases, cell fusion cannot be ruled out as reason for the double-labeling. However, the multipotency of the neural progenitors has been demonstrated both *in vitro* and *in vivo*, including the capability of oligodendrocyte differentatiation. The oligodendrocytes that

did double-label appeared in some cases to be satellite cells located near neurons. The functions of the perineuronal satellite oligodendrocyte remain incompletely understood, though certain aspects of their role have been clarified. Under normal circumstances, they are not thought to be involved in myelination. While they can be involved in remyelinating growing axons following injury, their main role appears to be related to metabolic support of neurons. They have been shown to localize more often with glutamatergic cortical neurons, but can also localize with GABAergic interneurons [232]. Perineuronal oligodendrocytes express glial enzymes associated with neuronal survival and have been suggested to protect against neuronal apoptosis, but do not appear to be heavily involved in regulation of extracellular glutamate [233]. Neural progenitors with the capability to differentiate into perineuronal oligodendrocytes, may be promising candidates for neuroprotection following injury. Establishing such an effect is difficult in this work due to the size of the lesion, but it is nonetheless likely that the differentiated progenitors have a beneficial effect on neurons to which they have localized. In the event that those neurons may have suffered injury or axonal damage, the perineuronal oligodendrocytes may also be an aid in remyelination.

Most of the double-labeled oligodendrocytes seemed to be of a myelinating phenotype. They were found in or near white matter tracts, and were sometimes found in clusters. These cells could clearly be of benefit in replacing oligodendrocytes lost during injury, and might also be involved in myelination of damaged or regenerating axons. The ability of the implanted progenitors to take on oligodendrocyte phenotypes with varying function suggests their potential utility for further application to brain injuries.

The distribution of NeuN-positive cells confirmed that while neurons were present in areas surrounding the lesion, no neurons were present within the scaffold. Within areas of viable brain tissue, only an occasional neuron double-labeled with BrdU could be identified. While the number of such cells was very few, it does appear that the neural progenitors have the capability of developing into mature neurons after implantation. In larger numbers, the presence of such neurons might be able to replace certain populations of GABAergic neurons lost after injury. It has been demonstrated that neural progenitors from the subventricular zone can migrate to sites of striatal injury and differentiate into medium spiny neurons. It has not been definitively determined that hippocampal progenitors have the same differentiation potential, but they have been shown *in vitro* to express markers for various neuronal phenotypes. Additional staining with a marker such as DARPP-32 might enable one to determine whether any implanted cells might have differentiated into medium spiny neurons in the striatum. A longer term study might also result in more neuronal differentiation.

While we have observed implanted progenitors that differentiated into astrocytes, oligodendrocytes, neurons, endothelial cells, and possibly macrophages, there appeared to be many BrdU positive cells that remained undifferentiated. Similar findings have been reported in various studies of cell implantation into brain and spinal cord injury. It has been suggested that undifferentiated cells persisting long-term in the brain may play anti-inflammatory roles. Being able to perform labeling with 3, 4, or 5 fluorophores simultaneously would enable a more precise determination of the proportion of differentiated and undifferentiated cells.

Acknowledgements

We thank Dr. Fred Gage for kindly providing the cells used in this work. We thank Karen Shu for assistance with the handling of the biomaterials prior to the implantation surgery. We thank Alix Weaver for assistance with hematoxylin and eosin staining.

Chapter 6: Conclusions and Future Work

This thesis investigated the use of a collagen biomaterial scaffold for treatment of penetrating brain injury in a rat model. Characterization of the injury revealed a 29% increase in the lesion volume between 1 week and 5 weeks post-injury. Immunohistochemistry showed a pattern of glial scarring surrounding the lesion that consisted of reactive astrocytes and chondroitin sulfate proteoglycans.

Collagen scaffolds implanted immediately after injury showed modest cellular infiltration after 1 week. Macrophages were the most numerous cell type, followed by astrocytes and a small number of endothelial cells. Scaffolds implanted 1 week post-injury (3 mm diameter) showed similar results after 4 weeks *in vivo*. However, the scaffolds were small relative to the cavity size, which limited the potential interaction with the surrounding brain.

Larger scaffolds (6 mm diameter) implanted 1 week post-injury were found to fill most of the PBI cavity. Macrophages, astrocytes, and endothelial cells were present within the scaffolds. In a few areas, neurons, axons, and oligodendrocytes could be detected slightly within the scaffold margins. The lack of these cells at significant distances within the scaffold indicate that a regenerative response did not take place. Rather, the results showed that the scaffold can integrate with surrounding viable brain in some areas and that neurons and oligodendrocytes can reside along the scaffold struts.

When soluble Nogo receptor was loaded into the scaffold prior to implantation, a significant increase in macrophage and endothelial cell infiltration was noted after 4 weeks *in vivo*. Deposition of extracellular matrix was noted within the scaffold pores in some cases, and there was a variable degree of vascularization with the scaffolds. In

some cases, there were small vessels distributed throughout a large area within the scaffold. This result suggested a promising step in modulating the lesion environment to promote regeneration. In particular, a lesion which would otherwise be a fluid-filled space, was thoroughly filled with a continuous extracellular matrix analog that was vascularized and supportive of cellular infiltration. Future work may be aimed at designing a scaffold that can be resorbed over time to limit the macrophage and giant cell response while remaining *in vivo* long enough to promote vascularization. Additionally, one may attempt to deliver a cellular or pharmacological therapy to the vascularized lesion site to promote a regenerative response.

Implantation of a collagen scaffold seeded with neural progenitor cells was resulted in the survival and differentiation of numerous cells into a variety of phenotypes. Differentiation into astrocytes, oligodendrocytes, endothelial cells, neurons, and potentially macrophages was observed. Future work might focus on implanting a similar construct into a smaller lesion, such that the cavity is better filled by the scaffold. This would allow for increased interaction of the implanted cells with the surrounding brain tissue. Additionally, potential positive effects of the cells are more likely to be detected when the lesion is not overwhelmingly large.

With the information gained from this work, another logical next step would be to combine the therapies we have investigated. This could be done in a sequential manner by beginning with implantation of a sNgR loaded scaffold following the injury. After allowing several weeks for vascularization, one might then inject a population of neural progenitors into the lesion site. It is hypothesized that the cells would show an increased

survival rate relative to implantation of a cell-seeded scaffold into the unvascularized lesion.

This research has demonstrated the complexity of trying to develop therapeutic options for CNS injuries. The knowledge gained will hopefully contribute to further work in the area and eventually treatment options for affected patients.

References

1. Kadoya, K., et al., *Combined intrinsic and extrinsic neuronal mechanisms facilitate bridging axonal regeneration one year after spinal cord injury.* Neuron, 2009. **64**(2): p. 165-72.
2. Afshari, F.T., S. Kappagantula, and J.W. Fawcett, *Extrinsic and intrinsic factors controlling axonal regeneration after spinal cord injury.* Expert Rev Mol Med, 2009. **11**: p. e37.
3. Benowitz, L.I. and A. Routtenberg, *GAP-43: an intrinsic determinant of neuronal development and plasticity.* Trends Neurosci, 1997. **20**(2): p. 84-91.
4. Giger, R.J., et al., *Mechanisms of CNS myelin inhibition: evidence for distinct and neuronal cell type specific receptor systems.* Restor Neurol Neurosci, 2008. **26**(2-3): p. 97-115.
5. Benfey, M. and A.J. Aguayo, *Extensive elongation of axons from rat brain into peripheral nerve grafts.* Nature, 1982. **296**(5853): p. 150-2.
6. Schwab, M.E. and H. Thoenen, *Dissociated neurons regenerate into sciatic but not optic nerve explants in culture irrespective of neurotrophic factors.* J Neurosci, 1985. **5**(9): p. 2415-23.
7. GrandPre, T., et al., *Identification of the Nogo inhibitor of axon regeneration as a Reticulon protein.* Nature, 2000. **403**(6768): p. 439-44.
8. Wang, K.C., et al., *Oligodendrocyte-myelin glycoprotein is a Nogo receptor ligand that inhibits neurite outgrowth.* Nature, 2002. **417**(6892): p. 941-4.
9. McKerracher, L., et al., *Identification of myelin-associated glycoprotein as a major myelin-derived inhibitor of neurite growth.* Neuron, 1994. **13**(4): p. 805-11.
10. Liu, B.P., et al., *Myelin-associated glycoprotein as a functional ligand for the Nogo-66 receptor.* Science, 2002. **297**(5584): p. 1190-3.
11. Domeniconi, M., et al., *Myelin-associated glycoprotein interacts with the Nogo66 receptor to inhibit neurite outgrowth.* Neuron, 2002. **35**(2): p. 283-90.
12. Fournier, A.E., T. GrandPre, and S.M. Strittmatter, *Identification of a receptor mediating Nogo-66 inhibition of axonal regeneration.* Nature, 2001. **409**(6818): p. 341-6.
13. Barton, W.A., et al., *Structure and axon outgrowth inhibitor binding of the Nogo-66 receptor and related proteins.* Embo J, 2003. **22**(13): p. 3291-302.
14. He, X.L., et al., *Structure of the Nogo receptor ectodomain: a recognition module implicated in myelin inhibition.* Neuron, 2003. **38**(2): p. 177-85.
15. Wang, K.C., et al., *P75 interacts with the Nogo receptor as a co-receptor for Nogo, MAG and OMgp.* Nature, 2002. **420**(6911): p. 74-8.
16. Wong, S.T., et al., *A p75(NTR) and Nogo receptor complex mediates repulsive signaling by myelin-associated glycoprotein.* Nat Neurosci, 2002. **5**(12): p. 1302-8.
17. Mi, S., et al., *LINGO-1 is a component of the Nogo-66 receptor/p75 signaling complex.* Nat Neurosci, 2004. **7**(3): p. 221-8.
18. Park, J.B., et al., *A TNF receptor family member, TROY, is a coreceptor with Nogo receptor in mediating the inhibitory activity of myelin inhibitors.* Neuron, 2005. **45**(3): p. 345-51.

19. Shao, Z., et al., *TAJ/TROY, an orphan TNF receptor family member, binds Nogo-66 receptor 1 and regulates axonal regeneration.* Neuron, 2005. **45**(3): p. 353-9.
20. Zhang, S., et al., *NgR acts as an inhibitor to axonal regeneration in adults.* Front Biosci, 2008. **13**: p. 2030-40.
21. Schmandke, A., A. Schmandke, and S.M. Strittmatter, *ROCK and Rho: biochemistry and neuronal functions of Rho-associated protein kinases.* Neuroscientist, 2007. **13**(5): p. 454-69.
22. Fournier, A.E., B.T. Takizawa, and S.M. Strittmatter, *Rho kinase inhibition enhances axonal regeneration in the injured CNS.* J Neurosci, 2003. **23**(4): p. 1416-23.
23. Atwal, J.K., et al., *PirB is a functional receptor for myelin inhibitors of axonal regeneration.* Science, 2008. **322**(5903): p. 967-70.
24. Teng, F.Y. and B.L. Tang, *Why do Nogo/Nogo-66 receptor gene knockouts result in inferior regeneration compared to treatment with neutralizing agents?* J Neurochem, 2005. **94**(4): p. 865-74.
25. Wang, F. and Y. Zhu, *The interaction of Nogo-66 receptor with Nogo-p4 inhibits the neuronal differentiation of neural stem cells.* Neuroscience, 2008. **151**(1): p. 74-81.
26. Wang, B., et al., *Nogo-66 promotes the differentiation of neural progenitors into astroglial lineage cells through mTOR-STAT3 pathway.* PLoS One, 2008. **3**(3): p. e1856.
27. Li, X., et al., *Myelin-associated glycoprotein inhibits the neuronal differentiation of neural progenitors.* Neuroreport, 2009. **20**(7): p. 708-12.
28. Silver, J. and J.H. Miller, *Regeneration beyond the glial scar.* Nat Rev Neurosci, 2004. **5**(2): p. 146-56.
29. Pekny, M. and M. Nilsson, *Astrocyte activation and reactive gliosis.* Glia, 2005. **50**(4): p. 427-34.
30. Fitch, M.T. and J. Silver, *CNS injury, glial scars, and inflammation: Inhibitory extracellular matrices and regeneration failure.* Exp Neurol, 2008. **209**(2): p. 294-301.
31. Crespo, D., et al., *How does chondroitinase promote functional recovery in the damaged CNS?* Exp Neurol, 2007. **206**(2): p. 159-71.
32. Shen, Y., et al., *PTPsigma is a receptor for chondroitin sulfate proteoglycan, an inhibitor of neural regeneration.* Science, 2009. **326**(5952): p. 592-6.
33. Hou, S., et al., *The repair of brain lesion by implantation of hyaluronic acid hydrogels modified with laminin.* J Neurosci Methods, 2005. **148**(1): p. 60-70.
34. Galtrey, C.M., et al., *Promoting plasticity in the spinal cord with chondroitinase improves functional recovery after peripheral nerve repair.* Brain, 2007. **130**(Pt 4): p. 926-39.
35. Myer, D.J., et al., *Essential protective roles of reactive astrocytes in traumatic brain injury.* Brain, 2006. **129**(Pt 10): p. 2761-72.
36. Rolls, A., R. Shechter, and M. Schwartz, *The bright side of the glial scar in CNS repair.* Nat Rev Neurosci, 2009. **10**(3): p. 235-41.
37. Hou, S.T., S.X. Jiang, and R.A. Smith, *Permissive and repulsive cues and signalling pathways of axonal outgrowth and regeneration.* Int Rev Cell Mol Biol, 2008. **267**: p. 125-81.

38. Cui, Q., *Actions of neurotrophic factors and their signaling pathways in neuronal survival and axonal regeneration.* Mol Neurobiol, 2006. **33**(2): p. 155-79.
39. Sapsford, W., *Penetrating brain injury in military conflict: does it merit more research?* J R Army Med Corps, 2003. **149**(1): p. 5-14.
40. Williams, A.J., et al., *Characterization of a new rat model of penetrating ballistic brain injury.* J Neurotrauma, 2005. **22**(2): p. 313-31.
41. Bramlett, H.M. and W.D. Dietrich, *Pathophysiology of cerebral ischemia and brain trauma: similarities and differences.* J Cereb Blood Flow Metab, 2004. **24**(2): p. 133-50.
42. Williams, A.J., et al., *Acute and delayed neuroinflammatory response following experimental penetrating ballistic brain injury in the rat.* J Neuroinflammation, 2007. **4**: p. 17.
43. Williams, A.J., et al., *Penetrating ballistic-like brain injury in the rat: differential time courses of hemorrhage, cell death, inflammation, and remote degeneration.* J Neurotrauma, 2006. **23**(12): p. 1828-46.
44. Rosenfeld, J.V., *Gunshot injury to the head and spine.* J Clin Neurosci, 2002. **9**(1): p. 9-16.
45. Izci, Y., et al., *The clinical, radiological and surgical characteristics of supratentorial penetrating craniocerebral injuries: a retrospective clinical study.* Tohoku J Exp Med, 2003. **201**(1): p. 39-46.
46. Eftekhar, B., et al., *Prognostic factors in the persistence of posttraumatic epilepsy after penetrating head injuries sustained in war.* J Neurosurg, 2009. **110**(2): p. 319-26.
47. Schulz, C., U. Woerner, and P. Luelsdorf, *Image-guided neurosurgery for secondary operative removal of projectiles after missile injury of the brain.* Surg Neurol, 2008. **69**(4): p. 364-8; discussion 368.
48. Sidaros, A., et al., *Long-term global and regional brain volume changes following severe traumatic brain injury: a longitudinal study with clinical correlates.* Neuroimage, 2009. **44**(1): p. 1-8.
49. Mergenthaler, P., U. Dirnagl, and A. Meisel, *Pathophysiology of stroke: lessons from animal models.* Metab Brain Dis, 2004. **19**(3-4): p. 151-67.
50. Muir, K.W. and P.A. Teal, *Why have neuro-protectants failed? lessons learned from stroke trials.* J Neurol, 2005. **252**(9): p. 1011-20.
51. Taoufik, E. and L. Probert, *Ischemic neuronal damage.* Curr Pharm Des, 2008. **14**(33): p. 3565-73.
52. Xi, G., R.F. Keep, and J.T. Hoff, *Mechanisms of brain injury after intracerebral haemorrhage.* Lancet Neurol, 2006. **5**(1): p. 53-63.
53. Branco, F., D.D. Cardenas, and J.N. Svircev, *Spinal cord injury: a comprehensive review.* Phys Med Rehabil Clin N Am, 2007. **18**(4): p. 651-79, v.
54. Rowland, J.W., et al., *Current status of acute spinal cord injury pathophysiology and emerging therapies: promise on the horizon.* Neurosurg Focus, 2008. **25**(5): p. E2.
55. Astradsson, A., et al., *Recent advances in cell-based therapy for Parkinson disease.* Neurosurg Focus, 2008. **24**(3-4): p. E6.

56. Park, J.H. and S.M. Strittmatter, *Nogo receptor interacts with brain APP and Abeta to reduce pathologic changes in Alzheimer's transgenic mice.* Curr Alzheimer Res, 2007. **4**(5): p. 568-70.
57. Clelland, C.D., R.A. Barker, and C. Watts, *Cell therapy in Huntington disease.* Neurosurg Focus, 2008. **24**(3-4): p. E9.
58. Riley, J., W. Sweeney, and N. Boulis, *Shifting the balance: cell-based therapeutics as modifiers of the amyotrophic lateral sclerosis-specific neuronal microenvironment.* Neurosurg Focus, 2008. **24**(3-4): p. E10.
59. Payne, N., C. Siatskas, and C.C. Bernard, *The promise of stem cell and regenerative therapies for multiple sclerosis.* J Autoimmun, 2008. **31**(3): p. 288-94.
60. Rabinovici, G.D. and B.L. Miller, *Frontotemporal lobar degeneration: epidemiology, pathophysiology, diagnosis and management.* CNS Drugs, 2010. **24**(5): p. 375-98.
61. Willerth, S.M. and S.E. Sakiyama-Elbert, *Approaches to neural tissue engineering using scaffolds for drug delivery.* Adv Drug Deliv Rev, 2007. **59**(4-5): p. 325-38.
62. Robertson, M.J., P. Gip, and D.V. Schaffer, *Neural stem cell engineering: directed differentiation of adult and embryonic stem cells into neurons.* Front Biosci, 2008. **13**: p. 21-50.
63. Lu, P. and M.H. Tuszynski, *Growth factors and combinatorial therapies for CNS regeneration.* Exp Neurol, 2008. **209**(2): p. 313-20.
64. Logan, A., et al., *Neurotrophic factor synergy is required for neuronal survival and disinhibited axon regeneration after CNS injury.* Brain, 2006. **129**(Pt 2): p. 490-502.
65. Benowitz, L.I., D.E. Goldberg, and N. Irwin, *Inosine stimulates axon growth in vitro and in the adult CNS.* Prog Brain Res, 2002. **137**: p. 389-99.
66. Lorber, B., et al., *Mst3b, an Ste20-like kinase, regulates axon regeneration in mature CNS and PNS pathways.* Nat Neurosci, 2009. **12**(11): p. 1407-14.
67. Irwin, N., et al., *Mst3b, a purine-sensitive Ste20-like protein kinase, regulates axon outgrowth.* Proc Natl Acad Sci U S A, 2006. **103**(48): p. 18320-5.
68. Lee, D.H., S.M. Strittmatter, and D.W. Sah, *Targeting the Nogo receptor to treat central nervous system injuries.* Nat Rev Drug Discov, 2003. **2**(11): p. 872-8.
69. Pena, A., et al., *Brain tissue biomechanics in cortical contusion injury: a finite element analysis.* Acta Neurochir Suppl, 2005. **95**: p. 333-6.
70. Sawauchi, S. and T. Abe, *The effect of haematoma, brain injury, and secondary insult on brain swelling in traumatic acute subdural haemorrhage.* Acta Neurochir (Wien), 2008. **150**(6): p. 531-6; discussion 536.
71. Bain, A.C. and D.F. Meaney, *Tissue-level thresholds for axonal damage in an experimental model of central nervous system white matter injury.* J Biomech Eng, 2000. **122**(6): p. 615-22.
72. Schettini, A. and E.K. Walsh, *Brain tissue elastic behavior and experimental brain compression.* Am J Physiol, 1988. **255**(5 Pt 2): p. R799-805.
73. Kyriacou, S.K., et al., *Brain mechanics For neurosurgery: modeling issues.* Biomech Model Mechanobiol, 2002. **1**(2): p. 151-64.

74. Lemole, G.M., Jr., et al., *Virtual reality in neurosurgical education: part-task ventriculostomy simulation with dynamic visual and haptic feedback.* Neurosurgery, 2007. **61**(1): p. 142-8; discussion 148-9.
75. Laine, F.J., et al., *Acquired intracranial herniations: MR imaging findings.* AJR Am J Roentgenol, 1995. **165**(4): p. 967-73.
76. Zacharaki, E.I., et al., *A comparative study of biomechanical simulators in deformable registration of brain tumor images.* IEEE Trans Biomed Eng, 2008. **55**(3): p. 1233-6.
77. Vloeberghs, M., et al., *Virtual neurosurgery, training for the future.* Br J Neurosurg, 2007. **21**(3): p. 262-7.
78. Yc Goha, K., *Virtual reality applications in neurosurgery.* Conf Proc IEEE Eng Med Biol Soc, 2005. **4**: p. 4171-3.
79. Balgude, A.P., et al., *Agarose gel stiffness determines rate of DRG neurite extension in 3D cultures.* Biomaterials, 2001. **22**(10): p. 1077-84.
80. Flanagan, L.A., et al., *Neurite branching on deformable substrates.* Neuroreport, 2002. **13**(18): p. 2411-5.
81. Georges, P.C., et al., *Matrices with compliance comparable to that of brain tissue select neuronal over glial growth in mixed cortical cultures.* Biophys J, 2006. **90**(8): p. 3012-8.
82. Engler, A.J., et al., *Matrix elasticity directs stem cell lineage specification.* Cell, 2006. **126**(4): p. 677-89.
83. Saha, K., et al., *Substrate modulus directs neural stem cell behavior.* Biophys J, 2008. **95**(9): p. 4426-38.
84. Compton, C.C., et al., *Organized skin structure is regenerated in vivo from collagen-GAG matrices seeded with autologous keratinocytes.* J Invest Dermatol, 1998. **110**(6): p. 908-16.
85. Hsu, W.C., et al., *Inhibition of conjunctival scarring and contraction by a porous collagen-glycosaminoglycan implant.* Invest Ophthalmol Vis Sci, 2000. **41**(9): p. 2404-11.
86. Harley, B.A., et al., *Optimal degradation rate for collagen chambers used for regeneration of peripheral nerves over long gaps.* Cells Tissues Organs, 2004. **176**(1-3): p. 153-65.
87. Spilker, M.H., et al., *The effects of tubulation on healing and scar formation after transection of the adult rat spinal cord.* Restor Neurol Neurosci, 2001. **18**(1): p. 23-38.
88. Miller, K., *Method of testing very soft biological tissues in compression.* J Biomech, 2005. **38**(1): p. 153-8.
89. Cheng, L., et al., *Spherical-tip indentation of viscoelastic material.* Mech. Mater., 2005. **37**(1): p. 213-226.
90. Cheng, L., et al., *Flat-punch indentation of viscoelastic material.* J Polym Sci B: Polym Phys, 2000. **38**(1): p. 10-22.
91. Prange, M.T. and S.S. Margulies, *Regional, directional, and age-dependent properties of the brain undergoing large deformation.* J Biomech Eng, 2002. **124**(2): p. 244-52.
92. Gefen, A., et al., *Age-dependent changes in material properties of the brain and braincase of the rat.* J Neurotrauma, 2003. **20**(11): p. 1163-77.

93. Thibault, K.L. and S.S. Margulies, *Age-dependent material properties of the porcine cerebrum: effect on pediatric inertial head injury criteria.* J Biomech, 1998. **31**(12): p. 1119-26.
94. Fountoulakis, M., et al., *Postmortem changes in the level of brain proteins.* Exp Neurol, 2001. **167**(1): p. 86-94.
95. Gefen, A. and S.S. Margulies, *Are in vivo and in situ brain tissues mechanically similar?* J Biomech, 2004. **37**(9): p. 1339-52.
96. Olde Damink, L.H., et al., *Cross-linking of dermal sheep collagen using a water-soluble carbodiimide.* Biomaterials, 1996. **17**(8): p. 765-73.
97. Lee, E.H. and J.R.M. Radok, *The contact problem for viscoelastic bodies.* J App Mech, 1960. **27**: p. 438-444.
98. Wang, T.W. and M. Spector, *Development of hyaluronic acid-based scaffolds for brain tissue engineering.* Acta Biomater, 2009. **5**(7): p. 2371-84.
99. Harley, B.A., et al., *Mechanical characterization of collagen-glycosaminoglycan scaffolds.* Acta Biomater, 2007. **3**(4): p. 463-74.
100. Pieper, J.S., et al., *Preparation and characterization of porous crosslinked collagenous matrices containing bioavailable chondroitin sulphate.* Biomaterials, 1999. **20**(9): p. 847-58.
101. Gibson, L.J., *Biomechanics of cellular solids.* J Biomech, 2005. **38**(3): p. 377-99.
102. Vickers, S.M., L.S. Squitieri, and M. Spector, *Effects of cross-linking type II collagen-GAG scaffolds on chondrogenesis in vitro: dynamic pore reduction promotes cartilage formation.* Tissue Eng, 2006. **12**(5): p. 1345-55.
103. Freyman, T.M., et al., *Fibroblast contraction of a collagen-GAG matrix.* Biomaterials, 2001. **22**(21): p. 2883-91.
104. Huang, C. and I.V. Yannas, *Mechanochemical studies of enzymatic degradation of insoluble collagen fibers.* J Biomed Mater Res, 1977. **11**(1): p. 137-54.
105. Tang, S., et al., *Fabrication and characterization of porous hyaluronic acid-collagen composite scaffolds.* J Biomed Mater Res A, 2007. **82**(2): p. 323-35.
106. Miller, K., et al., *Mechanical properties of brain tissue in-vivo: experiment and computer simulation.* J Biomech, 2000. **33**(11): p. 1369-76.
107. Karger, B., *Penetrating gunshots to the head and lack of immediate incapacitation. I. Wound ballistics and mechanisms of incapacitation.* Int J Legal Med, 1995. **108**(2): p. 53-61.
108. Bell, R.S., et al., *Early decompressive craniectomy for severe penetrating and closed head injury during wartime.* Neurosurg Focus, 2010. **28**(5): p. E1.
109. Izci, Y., et al., *Comparison of clinical outcomes between anteroposterior and lateral penetrating craniocerebral gunshot wounds.* Emerg Med J, 2005. **22**(6): p. 409-10.
110. Kim, T.W., et al., *Penetrating gunshot injuries to the brain.* J Trauma, 2007. **62**(6): p. 1446-51.
111. Murano, T., et al., *Civilian craniocerebral gunshot wounds: an update in predicting outcomes.* Am Surg, 2005. **71**(12): p. 1009-14.
112. Pabuscu, Y., et al., *A different approach to missile induced head injuries.* Comput Med Imaging Graph, 2003. **27**(5): p. 397-409.
113. Carey, M.E., et al., *Experimental missile wound to the brain.* J Neurosurg, 1989. **71**(5 Pt 1): p. 754-64.

114. Soblosky, J.S., et al., *Central and peripheral biogenic amine effects of brain missile wounding and increased intracranial pressure.* J Neurosurg, 1992. **76**(1): p. 119-26.
115. Novozhilova, A.P., et al., *State of the cerebral cortex in severe penetrating gunshot injuries to the skull and brain (experimental studies).* Neurosci Behav Physiol, 1997. **27**(2): p. 183-8.
116. Allen, I.V., R. Scott, and J.A. Tanner, *Experimental high-velocity missile head injury.* Injury, 1982. **14**(2): p. 183-93.
117. Allen, I.V., et al., *An ultrastructural study of experimental high velocity penetrating head injury.* Acta Neuropathol, 1983. **59**(4): p. 277-82.
118. Zhang, J., et al., *Temporal cavity and pressure distribution in a brain simulant following ballistic penetration.* J Neurotrauma, 2005. **22**(11): p. 1335-47.
119. Zhang, J., et al., *Experimental model for civilian ballistic brain injury biomechanics quantification.* J Biomech, 2007. **40**(10): p. 2341-6.
120. Lu, X.C., et al., *Electrocortical Pathology in a Rat Model of Penetrating Ballistic-Like Brain Injury.* J Neurotrauma, 2010.
121. Jankovic, S., et al., *Craniocerebral war missile injuries: clinical and radiological study.* Acta Neurochir (Wien), 2000. **142**(1): p. 101-2.
122. Williams, A.J., G.S. Ling, and F.C. Tortella, *Severity level and injury track determine outcome following a penetrating ballistic-like brain injury in the rat.* Neurosci Lett, 2006. **408**(3): p. 183-8.
123. Cromey, D.W., *Avoiding twisted pixels: ethical guidelines for the appropriate use and manipulation of scientific digital images.* Sci Eng Ethics, 2010. **16**(4): p. 639-67.
124. Jain, K.K., *Neuroprotection in traumatic brain injury.* Drug Discov Today, 2008. **13**(23-24): p. 1082-9.
125. Keep, R.F., et al., *The deleterious or beneficial effects of different agents in intracerebral hemorrhage: think big, think small, or is hematoma size important?* Stroke, 2005. **36**(7): p. 1594-6.
126. Deguchi, K., et al., *Implantation of a new porous gelatin-siloxane hybrid into a brain lesion as a potential scaffold for tissue regeneration.* J Cereb Blood Flow Metab, 2006. **26**(10): p. 1263-73.
127. Tian, W.M., et al., *Hyaluronic acid-poly-D-lysine-based three-dimensional hydrogel for traumatic brain injury.* Tissue Eng, 2005. **11**(3-4): p. 513-25.
128. Woerly, S., C. Lavallee, and R. Marchand, *Intracerebral implantation of ionic synthetic hydrogels: effect of polar substrata on astrocytosis and axons.* J Neural Transplant Plast, 1992. **3**(1): p. 21-34.
129. Woerly, S., et al., *Neural tissue formation within porous hydrogels implanted in brain and spinal cord lesions: ultrastructural, immunohistochemical, and diffusion studies.* Tissue Eng, 1999. **5**(5): p. 467-88.
130. Wong, D.Y., P.H. Krebsbach, and S.J. Hollister, *Brain cortex regeneration affected by scaffold architectures.* J Neurosurg, 2008. **109**(4): p. 715-22.
131. Tian, W. and T.R. Kyriakides, *Thrombospondin 2-null mice display an altered brain foreign body response to polyvinyl alcohol sponge implants.* Biomed Mater, 2009. **4**(1): p. 015010.

132. Plant, G.W., S. Woerly, and A.R. Harvey, *Hydrogels containing peptide or aminosugar sequences implanted into the rat brain: influence on cellular migration and axonal growth.* Exp Neurol, 1997. **143**(2): p. 287-99.
133. Nakada, A., et al., *Regeneration of central nervous tissue using a collagen scaffold and adipose-derived stromal cells.* Cells Tissues Organs, 2009. **190**(6): p. 326-35.
134. Wong, D.Y., et al., *Poly(epsilon-caprolactone) and poly (L-lactic-co-glycolic acid) degradable polymer sponges attenuate astrocyte response and lesion growth in acute traumatic brain injury.* Tissue Eng, 2007. **13**(10): p. 2515-23.
135. Zhang, H., et al., *Vascular endothelial growth factor promotes brain tissue regeneration with a novel biomaterial polydimethylsiloxane-tetraethoxysilane.* Brain Res, 2007. **1132**(1): p. 29-35.
136. Faulkner, J.R., et al., *Reactive astrocytes protect tissue and preserve function after spinal cord injury.* J Neurosci, 2004. **24**(9): p. 2143-55.
137. Galtrey, C.M. and J.W. Fawcett, *The role of chondroitin sulfate proteoglycans in regeneration and plasticity in the central nervous system.* Brain Res Rev, 2007. **54**(1): p. 1-18.
138. Tester, N.J. and D.R. Howland, *Chondroitinase ABC improves basic and skilled locomotion in spinal cord injured cats.* Exp Neurol, 2008. **209**(2): p. 483-96.
139. Knowlson, G.T., *Gel-foam granuloma in the brain.* J Neurol Neurosurg Psychiatry, 1974. **37**(8): p. 971-3.
140. Vargas, M.E. and B.A. Barres, *Why is Wallerian degeneration in the CNS so slow?* Annu Rev Neurosci, 2007. **30**: p. 153-79.
141. Ma, J., et al., *An experimental test of stroke recovery by implanting a hyaluronic acid hydrogel carrying a Nogo receptor antibody in a rat model.* Biomed Mater, 2007. **2**(4): p. 233-40.
142. Arvidsson, A., et al., *Neuronal replacement from endogenous precursors in the adult brain after stroke.* Nat Med, 2002. **8**(9): p. 963-70.
143. Parent, J.M., et al., *Rat forebrain neurogenesis and striatal neuron replacement after focal stroke.* Ann Neurol, 2002. **52**(6): p. 802-13.
144. Yamashita, T., et al., *Subventricular zone-derived neuroblasts migrate and differentiate into mature neurons in the post-stroke adult striatum.* J Neurosci, 2006. **26**(24): p. 6627-36.
145. Picard-Riera, N., B. Nait-Oumesmar, and A. Baron-Van Evercooren, *Endogenous adult neural stem cells: limits and potential to repair the injured central nervous system.* J Neurosci Res, 2004. **76**(2): p. 223-31.
146. Salman, H., P. Ghosh, and S.G. Kernie, *Subventricular zone neural stem cells remodel the brain following traumatic injury in adult mice.* J Neurotrauma, 2004. **21**(3): p. 283-92.
147. Ramaswamy, S., et al., *Cellular proliferation and migration following a controlled cortical impact in the mouse.* Brain Res, 2005. **1053**(1-2): p. 38-53.
148. Goings, G.E., V. Sahni, and F.G. Szele, *Migration patterns of subventricular zone cells in adult mice change after cerebral cortex injury.* Brain Res, 2004. **996**(2): p. 213-26.
149. Richardson, R.M., D. Sun, and M.R. Bullock, *Neurogenesis after traumatic brain injury.* Neurosurg Clin N Am, 2007. **18**(1): p. 169-81, xi.

150. Sun, L., J. Lee, and H.A. Fine, *Neuronally expressed stem cell factor induces neural stem cell migration to areas of brain injury.* J Clin Invest, 2004. **113**(9): p. 1364-74.
151. Chang, Y.C., et al., *Regenerative therapy for stroke.* Cell Transplant, 2007. **16**(2): p. 171-81.
152. Fitch, M.T., et al., *Cellular and molecular mechanisms of glial scarring and progressive cavitation: in vivo and in vitro analysis of inflammation-induced secondary injury after CNS trauma.* J Neurosci, 1999. **19**(19): p. 8182-98.
153. Tang, S., et al., *Soluble myelin-associated glycoprotein released from damaged white matter inhibits axonal regeneration.* Mol Cell Neurosci, 2001. **18**(3): p. 259-69.
154. Buss, A. and M.E. Schwab, *Sequential loss of myelin proteins during Wallerian degeneration in the rat spinal cord.* Glia, 2003. **42**(4): p. 424-32.
155. Grandpre, T. and S.M. Strittmatter, *Nogo: a molecular determinant of axonal growth and regeneration.* Neuroscientist, 2001. **7**(5): p. 377-86.
156. Quarles, R.H., *Myelin-associated glycoprotein (MAG): past, present and beyond.* J Neurochem, 2007. **100**(6): p. 1431-48.
157. Vourc'h, P. and C. Andres, *Oligodendrocyte myelin glycoprotein (OMgp): evolution, structure and function.* Brain Res Brain Res Rev, 2004. **45**(2): p. 115-24.
158. Schwab, J.M., S.K. Tuli, and V. Failli, *The Nogo receptor complex: confining molecules to molecular mechanisms.* Trends Mol Med, 2006. **12**(7): p. 293-7.
159. Weinreb, P.H., et al., *Resolution of disulfide heterogeneity in Nogo receptor I fusion proteins by molecular engineering.* Biotechnol Appl Biochem, 2010. **57**(1): p. 31-45.
160. Lee, J.K., et al., *Nogo receptor antagonism promotes stroke recovery by enhancing axonal plasticity.* J Neurosci, 2004. **24**(27): p. 6209-17.
161. Li, S., et al., *Blockade of Nogo-66, myelin-associated glycoprotein, and oligodendrocyte myelin glycoprotein by soluble Nogo-66 receptor promotes axonal sprouting and recovery after spinal injury.* J Neurosci, 2004. **24**(46): p. 10511-20.
162. Ji, B., et al., *Effect of combined treatment with methylprednisolone and soluble Nogo-66 receptor after rat spinal cord injury.* Eur J Neurosci, 2005. **22**(3): p. 587-94.
163. Harvey, P.A., et al., *Blockade of Nogo receptor ligands promotes functional regeneration of sensory axons after dorsal root crush.* J Neurosci, 2009. **29**(19): p. 6285-95.
164. Agarwalla, P.K., G.P. Dunn, and E.R. Laws, *An historical context of modern principles in the management of intracranial injury from projectiles.* Neurosurg Focus, 2010. **28**(5): p. E23.
165. Yao, C., et al., *Detection of protein biomarkers using high-throughput immunoblotting following focal ischemic or penetrating ballistic-like brain injuries in rats.* Brain Inj, 2008. **22**(10): p. 723-32.
166. Lu, X.C., et al., *NNZ-2566, a glypromate analog, improves functional recovery and attenuates apoptosis and inflammation in a rat model of penetrating ballistic-type brain injury.* J Neurotrauma, 2009. **26**(1): p. 141-54.

167. Chen, Z., et al., *Human amnion-derived multipotent progenitor cell treatment alleviates traumatic brain injury-induced axonal degeneration.* J Neurotrauma, 2009. **26**(11): p. 1987-97.
168. Davis, A.R., et al., *A comparison of two cognitive test paradigms in a penetrating brain injury model.* J Neurosci Methods, 2010. **189**(1): p. 84-7.
169. Shear, D.A., et al., *Longitudinal characterization of motor and cognitive deficits in a model of penetrating ballistic-like brain injury.* J Neurotrauma, 2010. **27**(10): p. 1911-23.
170. Chen, Z., et al., *Synergism of human amnion-derived multipotent progenitor (AMP) cells and a collagen scaffold in promoting brain wound recovery: Pre-clinical studies in an experimental model of penetrating ballistic-like brain injury.* Brain Res, 2010. **1368**: p. 71-81.
171. Dewar, D., S.M. Underhill, and M.P. Goldberg, *Oligodendrocytes and ischemic brain injury.* J Cereb Blood Flow Metab, 2003. **23**(3): p. 263-74.
172. Irving, E.A., D.L. Bentley, and A.A. Parsons, *Assessment of white matter injury following prolonged focal cerebral ischaemia in the rat.* Acta Neuropathol, 2001. **102**(6): p. 627-35.
173. Ksiezak-Reding, H., et al., *Tau protein expression in adult bovine oligodendrocytes: functional and pathological significance.* Neurochem Res, 2003. **28**(9): p. 1385-92.
174. LoPresti, P., et al., *Functional implications for the microtubule-associated protein tau: localization in oligodendrocytes.* Proc Natl Acad Sci U S A, 1995. **92**(22): p. 10369-73.
175. Migheli, A., et al., *Light and electron microscope localization of the microtubule-associated tau protein in rat brain.* J Neurosci, 1988. **8**(6): p. 1846-51.
176. Crompton, K.E., et al., *Inflammatory response on injection of chitosan/GP to the brain.* J Mater Sci Mater Med, 2006. **17**(7): p. 633-9.
177. Tate, M.C., et al., *Fibronectin promotes survival and migration of primary neural stem cells transplanted into the traumatically injured mouse brain.* Cell Transplant, 2002. **11**(3): p. 283-95.
178. Tate, C.C., et al., *Laminin and fibronectin scaffolds enhance neural stem cell transplantation into the injured brain.* J Tissue Eng Regen Med, 2009. **3**(3): p. 208-17.
179. Lee, J., et al., *Intracranial drug-delivery scaffolds: biocompatibility evaluation of sucrose acetate isobutyrate gels.* Toxicol Appl Pharmacol, 2006. **215**(1): p. 64-70.
180. Gilbert, R.J., et al., *CS-4,6 is differentially upregulated in glial scar and is a potent inhibitor of neurite extension.* Mol Cell Neurosci, 2005. **29**(4): p. 545-58.
181. Jones, L.L., R.U. Margolis, and M.H. Tuszynski, *The chondroitin sulfate proteoglycans neurocan, brevican, phosphacan, and versican are differentially regulated following spinal cord injury.* Exp Neurol, 2003. **182**(2): p. 399-411.
182. Ma, L., et al., *Enhanced biological stability of collagen porous scaffolds by using amino acids as novel cross-linking bridges.* Biomaterials, 2004. **25**(15): p. 2997-3004.
183. David, S., E.J. Fry, and R. Lopez-Vales, *Novel roles for Nogo receptor in inflammation and disease.* Trends Neurosci, 2008.

184. Fry, E.J., C. Ho, and S. David, *A role for Nogo receptor in macrophage clearance from injured peripheral nerve.* Neuron, 2007. **53**(5): p. 649-62.
185. Martini, R., et al., *Interactions between Schwann cells and macrophages in injury and inherited demyelinating disease.* Glia, 2008. **56**(14): p. 1566-77.
186. Satoh, J., et al., *Nogo-A and nogo receptor expression in demyelinating lesions of multiple sclerosis.* J Neuropathol Exp Neurol, 2005. **64**(2): p. 129-38.
187. Cui, Q., Y. Yin, and L.I. Benowitz, *The role of macrophages in optic nerve regeneration.* Neuroscience, 2009. **158**(3): p. 1039-48.
188. Andres, R.H., et al., *Cell replacement therapy for intracerebral hemorrhage.* Neurosurg Focus, 2008. **24**(3-4): p. E16.
189. Chopp, M. and Y. Li, *Treatment of stroke and intracerebral hemorrhage with cellular and pharmacological restorative therapies.* Acta Neurochir Suppl, 2008. **105**: p. 79-83.
190. Delcroix, G.J., et al., *Adult cell therapy for brain neuronal damages and the role of tissue engineering.* Biomaterials, 2010. **31**(8): p. 2105-20.
191. Harting, M.T., et al., *Cell therapies for traumatic brain injury.* Neurosurg Focus, 2008. **24**(3-4): p. E18.
192. Jain, K.K., *Cell therapy for CNS trauma.* Mol Biotechnol, 2009. **42**(3): p. 367-76.
193. Naegele, J.R., et al., *Recent advancements in stem cell and gene therapies for neurological disorders and intractable epilepsy.* Neuropharmacology, 2010. **58**(6): p. 855-64.
194. Walker, P.A., et al., *Progenitor cell therapy for the treatment of central nervous system injury: a review of the state of current clinical trials.* Stem Cells Int. **2010**: p. 369578.
195. Ben-Hur, T. and S.A. Goldman, *Prospects of cell therapy for disorders of myelin.* Ann N Y Acad Sci, 2008. **1142**: p. 218-49.
196. Al Nimer, F., et al., *MHC expression after human neural stem cell transplantation to brain contused rats.* Neuroreport, 2004. **15**(12): p. 1871-5.
197. Bakshi, A., et al., *Caspase-mediated cell death predominates following engraftment of neural progenitor cells into traumatically injured rat brain.* Brain Res, 2005. **1065**(1-2): p. 8-19.
198. Bakshi, A., et al., *Neural progenitor cells engineered to secrete GDNF show enhanced survival, neuronal differentiation and improve cognitive function following traumatic brain injury.* Eur J Neurosci, 2006. **23**(8): p. 2119-34.
199. Ben-Shaanan, T.L., T. Ben-Hur, and J. Yanai, *Transplantation of neural progenitors enhances production of endogenous cells in the impaired brain.* Mol Psychiatry, 2008. **13**(2): p. 222-31.
200. Chiba, S., et al., *Anatomical and functional recovery by embryonic stem cell-derived neural tissue of a mouse model of brain damage.* J Neurol Sci, 2004. **219**(1-2): p. 107-17.
201. Dayer, A.G., et al., *Expression of FGF-2 in neural progenitor cells enhances their potential for cellular brain repair in the rodent cortex.* Brain, 2007. **130**(Pt 11): p. 2962-76.
202. Gao, J., et al., *Transplantation of primed human fetal neural stem cells improves cognitive function in rats after traumatic brain injury.* Exp Neurol, 2006. **201**(2): p. 281-92.

203. Hagan, M., et al., *Neuroprotection by human neural progenitor cells after experimental contusion in rats.* Neurosci Lett, 2003. **351**(3): p. 149-52.
204. Harting, M.T., et al., *Subacute neural stem cell therapy for traumatic brain injury.* J Surg Res, 2009. **153**(2): p. 188-94.
205. Lu, D., et al., *Neural and marrow-derived stromal cell sphere transplantation in a rat model of traumatic brain injury.* J Neurosurg, 2002. **97**(4): p. 935-40.
206. Muir, J.K., et al., *Terminally differentiated human neurons survive and integrate following transplantation into the traumatically injured rat brain.* J Neurotrauma, 1999. **16**(5): p. 403-14.
207. Pagani, L., et al., *Identification and early characterization of genetically modified NGF-producing neural stem cells grafted into the injured adult rat brain.* Neurol Res, 2008. **30**(3): p. 244-50.
208. Philips, M.F., et al., *Survival and integration of transplanted postmitotic human neurons following experimental brain injury in immunocompetent rats.* J Neurosurg, 1999. **90**(1): p. 116-24.
209. Prajerova, I., et al., *Neural stem/progenitor cells derived from the embryonic dorsal telencephalon of D6/GFP mice differentiate primarily into neurons after transplantation into a cortical lesion.* Cell Mol Neurobiol, 2010. **30**(2): p. 199-218.
210. Riess, P., et al., *Transplanted neural stem cells survive, differentiate, and improve neurological motor function after experimental traumatic brain injury.* Neurosurgery, 2002. **51**(4): p. 1043-52; discussion 1052-4.
211. Roshal, L.M., et al., *Effect of cell therapy on recovery of cognitive functions in rats during the delayed period after brain injury.* Bull Exp Biol Med, 2009. **148**(1): p. 140-7.
212. Shear, D.A., et al., *Neural progenitor cell transplants promote long-term functional recovery after traumatic brain injury.* Brain Res, 2004. **1026**(1): p. 11-22.
213. Park, K.I., Y.D. Teng, and E.Y. Snyder, *The injured brain interacts reciprocally with neural stem cells supported by scaffolds to reconstitute lost tissue.* Nat Biotechnol, 2002. **20**(11): p. 1111-7.
214. Shindo, T., et al., *Differences in the neuronal stem cells survival, neuronal differentiation and neurological improvement after transplantation of neural stem cells between mild and severe experimental traumatic brain injury.* J Med Invest, 2006. **53**(1-2): p. 42-51.
215. Sinson, G., M. Voddi, and T.K. McIntosh, *Combined fetal neural transplantation and nerve growth factor infusion: effects on neurological outcome following fluid-percussion brain injury in the rat.* J Neurosurg, 1996. **84**(4): p. 655-62.
216. Gage, F.H., et al., *Survival and differentiation of adult neuronal progenitor cells transplanted to the adult brain.* Proc Natl Acad Sci U S A, 1995. **92**(25): p. 11879-83.
217. Palmer, T.D., J. Takahashi, and F.H. Gage, *The adult rat hippocampus contains primordial neural stem cells.* Mol Cell Neurosci, 1997. **8**(6): p. 389-404.
218. Takahashi, J., T.D. Palmer, and F.H. Gage, *Retinoic acid and neurotrophins collaborate to regulate neurogenesis in adult-derived neural stem cell cultures.* J Neurobiol, 1999. **38**(1): p. 65-81.

219. Aberg, M.A., et al., *IGF-I has a direct proliferative effect in adult hippocampal progenitor cells.* Mol Cell Neurosci, 2003. **24**(1): p. 23-40.
220. Hsieh, J., et al., *IGF-I instructs multipotent adult neural progenitor cells to become oligodendrocytes.* J Cell Biol, 2004. **164**(1): p. 111-22.
221. Hsieh, J., et al., *Histone deacetylase inhibition-mediated neuronal differentiation of multipotent adult neural progenitor cells.* Proc Natl Acad Sci U S A, 2004. **101**(47): p. 16659-64.
222. Jessberger, S., et al., *Directed differentiation of hippocampal stem/progenitor cells in the adult brain.* Nat Neurosci, 2008. **11**(8): p. 888-93.
223. Klassen, H., et al., *The immunological properties of adult hippocampal progenitor cells.* Vision Res, 2003. **43**(8): p. 947-56.
224. Li, Y. and M. Chopp, *Marrow stromal cell transplantation in stroke and traumatic brain injury.* Neurosci Lett, 2009. **456**(3): p. 120-3.
225. Lu, D., et al., *Intravenous administration of human umbilical cord blood reduces neurological deficit in the rat after traumatic brain injury.* Cell Transplant, 2002. **11**(3): p. 275-81.
226. Richardson, R.M., et al., *Stem cell biology in traumatic brain injury: effects of injury and strategies for repair.* J Neurosurg, 2010. **112**(5): p. 1125-38.
227. Ruoslahti, E., *Brain extracellular matrix.* Glycobiology, 1996. **6**(5): p. 489-92.
228. Wurmser, A.E. and F.H. Gage, *Stem cells: cell fusion causes confusion.* Nature, 2002. **416**(6880): p. 485-7.
229. Wurmser, A.E., et al., *Cell fusion-independent differentiation of neural stem cells to the endothelial lineage.* Nature, 2004. **430**(6997): p. 350-6.
230. Wang, F., et al., *Nogo-A is involved in secondary axonal degeneration of thalamus in hypertensive rats with focal cortical infarction.* Neurosci Lett, 2007. **417**(3): p. 255-60.
231. Sun, J., et al., *Endothelial cells promote neural stem cell proliferation and differentiation associated with VEGF activated Notch and Pten signaling.* Dev Dyn, 2010. **239**(9): p. 2345-53.
232. Takasaki, C., et al., *Cytochemical and cytological properties of perineuronal oligodendrocytes in the mouse cortex.* Eur J Neurosci, 2010. **32**(8): p. 1326-36.
233. Taniike, M., et al., *Perineuronal oligodendrocytes protect against neuronal apoptosis through the production of lipocalin-type prostaglandin D synthase in a genetic demyelinating model.* J Neurosci, 2002. **22**(12): p. 4885-96.